

Biochemistry and physiological role of otoferlin

Dissertation

In partial fulfillment of the requirements for the degree “Doctor rerum
naturalium” in the Neuroscience Program at the Georg August University
Goettingen, Faculty of Biology

Submitted by

Kirsten Reuter

Born in Sulz am Neckar

Inner Ear Lab

Department of Otolaryngology, University Medical Center Goettingen

Goettingen, 29th August 2011

Supervision: Prof. Tobias Moser

**PhD committee: Prof. Reinhard Jahn
Prof. Nils Brose**

Day of Oral Exam: 10th October 2011

Herewith I declare that I prepared the PhD Thesis 'Biochemistry and Physiological Role of Otoferlin' on my own and with no other sources and aids than quoted.

Goettingen, 29th August 2011

Kirsten Reuter

For my Parents and my Family...

Table of Contents

Table of Contents	i
Figures	iii
Tables	iv
Introduction	1
Hearing and deafness	1
Outer and middle ear	1
Inner ear	2
Comparing exocytosis in inner hair cells and neurons	7
Otoferlin	9
Structure of otoferlin	9
Proposed functions	10
Pathogenic mutations	11
Monitoring synaptic vesicle fusion	12
Viral transduction	13
Adeno-Associated Virus (AAV)	14
Adenovirus (Ad)	15
Research goals	16
Materials and methods	17
Equipment	17
Subcloning of expression- and viral vectors	19
Protein expression / purification	24
SDS PAGE	25
Isothermal titration calorimetry (ITC)	26
CD spectroscopy	26
Fluorimetry	27
Floation assay	27
Animals	28
Virus production	29
Immunohistochemistry	29
Real time PCR	31
Organotypic cultures of the dissected organ of Corti	32
Embryonic transuterine otocyst injections	33
Auditory brainstem responses	33
Distortion product oto-acoustic emissions (DPOAE)	35
PHluorin imaging and unquenching	36

Results	37
Biochemistry and structure of otoferlin C ₂ F _{wt} and the <i>pachanga</i> variant	37
Ca ²⁺ binding of C ₂ F _{wt} is unlikely	37
Similar secondary structure of C ₂ F _{wt} and C ₂ F _{Pga}	40
Otoferlin C ₂ F does not seem to bind phospholipids in a Ca ²⁺ dependent manner	41
<i>Otof</i> ^{Pga/Pga} mRNA level increased but protein level decreased	42
Towards “rescue” of otoferlin knock out mice	44
<i>In vitro</i> and <i>in vivo</i> transduction of IHCs	44
Syt1 does not rescue hearing ability in otoferlin knock out mice	56
Transgenic otoferlin does not restore hearing in <i>Otof</i> ^{-/-} mice	59
Visualizing exocytosis in IHCs	66
Discussion and conclusion	70
Ca ²⁺ or phospholipid binding of C ₂ F _{wt} and C ₂ F _{Pga} still unclear	70
The <i>pachanga</i> mutation causes reduction in protein but not in mRNA levels	72
Embryonic transuterine otocyst injections into the inner ear	72
Replacement of otoferlin with synaptotagmin 1 does not suffice to restore hearing ability	74
Expression of transgenic otoferlin in IHCs does not restore hearing in <i>Otof</i> ^{-/-} mice	76
pH sensitive GFP variants for monitoring exocytosis in IHCs	78
Summary	80
References	81
Acknowledgements	I
Appendix 1	II
Abbreviations	II
Appendix 2	IV
Vector Maps	IV
Curriculum Vitae	V
Publications	VI

Figures

Figure I1: Structure of outer, middle and inner ear	2
Figure I2: Inner ear and cross section through the cochlea	3
Figure I3: Schematic view of uncoiled cochlea	4
Figure I4: Illustration of organ of Corti	4
Figure I5: Apical section of a hair cell	5
Figure I7: The SNARE complex	7
Figure I6: The inner hair cell ribbon synapse	8
Figure I8: Otoferlin model	10
Figure I9: pHluorin fluorescence characteristics	13
Figure I10: AAV vector and infection strategy	14
Figure 1: ITC to determine Ca^{2+} binding of $\text{C}_2\text{F}_{\text{wt}}$	38
Figure 2: Ca^{2+} binding analysis of $\text{C}_2\text{F}_{\text{wt}}$	39
Figure 3: Secondary structure of $\text{C}_2\text{F}_{\text{wt}}$ and $\text{C}_2\text{F}_{\text{Pga}}$	40
Figure 4: Flootation assay of C_2F .	41
Figure 5: Expression of otoferlin _{wt} and otoferlin _{Pga}	42
Figure 6: Viral gene expression in organotypic culture	45
Figure 7: Embryonic trans-uterine-otocyst injections	46
Figure 8: Statistical analysis of trans-uterine otocyst injections	47
Figure 9: Transgenic eGFP expression.	48
Figure 10: DPOAEs of animals expressing transgenic eGFP	50
Figure 11: Threshold and wave I amplitude determination in ABR recordings	51
Figure 12: Chirp stimuli in mouse	52
Figure 13: ABR thresholds of mouse litters injected with eGFP viruses	53
Figure 14: ABR wave I amplitudes after eGFP virus injection	55
Figure 15: Transgenic Syt1 expression.	56
Figure 16. Effect of Syt1 expression on DPOAEs.	57
Figure 17: ABR recordings of AAV1/2-Syt1-eGFP injected animals	58
Figure 18: In vivo transduction by Ad5-mOtof ^{wt} -eGFP	60
Figure 19: DPOAEs of Ad5-mOtof ^{wt} -eGFP injected mice	61
Figure 20: Effect of transgenic otoferlin on ABR thresholds of <i>Otof</i> ^{-/-} mice	63
Figure 21: Correlation of transduction rate with ABR wave I amplitude	64
Figure 22: Expression of vGlut1-pHluorin	66
Figure 23: Apical versus basal expression of vGlut1-pHluorin in IHCs	67
Figure 24: Phenotype of AAV1/2-VGlut1-pHluorin injected mice	68
Figure 25: VGlut1-pHluorin unquenching with NH_4Cl	69

Tables

Table M2: Lipid composition of solutions for the production of liposomes	27
Table M1: Virus titers	29
Table M3: Primary antibodies used for immunohistochemistry	30
Table M4: Secondary antibodies used for immunohistochemistry	31
Table M4: Frequency combinations used for DPOAE measurements.	35
Table 1: eGFP expression after <i>in vivo</i> viral transduction.	48
Table 2: Transgenic synaptotagmin 1 expression of positive animals.	56
Table 3: Transduction rates after injection of Ad5-mOtof ^{wt} -eGFP	59

Introduction

Hearing and deafness

Hearing is a sense of great importance. Humans as well as many other species rely on their hearing ability for communication but also for other purposes like detection of prey and predators or navigation. For most animals deafness is fatal; prey cannot escape their predators and predators cannot find their prey. Although not being fatal for humans, deafness often means living a life isolated from most of the hearing society.

Proper hearing requires the detection and interpretation of the information carried by sound: frequency, intensity and temporal structure. Additionally binaural hearing enables the localization of sound. Time differences of the order of tens of microseconds of sound arrival at the two ears (interaural time difference) can be detected due to efficient signal transmission. The sound enters the external ear canal, is transmitted from the tympanic membrane to the oval window of the cochlea via the ossicles of the middle ear and then leads to vibration of the basilar membrane in the inner ear and consequently to stimulation of inner hair cells (IHCs). Outer hair cells (OHCs) locally amplify the basilar membrane vibration. IHCs then transmit the information to spiral ganglion neurons (SGN) at their ribbon synapses. SGN then conduct information as a spike code to the brain.

Damage of any part of the auditory system may lead to deafness; often defects in the inner ear are involved. They can be caused by excessive exposure to sound, by inflammation or infections as well as by genetic defects. One of these genetic cases is DFNB9, an autosomal recessive nonsyndromic hearing loss caused by mutations in *OTOF*, the gene encoding the protein otoferlin. This protein is mainly expressed in IHCs, but also in low amounts in the brain (Yasunaga et al., 2000).

Outer and middle ear

The outer ear consists of the pinna and the external ear canal. The pinna funnels the sound into the external ear canal toward the tympanic membrane. In the middle ear the ossicles (malleus, incus and stapes) convey the vibration to the oval

window membrane (Figure I1). The surface ratio of tympanic membrane to oval window membrane, that is 20:1, and the lever action of the ossicles permit an adequate transfer of pressure waves from the low impedance medium air to the non-compressible fluid filled space of the cochlea.

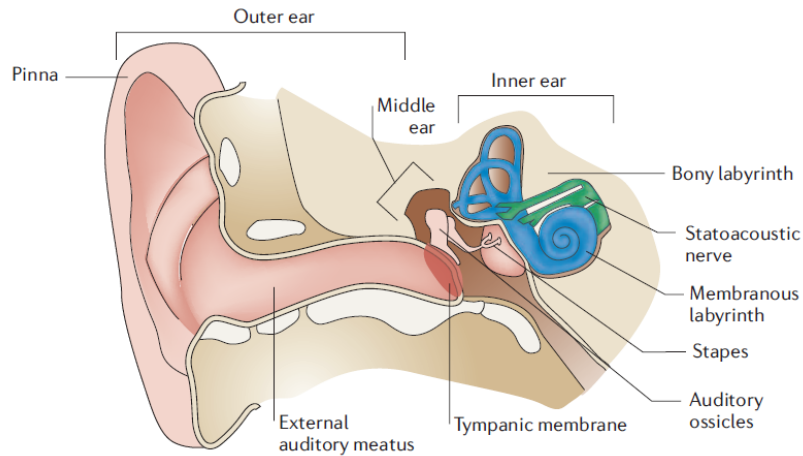


Figure I1: Structure of outer, middle and inner ear (Kelley, 2006)

Inner ear

The vestibular system and the cochlea make up the mammalian inner ear. The vestibular system with the saccule, the utricle and the three semicircular canals contribute to the sense of balance, whereas sound is transduced only in the cochlea. Both senses rely on hair cells, cells specialized for the detection of mechanical vibration.

Cochlea

In a bony shell three fluid filled compartments are coiled up around the so called modiolus making up the cochlea. The modiolus contains the spiral ganglion neurons, the first neurons of the auditory pathway. They have synaptic contact with the cochlear hair cells, which are localized in the organ of Corti. It is found in the middle fluid filled compartment (Figure I2), the scala media. Localized above the scala media is the scala vestibuli and below the scala media the scala tympani is found.

Both scala vestibuli and scala tympani are filled with perilymph, the two compartments communicate at a gap in the membrane called the helicotrema. Only the

scala media is filled with endolymph, it contains a high concentration (~150 mM) of K^+ , which is maintained by the stria vascularis, a tissue lining the outward pointing side of the scala media.

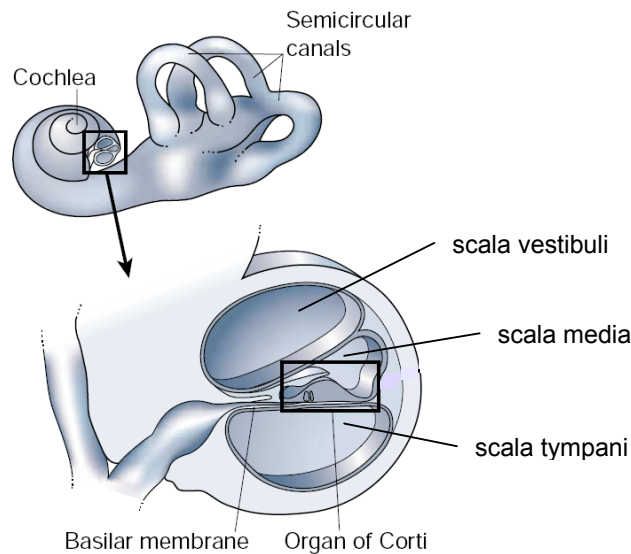


Figure I2: Inner ear and cross section through the cochlea (adapted from Gillespie and Walker, 2001)

The cross section through the cochlea shows three fluid filled compartments. Bottom most is the scala tympani above which the Organ of Corti is located in the scala media. The third compartment is called the scala vestibuli.

At the basal end of the cochlea at the oval window a membrane separates the fluid inside the scala vestibuli from the middle ear. When the ossicles transmit sound to the cochlea pressure waves are elicited in the fluid of the scala vestibuli which are being transmitted to the scala tympani and released at the round window. These pressure waves lead to a traveling wave along the basilar membrane, that has a maximum deflection at a certain position along the way from base to apex, where most of the energy is dissipated, stopping the wave abruptly. The physical properties of the basilar membrane define this point of strongest vibration dependent on the input frequency. Low frequencies result in a maximal deflection of the basilar membrane at the apex, where the membrane is less stiff, wider and thicker than at the base. Thus, the sound frequency defines the location of the peak of the traveling wave.

This effect is the basis for a tonotopic organization of signal transmission throughout the auditory pathway (Figure I3). In humans the cochlea has 2.5 turns and detects frequencies from 0.1 to 20 kHz (Fettiplace and Hackney, 2006), in mice only 1.75 turns are found with a frequency range of 1 to 100 kHz.

- Introduction -

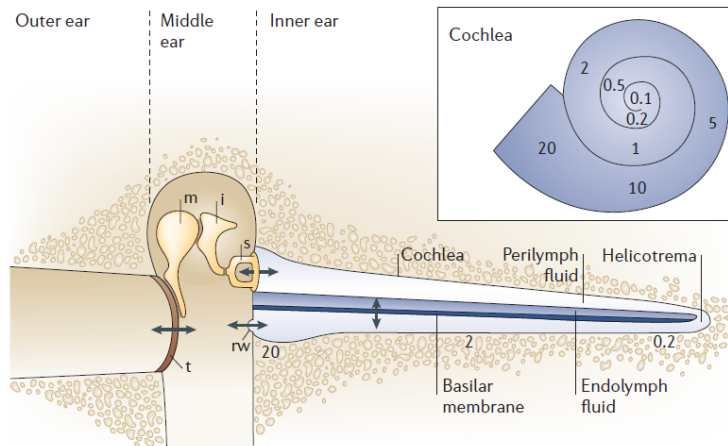


Figure I3: Schematic view of uncoiled cochlea

Inset: tonotopic distribution of maximal response to specific sound frequencies (in kHz) along basilar membrane of a human cochlea. (Fettiplace and Hackney, 2006)

Organ of Corti

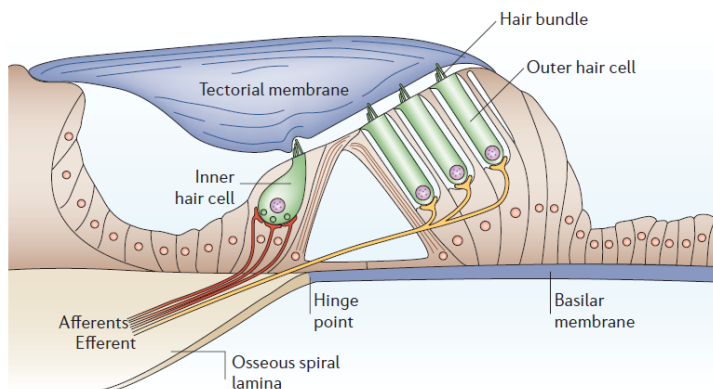


Figure I4: Illustration of organ of Corti

The illustration of the organ of Corti is pointing out the tectorial and basilar membrane, supporting cells and hair cells and afferent and efferent nerve fibers. (Fettiplace and Hackney, 2006)

On top of the basilar membrane the organ of Corti is situated (Figure 14), different cell types (inner and outer pillar cells, Hensen's cells, phalangeal cells and Deiters' cells) support the cochlear hair cells and maintain their homeostasis (Figure 14).

The cochlear hair cells are required for signal amplification and for converting the mechanical stimulus of sound into an electrical signal.

Cochlear hair cells

Hair cells in the cochlea can be separated into two groups, outer and inner hair cells (OHCs and IHCs), both are specialized to detect the mechanical movement induced by sound via a bundle of stereocilia at the apical surface of the cells. In humans about 12000 OHCs and 3500 IHCs are found (Dallos, 1992). The stereocilia form rows of increasing length and are interconnected by side links and top links. At the very top of a stereocilium a tip link connects it to the next taller stereocilium (Fettiplace and Hackney, 2006). At each lower end of a tip link mechano-electrical transduction (MET) channels are located in the proximity to the link (Figure I5) (Beurg et al., 2009; Sakaguchi et al., 2009). Stereociliar deflection applies tension to the tip links which leads to opening of the MET channels.

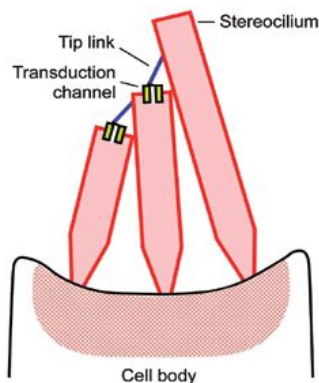


Figure I5: Apical section of a hair cell

The connection of MET channel with tip links is depicted in this schematic of an apical hair cell section. (LeMasurier and Gillespie, 2007)

The hair bundles of IHCs have no physical contact to the lower surface of the tectorial membrane, whereas the tips of the hair bundles of OHCs touch the tectorial membrane. Vertical vibration of the basilar membrane due to a sound stimulus lifts and lowers the Organ of Corti which causes a shearing force between the hair bundle of OHCs and the tectorial membrane leading to a displacement of the tips of the stereocilia bundle. The resulting fluid flow causes a deflection of the IHC hair bundles.

The hair bundles are immersed in the endolymph of the scala media; therefore the potential difference between endolymph (~ 80 mV) and IHCs (~ -70 mV) drives a cation flow, mainly K^+ , through open mechanotransducer channels leading to a depolarization of the cell in case of stereociliar deflection toward the tallest stereocilium.

Outer hair cells

The main function of OHCs is to increase the amplitude of basilar membrane deflection; thereby also shaping the frequency tuning (Dallos and Fakler, 2002). The cells are modulated by efferent synapses formed by medial superior olive (MSO) neurons. The lateral membrane of OHCs is densely packed with prestin, a protein which alters its conformation upon voltage changes (Oliver et al., 2001), the conformational change leads to the contraction under depolarized conditions and cell elongation in hyperpolarized state (Brownell et al., 1985; Kachar et al., 1986). This mechanism of electromotility is required for cochlear signal amplification (Liberman et al., 2002). However, the loss of outer hair cells also causes a reduction in frequency selectivity (Dallos and Harris, 1978) as the contraction – elongation cycle of OHCs enhances the maximum of the passive vibration of the basilar membrane. Recent findings also demonstrate that OHCs have relatively depolarized resting potential of about -40mV which lies near the highest voltage sensitivity of prestin (Johnson et al., 2011).

The non-linear cochlear amplification mediated by OHCs is read-out in distortion product oto-acoustic emission (DPOAE) analysis of OHC function. In DPOAE measurements two frequencies (f_1 and f_2) are played simultaneously and the non-linearity of the cochlea leads to a specific distortion, dependent on frequency and amplitude of f_1 and f_2 . This distortion product is amplified by OHCs like other signals too and can be recorded by a microphone. The amplitude of the recorded signal gives evidence for the extent of cochlear amplification, thus OHC function.

Inner hair cells

In contrast to OHCs IHCs and their synapses with SGN are responsible for sound coding. The mechanical input is transduced into a receptor potential at the IHC membrane which leads to Ca^{2+} influx through voltage gated Ca^{2+} channels triggering synaptic vesicle fusion. Then the neurotransmitter causes an excitatory postsynaptic current which is translated into action potentials by the SGN. Depending on the position along the basilar membrane, owing to its mechanical properties, different frequencies lead to maximal membrane vibration and hair bundle stimulation of the IHCs. Therefore each IHC senses a small range of frequencies, transducing only a narrow band of stimuli (Fettiplace and Fuchs, 1999).

IHCs mainly signal to afferent terminals of (type I) SGN. In the apex and during

development also efferent terminals from the lateral superior olive (LSO) are innervating the IHCs. Most efferent terminals in mature organs of Corti end on postsynaptic efferent boutons, possibly shaping the postsynaptic response.

Comparing exocytosis in inner hair cells and neurons

Exocytosis at conventional neuronal synapses

In conventional neuronal synapses fusion of synaptic vesicles is thought to be mediated by soluble N-ethylmaleimide-sensitive factor attachment protein receptor (SNARE) complex (Figure I7) and regulated by mainly two proteins, complexin I and synaptotagmin I (Syt1).

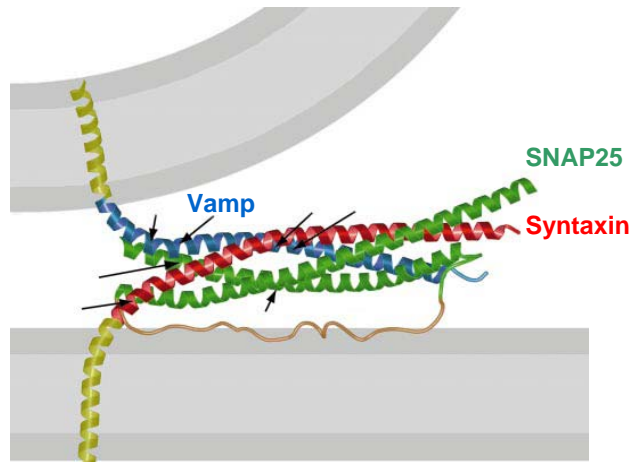


Figure I7: The SNARE complex
Image adapted from Sutton et al. (1998).

The SNARE complex is made up of the three neuronal SNAREs: 25-kilo Dalton (kDa) Synaptosome Associated Protein (SNAP-25), synaptobrevin (VAMP) and syntaxin 1 forming a parallel four-helix bundle (Poirier et al., 1998; Sutton et al., 1998; Jahn and Scheller, 2006). Formation and disassembly of the complex is regulated by several proteins including Rab GTP-ases, Munc18, N-ethylmaleimide sensitive factor (NSF) and α -soluble NSF attachment protein (α -SNAP) (Waters and Hughson, 2000; Whyte and Munro, 2002; Rosenmund et al., 2003; Bonifacino and Glick, 2004; Jahn and Scheller, 2006). RIMs and Munc13s also play a role in vesicle docking and SNARE complex formation (Rizo and Rosenmund, 2008). It is thought that once the SNARE complex is formed the synaptic vesicle is held in a pre-fusion state, ready to be fused upon Ca^{2+} triggering, a process regulated by complexin I and synaptotagmin I (Syt1).

Syt1 is thought to act as the Ca^{2+} sensor for vesicle fusion, responsible for fast and synchronous transmitter release upon Ca^{2+} influx (Söllner et al., 1993; Geppert et al., 1994; Fernandez-Chacon et al., 2001; Chapman, 2002; Yoshihara and Littleton, 2002; Südhof and Scheller, 2003). It contains two C_2 domains, C_2A and C_2B , which, *in vitro*, bind phospholipids in a Ca^{2+} dependent manner (Davletov and Südhof, 1993; Rickman et al., 2004). C_2 domains are independently folded protein domains with 8 parallel interconnected β -strands. The loops connecting the β -strands may contain aspartate residues with a pKa of 4.0 which often form negatively charged binding pockets, suggesting Ca^{2+} dependent substrate binding (Rizo and Südhof, 1998). It has also been suggested that Syt1 in part also operates by membrane bending and penetration (Martens et al., 2007; Hui et al., 2009).

Inner hair cell exocytosis

Inner hair cell depolarization due to cation influx through the MET channel leads to opening of voltage gated Ca^{2+} channels. An increased Ca^{2+} concentration triggers the fusion of glutamate filled vesicles at the IHC ribbon synapse (Figure I6). The synapse is able to fuse the vesicles with a sub millisecond precision; however, the machinery for the precise release is not yet fully understood.

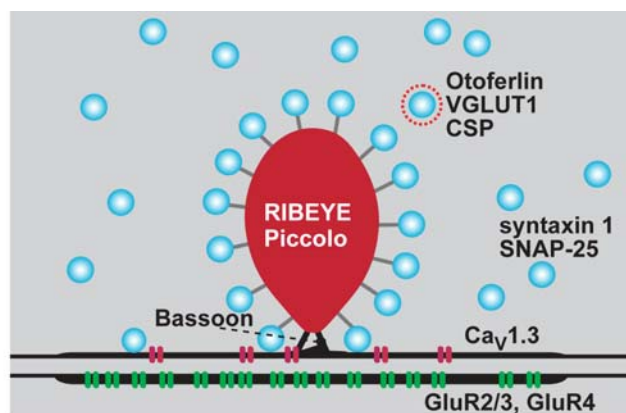


Figure I6: The inner hair cell ribbon synapse
Image adapted from Nouvian et al. (2006).

At the ribbon synapse the proteins RIBEYE, bassoon and piccolo are present, however the synapse lacks other major components of the neurotransmitter release machinery found in conventional synapses including synaptophysins, synapsins and synaptotagmins I and II (Mandell et al., 1990; Safieddine and Wenthold, 1997, 1999)

and apparently the synapse functions without neuronal SNAREs (syntaxin, SNAP25, synaptobrevin) (Nouvian et al., 2011). Instead it was shown that the protein otoferlin is involved in exocytosis at the inner hair cell ribbon synapse (Roux et al., 2006), however, its function still needs further investigation.

Otoferlin

Otoferlin belongs to the ferlins, a protein family involved in different membrane fusion events. It is mainly found in IHCs, but also in outer and vestibular hair cells and brain tissue. The absence of synaptotagmin I in IHCs, cells particularly relying on temporal precision of synaptic vesicle fusion, leads to the question which protein takes over the Ca^{2+} sensing function. Otoferlin is one candidate for inducing Ca^{2+} dependent neurotransmitter release at the inner hair cell ribbon synapse, however, this theory has not been proven yet. Analysis of the binding capacity of otoferlin C_2 domains to Ca^{2+} and phospholipids and replacing the entire protein with Syt1 may lead to an answer of this question.

Structure of otoferlin

OTOF, the gene encoding otoferlin, is localized in the human genome on chromosome 2p23 and contains 48 exons (Yasunaga et al., 2000) (Figure 18).

Otoferlin contains a C-terminal transmembrane domain, a coiled coil domain and at least 6 C_2 domains (Figure 18). The C_2 domains are labelled according to the alphabet and their position in the protein starting with C_2A as most N-terminal C_2 domain. Only C_2de , a proposed C_2 domain between C_2D and C_2E makes a difference in nomenclature as its existence is still unclear and it may be an incomplete C_2 domain (McNeil and Kirchhausen, 2005; Washington and Ward, 2006; Han and Campbell, 2007).

The C_2 domains of ferlins are evolutionary distinct to those of synaptotagmins, in fact, it is quite likely that functionally important motifs, such as the Ca^{2+} binding sites depart from known structures.

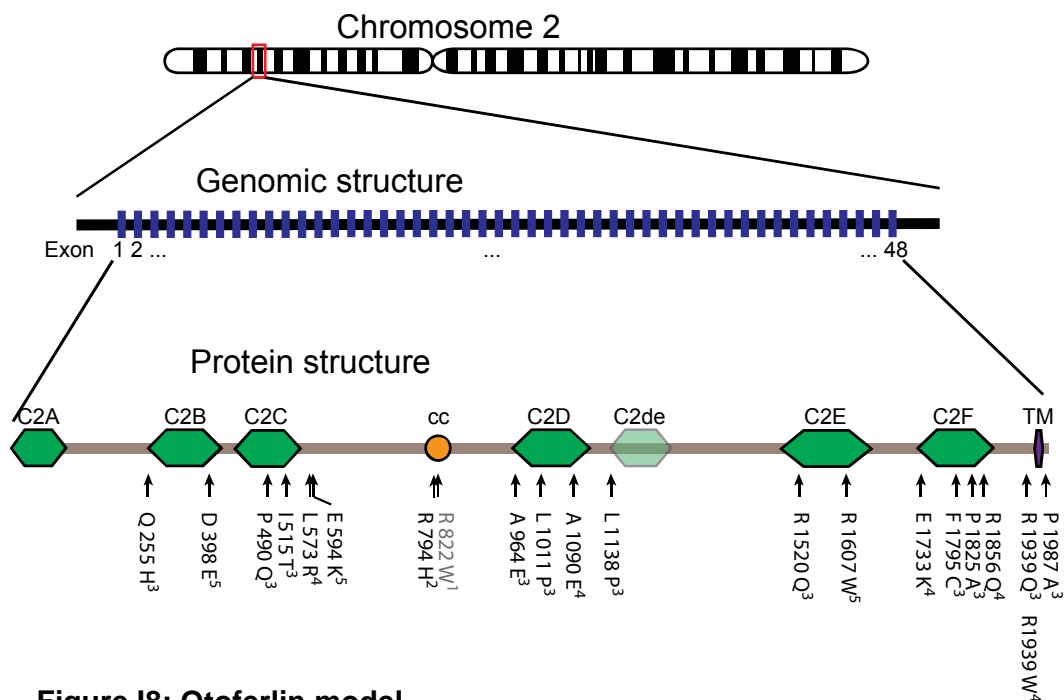


Figure I8: Otoferlin model

The genomic structure shows 48 exons depicted as vertical blue bars, the protein structure shows the C₂ domains as green hexagons, the coiled coil domain in yellow and the trans-membrane domain in violet, black arrows indicate pathogenic missense mutations.^(1)Hutchin et al., 2005; ²Varga et al., 2006; ³Rodríguez-Ballesteros et al., 2008; ⁴Choi et al., 2009; ⁵Wang et al., 2010)

Proposed functions

Otoferlin function at the IHC ribbon synapse is still unclear. It was shown to be involved in Ca²⁺ dependent exocytosis at the IHC synapse (Roux et al., 2006). IHCs lacking otoferlin hardly showed any Ca²⁺ triggered exocytosis. However, it is not clear from these experiments whether otoferlin, indeed, works as a Ca²⁺ sensor for exocytosis or takes over other functions for leading to the shown phenotype.

Other proposed functions include vesicle priming and replenishment (Pangrsic et al., 2010), control of coupling of Ca_v1.3 channels and ribbons (Heidrych et al., 2009) and endosome recycling (Heidrych et al., 2008).

Therefore, it is important to find out more about otoferlin, especially about its protein domain function. Hence, the Ca²⁺ binding and Ca²⁺ dependent phospholipid binding capacity, both are important for Syt1 protein function, can give evidence for or against the theory of otoferlin acting as Ca²⁺ sensor for exocytosis in IHCs.

It has been shown that otoferlin C₂A does not bind Ca²⁺ (Johnson and Chapman, 2010; Helfmann et al., 2011), nevertheless Ca²⁺ binding has been shown for

C₂B, C₂C, C₂D, C₂E and C₂F (Roux et al., 2006; Johnson and Chapman, 2010), with lower affinity than exhibited in synaptotagmin C₂ domains (Johnson and Chapman, 2010). Therefore the issue needs further characterization. The study by Johnson and Chapman (2010) also demonstrates binding of these six C₂ domains to liposomes again with low affinity. Only the structure of the C₂A domain of otoferlin has been solved so far (Helfmann et al., 2011).

Pathogenic mutations

In humans more than 40 pathogenic mutations in *OTOF* are known to date leading to DFNB9, an autosomal recessive nonsyndromic hearing loss (Yasunaga et al., 1999, 2000; Adato et al., 2000; Houseman et al., 2001; Migliosi et al., 2002; Mirghomizadeh et al., 2002; Rodríguez-Ballesteros et al., 2003; Varga et al., 2003, 2006; Hutchin et al., 2005; Tekin et al., 2005; Rouillon et al., 2006; Choi et al., 2009; Wang et al., 2010). 20 of these mutations are missense mutations, which are all located in or close to the regions of the proposed C₂ domains, the coiled coil domain or the trans-membrane domain, nonsense mutations are distributed along the entire gene (Rodríguez-Ballesteros et al., 2008). Patients suffering from mutations in *OTOF* may benefit from future gene therapeutic approaches for viral driven expression of otoferlin in the inner ear.

***Pachanga* (Pga) mutation**

Schwander et al. found recessive deafness traits in a forward genetics screen using N-ethyl-N-nitrosourea (ENU) as a mutagen. One of the mutations found to be leading to deafness was a missense mutation in the otoferlin C₂F domain, called *pachanga* mutation (D1767G in NP_0010903865, NCBI); mice carrying this mutation (*Otof*^{Pga/Pga}) are deaf but show no circling behaviour (Schwander et al., 2007).

The effect of the mutation on the C₂F domain of otoferlin is unclear; there might be an altered secondary structure or an effect on Ca²⁺ or phospholipid binding. Furthermore the phenotype of the *Otof*^{Pga/Pga} mice may arise due to transcription or protein folding problems induced by the mutation.

Monitoring synaptic vesicle fusion

Detailed physiological analysis of genetically manipulated inner hair cells can give evidence on the function of the manipulated proteins at the ribbon synapse and therefore elucidate further the function of this specialized synapse. In case of the hair cell synapse the process of exocytosis is of special interest as it must be extraordinarily precise to fulfill the requirements of sound coding. In people suffering from DFNB9 the effect of the mutation on exocytosis is often unclear and needs further characterization.

Hair cell exocytosis is often monitored by presynaptic patch-clamp capacitance measurements or postsynaptic patch-clamp recordings. However, a new method using a variant of green fluorescent protein (GFP) for monitoring exocytosis has been developed. Wild type GFP as well as its enhanced form eGFP show pH dependent fluorescence (Kneen et al., 1998). A mutagenesis screen then found GFP variants (ratiometric and ecliptic pHluorins) which displayed increased pH dependent absorbance changes. The absorbance of ecliptic pHluorin decreases with lowered pH, at pH<6 no 475nm excitation peak is present any longer (Figure I9) (Miesenbock et al., 1998). Additional point mutations leading to super-ecliptic pHluorin increased brightness of the original ecliptic pHluorin without affecting pH sensitivity (Sankaranarayanan et al., 2000).

These pHluorins have been used for monitoring exocytosis for example in hippocampal neuronal cultures by expressing a fusion protein of the vesicular protein VAMP coupled to the fluorophore. The pHluorin points into the vesicular lumen where it is quenched due to the vesicular pH of 5.6 and only fluoresces upon vesicle fusion and exposure to physiological pH (Sankaranarayanan et al., 2000). With this method it would be possible to correlate the site of exocytosis with fluorescence intensity hot spots, but also to estimate the time course and amount of exocytosis in the IHCs.

Establishing the use of pHluorins for monitoring exocytosis in hair cells would be of great benefit. The main advantages include single synapse analysis, the specificity for synaptic vesicle exocytosis and the measurement during depolarization. Recently, large heterogeneity of presynaptic calcium signals has been described (Meyer et al., 2009; Frank et al., 2010), therefore it is likely that exocytosis between the 5 - 20 synapses of a single IHC is also variable. However, the most commonly used method to monitor the IHC exocytosis, whole-cell membrane capacitance measurement, only measures capacitance changes of the entire cell without single synapse resolution.

Additionally, the observed changes in membrane capacitance do not necessarily represent synaptic vesicle exocytosis.

The use of pHluorins could also simplify the analysis of the effect of a transgene on IHC exocytosis by co-expressing both proteins. The transgene of interest, for example otoferlin with mutations found in DFNB9 patients, could be coexpressed with pHluorin via viral gene transfer. This would allow fast analysis of the effect of particular mutations in future screens.

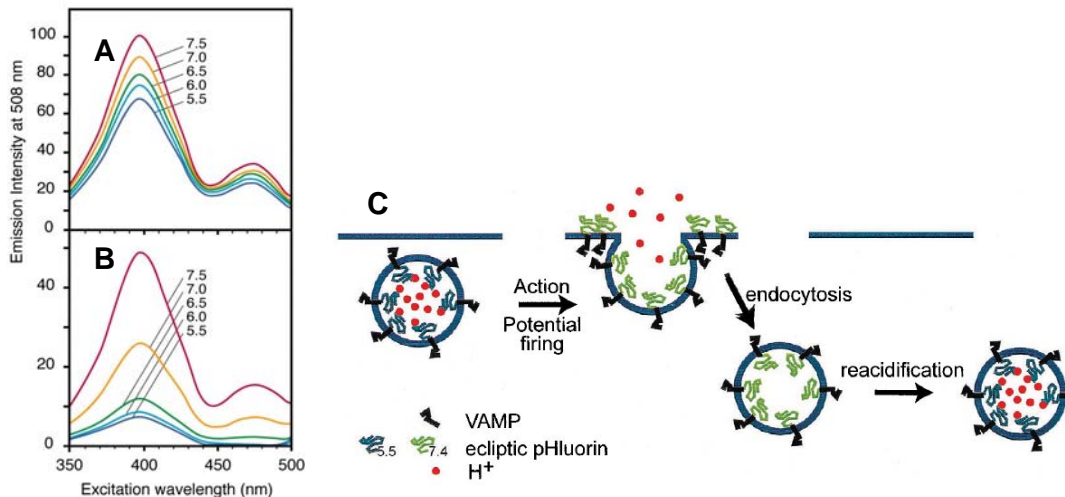


Figure I9: pHluorin fluorescence characteristics

A-B. pH dependent excitation spectra of **A.** wild-type GFP and **B.** ecliptic pHluorin (Miesenbock et al., 1998).

C. Schematic of pHluorin quenching and un-quenching during synaptic activity (Sankaranarayanan et al., 2000).

Viral transduction

Genetic manipulation of IHCs by viral transduction was shown to be efficient for adeno-associated virus (AAV) serotype 1/2, adenovirus (Ad) serotype 5 and lentivirus (Luebke, Foster, et al., 2001; Bedrosian et al., 2006). Therefore these virus types can be used for transgene expression in IHCs which can be monitored via fluorescent reporter proteins like green fluorescent protein (GFP). Viral transduction can be used on the one hand to analyze the effect of the corresponding transgene on IHC function and on the other hand for the use in gene therapy approaches which rely on the use of viral transduction.

Adeno-Associated Virus (AAV)

The AAV belongs to the family of paroviridae, it is a non-enveloped virus, has a diameter of about 25 nm and contains a genome of almost 5 kilo bases (kb) single stranded DNA, which, in recombinant AAVs, restricts the capacity for insertion of transgenes to roughly 2.5 – 3 kb depending on promoter and poly A tail length. Recombinant AAV cannot replicate itself but needs helper vector for this purpose (Figure I10) (Wu et al., 2006), which is one reason, besides its low immunogenicity, why it is favored for gene therapy approaches. Another important feature of the AAV is the long-term gene expression; the viral genome site specifically integrates into the host genome or remains in an episomal form (Figure I10) (Wu et al., 2006).

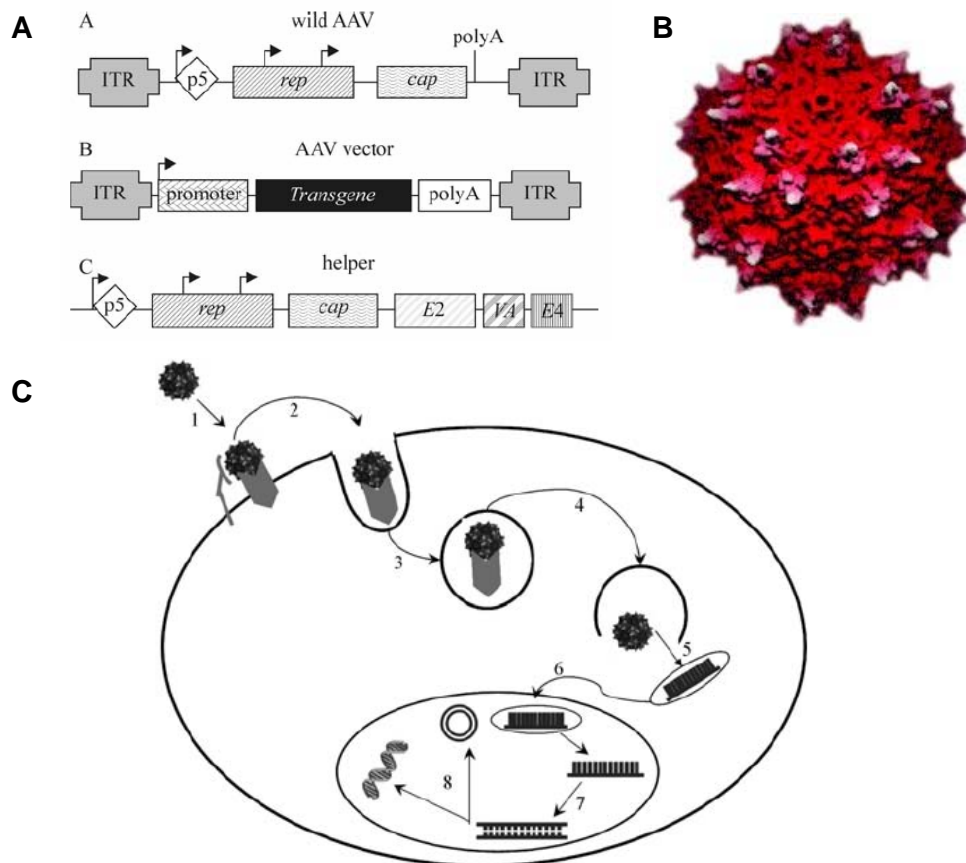


Figure I10: AAV vector and infection strategy

A. AAV vector maps: upper map: wild type AAV, then: AAV vector with transgene and last: helper vector for production of AAV with transgene (Coura and Nardi, 2008).

B. 3D structure of AAV serotype 2 (Xie et al., 2002).

C. Schematic of AAV infection of host cell (Coura and Nardi, 2008).

AAV serotype 2, meaning that replicon, capsid protein and inverted terminal repeats (ITRs) all originate from wild type AAV type 2, is very popular in AAV based research. It has a natural tropism for neurons (Bartlett et al., 1998) amongst other cell types. It binds to heparan sulfate proteoglycan as primary receptor on the host cell surface, while $\alpha V\beta 5$ integrin and fibroblast growth factor receptor 1 have co-receptor function facilitating receptor-mediated endocytosis of the virus (Summerford and Samulski, 1998; Qing et al., 1999; Summerford et al., 1999).

Also hybrids of virus serotypes were developed to enhance or enable tissue transduction which was not possible with naturally occurring AAV serotypes (Hildinger et al., 2001). Apart from mosaic AAV vectors, using capsid subunits from different serotypes, also chimeric virions were developed. In this case mutations have been performed leading to amino acid or even protein domain exchange between different serotypes. For gene therapy approaches in the inner ear the most suitable chimeric AAV vector is a combination of serotypes 2 and 1, this virion has a high transduction capacity for inner and outer hair cells (Bedrosian et al., 2006).

Adenovirus (Ad)

Like AAV the adenoviridae are non-enveloped viruses, they have a diameter of 80 - 100 nm, the large size allows a genome of 30 - 38 kb double stranded DNA and the virus can even hold up to 45 kb. Natural adenovirus contains several genes required for replication, divided into early (E1a E1b, E2a, E2b, E3, E4) and late (L1, L2, L3, L4, L5) genes. The late phase of replication begins with the onset of DNA replication.

Most adenovirus serotypes bind the coxsackievirus adenovirus receptor (CAR) of the host cell as primary receptor and then α_v integrin, which has a co-receptor function and initiates internalization via clathrin coated pits (Wu and Nemerow, 2004). Although the viral genome does not integrate into the host cell genome (Coura and Nardi, 2008) usually long-term gene expression is found.

Due to the capacity to hold large DNA fragments the adenovirus has a big advantage compared to AAV, nevertheless for the integration of small DNA fragments into the host cell genome the use of AAV is to be favored as adenovirus exhibits high immunogenicity (Coura and Nardi, 2008).

For applications involving hair cell transduction adenovirus serotype 5 with E1, E2 and E4 region deleted should be chosen (Praetorius et al., 2009) as first generation adenovirus (with only E1 and E2 deleted) led to ototoxicity and hair bundle loss (Holt et al., 1999; Luebke, Steiger, et al., 2001) .

Research goals

My PhD project had two major goals. First, contribute to clarifying the role of otoferlin at the hair cell ribbon synapse. It is still unclear whether and how otoferlin acts as calcium sensor. The focus was set on the C₂F and the *pachanga* variant of this domain. Ca²⁺ and phospholipid binding was characterized in both, wild type (C₂F_{wt}) and mutant (C₂F_{Pga}), variants.

The second goal was to establish and apply viral gene transfer into the inner ear using transuterine injection of the embryonic otocyst. As first application of this method we intend to open a principle way for gene therapy on deaf mice. Using an otoferlin knock out mouse (*Otof*^{-/-}) as model for deaf animals we aim to rescue their hearing ability via viral gene transfer. The potential to restore hearing by transgenic expression of the absent protein or ectopic synaptotagmin I as possible candidate for otoferlin replacement was tested.

The transuterine injections were also to be used for developing a method to simplify future ribbon synapse analysis. A known tool to visually monitor exocytosis needs to be established in hair cells. The key to this tool is the expression of a fusion protein constituted of a vesicular protein and the pH sensitive variant of GFP, pHluorin, at the hair cell ribbon synapse.

Materials and methods

Equipment

Molecular and cell biology

Applied Biosystems 7500 Real time PCR system

Beckmann Coulter® Avanti® J-30I centrifuge with JS-24 rotor

Biometra® Thermocycler

Bio Rad Smart Spec™ Plus Spectrophotometer

Bio Rad My Cycler™ thermal cycler

Bio Rad Power Pac 3000

Bio Rad Micro Pulser™

Eppendorf concentrator 5301

GE Healthcare Electrophoresis Power Supply – EPS301

Heraeus instruments HERA cell CO₂ incubator

Heraeus instruments HERA cell sterile bench

Heraeus instruments Pico 17 centrifuge with and without thermal aggregate

Intas UV-Systeme

Leica SP2

New Brunswick Scientific Innova® 40 incubator

Sartorius arium® 611 VF water filter system

VWR INCU-line incubator

Zeiss Axiovert 40 CFL with HBO 50 lamp

Zeiss Stemi 200-C

Otocyst injections

Drägerwerk AG TitusA Isofluran evaporator

Harvard Apparatus PLI-100 Pico Injector

Heraeus instruments LaminAir® HBB 2448

Sutter Instruments Co. P-2000 Laser Puller

Zeiss SteREO Discovery.V12, EMS2

PHluorin imaging

Cobolt Co. Cobolt Calypso 491nm laser
RedshirtImaging Neuro CCD camera
Uniblitz shutter system
Yokogawa CSU22 spinning disc confocal system
Zeiss AxoExaminer

Protein biochemistry

Applied Photophysics Chirascan CD spectrometer
Cuvette: 110-QS Quartz Glass, SUPRASIL® 1 mm optical pathlength, 350 μ l
Volume
Amersham Pharmacia BioSciences SMART system
Beckmann Coulter® TL-100 Ultracentrifuge, TLS 55 rotor
Beckmann Coulter® Allegra® X15-R with SX4750 and SX4750 μ rotors
Beckmann Coulter® Avanti® J-30I centrifuge with JS-24 and JA-18 rotors
Branson Sonifier 250
GE Healthcare High sensitivity isothermal titration calorimeter VP-ITC
Jobin Yvon Horiba Fluoromax-3
Cuvette: 100-QS Quartz Glass, SUPRASIL® 10 mm optical pathlength, 3500 μ l
Volume
New Brunswick Scientific I 26 incubator
ThermoScientific/PeqLab NanoDrop1000 Spectrophotometer

Systems physiology

ABR measurements

Hameb digital storage oscilloscope
JBL 2402 speaker
Tucker Davis Technologies HB6 Headphone buffer
Tucker Davis Technologies PA5 Programmable attenuator
Tucker Davis Technologies RA16 Medusa base station
Tucker Davis Technologies R.P. 2.1 Enhanced real time processors (two)

DPOAE measurements

M Audio DMP3™ dual microphone pre amplifier
Sennsheiser MKE 2 microphone

Technics SL-P320 compact disc player

Tucker-Davis Technologies EC1 Speaker

Tucker-Davis Technologies ED1 Electrostatic Speaker Driver

Tucker-Davis Technologies PA4 Programmable attenuators (two)

TerraTec DMX 6fire USB soundcard

Subcloning of expression- and viral vectors

In all subcloning procedures the sequence of intermediate and final DNA constructs was confirmed by DNA sequencing at the Institute DNA Core Facility of the Max-Planck-Institute for Experimental Medicine in Goettingen. Generally, plasmid DNA was amplified in XL1-blue or DH5 α cells, only for TOPO vectors TOP10 cells, and for viral vectors (AAV and Ad) SURE® electrocompetent cells (Stratagene) were used. The cells were transformed by electroporation (XL1blue, TOP10 and SURE®) or using chemical transformation (DH5 α), recovery took place for one hour at 37°C in LB medium and then the cells were spread on LB-agar plates containing 100 μ g/ml ampicillin for over night incubation at 37 °C. The next day colonies were picked, incubated over night at 37 °C in LB medium also containing 100 μ g/ml ampicillin. Plasmid purifications were then done with Qiagen, Fermentas or Peqlab purification kits and stored in 1:10 diluted elution buffer provided with the kits. If not stated otherwise, after restriction digests DNA fragments were separated via gel electrophoresis using 1% agarose gels in TAE buffer, gel extractions were done via Qiagen or Fermentas gel purification kits and PCRs were performed using Pfu DNA polymerase. From viral vectors the viruses were produced by Dr. Sebastian Kügler of the Viral Vectors Lab, Department of Neurology, University Medicine Goettingen and Dr. Samuel Young of the Department of Neurosciences of the Max Planck Florida Institute.

pGEX-2T-C₂F_{wt}, pGEX-2T-C₂F_{Pga}

Initially otoferlin C₂F_{wt} was inserted into pET44a via SmaI and XhoI restriction sites which were added to the termini of C₂F_{wt} via PCR using rat cDNA as template DNA.

forward primer: 5' atatcccgggacaaccctgacaagccaggcattg 3'

reverse primer: 5' atattcgagttagtcagggttcattgagccag 3'

- Materials and Methods -

Then otoferlin amino acids 1688 to 1927 (NPDK...NEPD) were subcloned into the pGEX-2T expression vector for expression of GST coupled to C₂F_{wt}.

Two restriction sites, BamHI upstream and EcoRI with a stop codon downstream of C₂F_{wt}, were added to the C₂ domain via PCR.

forward primer: 5' atatggatccaaccctgacaagccaggc 3'

reverse primer: 5' atatgaattctagtcaggttcattgcgagccag 3'

40 amplification cycles with an annealing temperature of 67 °C were performed in the presence of 4% DMSO and 150 µM dNTPs, pET-44a-C₂F vector was used as template DNA. The PCR product was then loaded on a 1% agarose gel, the corresponding band was extracted and the gel piece was minced to purify the DNA with a phenol chloroform extraction. Adenosine overhangs were then added to the PCR product and the construct was inserted into TOPO pCR2.1 vector. From TOPO pCR2.1 C₂F_{wt} was cut by a restriction digest with BamHI and EcoRI and inserted into pGEX-2T.

For the expression of C₂F_{Pga} an *in vitro* mutagenesis was performed. First two separate PCRs with 20 amplification cycles and an annealing temperature of 67 °C were performed on pGEX-2T-C₂F_{wt} again using 4% DMSO and 150 µM dNTPs, each PCR contained one primer carrying the pachanga mutation, and the original PCR primer for the subcloning of pGEX-2T-C₂F_{wt}.

PCR1:

forward primer: 5' cagcaggagggcaaacaggacacagacgtac 3' (original base: **a**)

reverse primer: 5' atatgaattctagtcaggttcattgcgagccag 3'

PCR2:

forward primer: 5' atatggatccaaccctgacaagccaggc 3'

reverse primer: 5' gtcctgtttgcctcctgctggcccttcag 3'

The PCR products were purified from an agarose gel, then they were combined, DNA Polymerase, DMSO and dNTPs were added anew, the reaction was heated to 94 °C, cooled down to 37 °C and an initial amplification step was performed for 5 min at 72 °C, then the temperature protocol was repeated once more. The original primers for the production of pGEX-2T-C₂F_{wt} were added to the reaction and the same PCR protocol was performed as for the first two PCRs. Adenosine overhangs were added to the

resulting PCR product and it was inserted into TOPO-pCR2.1. Finally C₂F_{Pga} inserted into pGEX-2T using the same procedure as for C₂F_{wt}.

AAV-HBA-EWB

AAV-HBA-EWB was provided by Dr. Sebastian Kügler, it contains, like all AAV vectors used in this study ITRs of AAV serotype 2 a human cytomegalovirus enhancer combined with a human β actin promoter (HBA), an eGFP (enhanced GFP) reporter protein, a woodchuck posttranscriptional regulatory element (WPRE) and a bovine growth hormone (BGH) polyadenylation sequence. In this vector EGFP, WPRE and BGH are together abbreviated as EWB, in other constructs the WPRE and BGH are not mentioned in the name anymore. Two different AAVs, using two types of capsid proteins were produced from this construct and called AAV1/2-eGFP (serotype 2 ITRs and serotype 1 and 2 chimeric capsid) and AAV6-eGFP (serotype 2 ITRs and serotype 6 capsid).

AAV-HBA-Syt1-IRES-EGFP

AAV-HBA-Syt1-IRES-eGFP (IRES: internal ribosomal entry site) was subcloned by Dr. Anna Bulankina. The purified adeno-associated virus for expression of Syt1 and eGFP will be referred to as AAV1/2-Syt1-eGFP.

AAV-HBA-VGlu1-pHluorin

To subclone VGlu1-pHluorin into the AAV vector two restriction sites, EcoRI upstream and HindIII downstream of VGlu1-pHluorin were added to the DNA via PCR.

forward primer: 5' atatgaattcgcacagccaccatggagttc 3'

reverse primer: 5' atataagcttgaggcacgtggtcagtagtc 3'

20 amplification cycles with an annealing temperature of 58 °C were performed in PCR buffer modified from Jeffreys et al. (1988). Approximately 15 μ g of DNA (pcDNA1-VGlu1-pHluorin kindly provided by Yongling Zhu) were amplified in 45 mM Tris-HCl pH 8.8, 11 mM (NH₄)₂SO₄, 4.5 mM MgCl₂, 6.7 mM β -mercaptoethanol, 4.4 μ M EDTA pH 8.0, 113 μ g/ml BSA and 1 mM dNTP (each). The PCR product and AAV-HBA-EWB were digested with EcoRI and HindIII restriction enzymes, corresponding bands of vector and PCR product were purified from an agarose gel and ligated. Ligation was done using T4 DNA Ligase (Fermentas) in the provided buffer. The ligated

vector was then concentrated by ethanol precipitation over night before electroporation. After sequence confirmation the DNA was amplified for virus production, the final AAV will be referred to as AAV1/2-VGlut1-pHluorin.

pcDNA3-HBA-mOtof^{wt}-IRES-EGFP / pcDNA3-HBA-mOtof^{Pga}-IRES-EGFP

Dr. Ellen Reisinger subcloned mOtof-eGFP in pECFP-N1 using *Otof* amplified from mouse cDNA. The vector was then used by Nina Dankenbrink-Werder to generate pcDNA3-mOtof^{wt}-IRES-eGFP.

In a first cloning step the *pachanga* variant was generated via a mutagenesis PCR with 20 amplification cycles, an annealing temperature of 52 °C – 65 °C and 10 min elongation period per cycle with pcDNA3-mOtof^{wt}-IRES-eGFP as template.

forward primer: 5' gccagcaggagggcaaacaggacacagac 3'

reverse primer: 5' gtctgtgtcctgtttgccctcctgctggc 3'

After the PCR the solution was digested with DpnI to remove all bacterially produced pcDNA3-mOtof^{wt}-IRES-eGFP vectors and transfected in XL1-blue cells to amplify the PCR product: pcDNA3-mOtof^{Pga}-IRES-eGFP.

In order to insert the promoter sequence upstream of otoferlin, a BamHI restriction site was generated and an XbaI restriction site was removed from the vector containing the promoter sequence (CMV enhancer coupled to human β -Actin Promoter) via two subsequent mutagenesis PCRs. The first PCR product was inserted into TOPO-pCR2.1 and the presence of the inserted BamHI restriction site was confirmed by DNA sequencing.

forward primer: 5' acatggatcctctagatcccatatatggagtcc 3'

reverse primer: 5' gctgaactgtggccggttac 3'

template DNA: AAV-HBA-EWB-eGFP

The PCR product of the second mutagenesis PCR was directly digested with BamHI and EcoRI and inserted upstream of otoferlin in pcDNA3-mOtof^{wt}-IRES-eGFP and pcDNA3-mOtof^{Pga}-IRES-eGFP between these two restriction sites.

forward primer 2: 5' ttacatggatccgctagatcc 3'

reverse primer 2: 5' ctgaactgtggccggttac 3'

When the absence of the XbaI restriction site was confirmed by DNA sequencing also the absence of the otoferlin stop codon, a remainder of the Otoferlin-eGFP fusion protein, was revealed. Therefore a new stop codon had to be inserted. Both vectors were digested with HindIII and dephosphorylated, then annealed oligos containing the stop codon were inserted.

leading oligo: 5' agcttagatgctagtcggc 3'

lacking oligo: 5' agctgccgactagcatctaa 3'

Ad-HBA-mOtof^{wt}-IRES-eGFP / Ad-HBA-mOtof^{Pga}-IRES-eGFP

Murine otoferlin was subcloned into Adenovirus vector. First the vector Ad-MCS-BGH-polyA was formed from syn-BGH-polyA (kindly provided by Samuel Young). An XbaI restriction site was removed from the backbone, by digesting the vector with XbaI, filling up the sticky ends and religation. Synapsin promoter was removed and HindIII, XbaI, BamHI and XhoI restriction sites were inserted into the multiple cloning site (MCS) in two steps by inserting annealed oligos containing the desired restriction sites.

leading oligo 1: 5' ccggctaggatccatcgcatctcgagtacttg 3'

lacking oligo 1: 5' agatcctaggtagcgtagagctcatgaacccgg 3'

leading oligo 2: 5' ccgggtgacctaagcttctgtgtctagaatgctg 3'

lacking oligo 2: 5' gatccagcattctagacacagaagcttaggtcaca 3'

Finally CMVe-βActinP-mOtof^{wt}-IRES-eGFP and CMVe-βActinP-mOtof^{Pga}-IRES-eGFP were inserted into Ad-MCS-BGH-polyA between XbaI and BamHI restriction sites. The finished vectors, Ad-CMVe-βActinP-mOtof^{wt}-IRES-eGFP and Ad-CMVe-βActinP-mOtof^{Pga}-IRES-eGFP were then used for virus production. For simplification the purified adenoviruses for expression of the two constructs will be called Ad5-mOtof^{wt}-eGFP and Ad5-mOtof^{Pga}-eGFP.

Ad-HBA-eGFP

To generate an adenovirus for eGFP expression without otoferlin for control experiments Ad-CMVe-βActinP-mOtof^{wt}-IRES-eGFP was digested with NheI and EcoRI in a sequential digest thus removing mOtof^{wt}-IRES from the vector. The sticky ends at

the restriction sites were then filled up using T4 DNA polymerase and the vector was religated. For simplification the purified adenovirus for expression of eGFP will be called Ad5-eGFP.

Protein expression / purification

For the expression of GST-C₂F_{wt} and GST-C₂F_{Pga} BL21-DE3 cells were transfected with pGEX-2T-C₂F_{wt} or pGEX-2T-C₂F_{Pga} and spread on LB-agar plates. 50-100 ml LB medium were inoculated with single colonies and incubated over night at 37°C. The next day 12-18 flasks with 450 ml TB (terrific broth) medium, 50 ml salt solution (0.17 M KH₂PO₄ 0.72 M K₂HPO₄), 13 ml EtOH (optional) and 10 mg/ml Ampicillin were inoculated with 8-10 ml over night culture. The cultures were incubated at 30°C at 175 – 200 rpm until an OD at 600 nm of 0.6 was reached, then 500 µM IPTG was added to each flask to induce expression and incubation was continued at 16°C over night.

The cells were pelleted for 15-20 min at 4 °C and 5000 g and frozen at -20 °C in case purification was not done immediately. 15-25 ml buffer (20 mM Tris-HCl pH 7.4, 500 mM NaCl, 2.5 mM glutathione, 10 µM ATP (optional), 5% EtOH (optional)) were used for cell resuspension per 500 ml expression volume. Then 1 mM MgCl₂, ~1 g DNase, ~1 g Lysosyme and ~1 g PMSF were added to the cell suspension which was then incubated on ice for 10 min. This incubation was repeated after addition of 50 µl 20% Triton-X-100 per 1 ml of suspension volume.

In order to break the cell envelope the suspension was sonicated 3-5 times for 40 sec at 50% intensity and the cell debris were pelleted for 60 min at 4 °C and 23000 g.

GST-C₂F_{wt} and GST-C₂F_{Pga} were then bound to glutathione coupled sepharose (170 µl 50% slurry per 500 ml expression volume) and unbound protein was removed by extensive washing with wash buffer (20 mM Tris-HCl pH 7.4, 500 mM NaCl, 2.5 mM glutathione, 10 µM ATP (optional), 5% EtOH (optional)). Then, in a final washing step the buffer was changed to resuspension buffer (20 mM Tris-HCl pH 7.4, 500 mM NaCl), and the sepharose was resuspended in 0.3 – 0.5 ml resuspension buffer per 500 ml expression volume depending on the cell pellet size.

The GST tag was then cleaved over night from the C₂F domain by adding ~ 20 mU/ml thrombin and incubating over night at 4 °C under constant mixing. The next day

the eluate from the sepharose column was collected and purity was estimated via sodiumdodecylsulfate polyacrylamide gel electrophoresis (SDS PAGE). Then the protein solution was dialyzed in 500 ml dialysis buffer pre-treated with Chelex100® (for floatation assays: 20 mM HEPES pH 7.4, 150 mM NaCl; for CD-spectroscopy and fluorimetry: 5 mM Tris-HCl pH 7.4) and in another 500 ml buffer over night using spectra Por® dialysis membranes with a molecular weight cut off (MWCO) of 6-8 kDa. In some experiments the protein solutions were frozen in liquid nitrogen and stored at -80 °C until they were used.

In order to determine the concentration, a control (buffer) and the protein solution were dissolved 1:10 in 6 M GnHCl and absorbance was measured at 280 and 320 nm. The control solution was used as baseline and the concentration of the protein solution was determined using equation 1:

$$(eq. 1) \quad c[\mu M] = \frac{Abs_{280} - Abs_{320}}{extinction\ coefficient} \bullet dilution\ factor \bullet 10^6$$

The extinction coefficient describes the strength of light absorption at 280 nm and was determined by protein sequence analysis using the online tool ProtParam at <http://www.expasy.org/>. In proteins the number of the amino acids tryptophane, tyrosine and cysteine define the extinction coefficient, all three chromophores contribute to the spectral properties of the protein and it is assumed that no other chromophore exists in the protein.

SDS PAGE

For SDS PAGE 12% polyacrylamide gels were poured with a resolving gel (0.375 M Tris-HCl pH 8.8, 12% acrylamide, 0.1% SDS, 0.05% APS, 0.05% N,N,N',N'-Tetramethylethylenediamine (TEMED)) and a stacking gel (0.125 M Tris-HCl pH 6.8, 12% acrylamide, 0.1% SDS, 0.05% APS, 0.1% TEMED). Anode and cathode were both immersed in 25 mM Tris-HCl 192 mM glycine and 1 g/L SDS. Sample buffer was added to the protein solution making a final concentration of 50 mM Tris HCl pH 6.8, 4% SDS, 12% Glycerol, 0.01% Serva Blue G and 2% β-Mercaptoethanol. The sample was then loaded on the gel, and electrophoresis was done at 80 V and 400 mA. After

size separation the gels were boiled in Coomassie blue staining solution (2.5 g Coomassie Brilliant Blue R250, 450 ml EtOH, 100 ml acetic acid, 400 ml H₂O) and then transferred into destaining solution (500 ml EtOH, 100 ml Acetic acid, ad 1 L H₂O), boiled and transferred into H₂O after sufficient destain.

Isothermal titration calorimetry (ITC)

ITC was performed using degassed buffer and protein solutions; protein concentrations of 10 - 50 μM were used. The reference cell was filled with ddH₂O and measurements were made at 25 °C. 0.5 - 6 mM (depending on protein concentration) Ca²⁺, diluted in the same buffer as C₂F, was titrated to the protein solution in 50 – 100 steps of 1 – 6 μl with a stirring speed of 250rpm.

CD spectroscopy

For circular dichroism (CD) spectroscopy the protein solution was diluted to a concentration of 1.5 – 2.5 μM in order to optimize signal to noise ratio. The spectra were measured from 190 – 260 nm at 25 °C in the presence of 100 μM CaCl₂ or EDTA. To control for sufficient light transmission high tension voltage was measured and above 700 V all CD values were discarded. Each measurement was corrected for buffer contribution by subtracting an initial measurement of buffer solution only. Finally the curves were normalized by calculating the mean residual ellipticity ([Θ]_{MRE}) using equation 2. Then the average and the standard error of mean were calculated.

$$(eq. 2) \quad [\Theta]_{MRE} = \frac{100 \cdot \Theta}{d \cdot c \cdot n}$$

Θ: measured ellipticity in deg,

d: path length in cm

c: concentration in M (mol/l),

n: number of amino acids

Fluorimetry

Autofluorescence was measured with a protein concentration of 2.36 μM with 295 nm excitation wave length. Fluorescence emission was recorded from 305 – 450 nm in 1 nm steps with an integration time of 0.2 sec, averaging 5 runs. Ca^{2+} or EDTA was added to a final concentration of 100 μM , respectively.

Floatation assay

Production of liposomes

Lipid stock solutions were prepared from commercially available lipid solutions (25 mg/ml lipid dissolved in Chloroform : Methanol 2:1 v/v) were mixed in an argon filled flask, the solvents were evaporated and the lipid film was dissolved over night in 1 ml sodium cholate solution (20 mM HEPES pH 7.4, 150 mM NaCl, 1 mM DTT, 5% w/v Na-Cholate) and stored at -80°C until use.

The lipid mixtures (13.5 μM lipids, 20 mM HEPES, 150 mM KCl, 5% Na-Cholate) for liposome production were then prepared from the stock solutions. The following mixtures were prepared:

Lipid	Mixture 1 (+PS)	Mixture 2 (-PS)	Mixture 3 (+PIP ₂)	Colored mixture
PC	40%	60%	40%	57%
PS	20%	-	20%	-
PE	20%	20%	20%	20%
PI	10%	10%	8%	10%
Cholesterol	10%	10%	10%	10%
PI-4,5-bis-P	-	-	2%	-
Texas red	-	-	-	3%

Table M2: Lipid composition of solutions for the production of liposomes

For the production of liposomes 40 μl of mixtures 1 to 3 were each combined with 10 μl of the colored mixture. Then 30 μl of buffer (dialysis buffer of protein solution: 20 mM HEPES pH 7.4, 150 mM NaCl) was added. Finally 20 μl of Synaptobrevin (13 kDa) solution were added as loading control in SDS PAGE. The solution was incubated for 30 min at room temperature (RT) and then centrifuged for 10 min at 4°C at 17000 g.

Finally liposomes were produced from the lipid mixtures using a desalting column (fast Desalting PC3.2/10, Amersham Pharmacia BioSci.) on a SMART system (Amersham Pharmacia BioSci.). The sample was loaded on the column and the detergent was washed from the column with dialysis buffer. This way the lipids formed liposomes and were eluted and collected in a single fraction of about 100 μ l - 150 μ l.

Floatation assay

20 μ l of liposomes, 1 μ l 10 mM Ca^{2+} or EGTA solution, 29 μ l protein solution containing 15-30 μ g of protein and 50 μ l 80% Nycodence (in dialysis buffer with 1 mM Ca^{2+} or EGTA) were mixed in a centrifugation vial. Then a second phase of dialysis buffer was carefully added on top of the first containing 30% Nycodence and 1 mM Ca^{2+} or EGTA. Finally a third phase was added only consisting of dialysis buffer with 1 mM Ca^{2+} or EGTA. This gradient was then centrifuged for 90 min at 197,400 g at 4 °C.

After centrifugation two phases formed and 50 μ l of each phase (upper and lower) were transferred into fresh tubes and analyzed via SDS PAGE.

Animals

Animal handling and experiments complied with national animal care guidelines, and were approved by the University of Goettingen Board for animal welfare and the animal welfare office of the state of Lower Saxony.

Wild type mice

Animals up to one year of age were used for various experiments. Immunohistochemistry and primary tissue culture on organs of Corti, real time PCR as well as ABR and DPOAE were performed on C57BL/6J, CD1 and CD1/C57BL6 (offspring of CD1 mice mated with C57BL/6J mice) mice. Embryonic transuterine otocyst injections were performed on CD1 dams mated with C57BL/6J males or, for experiments with *Otof*^{+/+} or *Otof*^{-/-} mice, C57BL/6J dams mated with C57BL/6J males.

Genetically modified mice

Otof^{Pga/Pga} mice (provided by Ulrich Mueller, Schwander et al. 2007), were used for real time PCR and immunohistochemistry. *Otof*^{+/+} and *Otof*^{-/-} mice, generated by Dr. Ellen Reisinger, were used for embryonic transuterine otocyst injections.

ABR and DPOAEs were measured from otocyst injected animals of all genetic

variants and immunohistochemistry was performed on organs of Corti of these mice.

Virus production

All AAV vectors used in this study contain inverted terminal repeats of AAV serotype 2. The capsid proteins used were either of serotype 1 and 2 (AAV1/2) or of serotype 6 (AAV6), all AAVs contain a human cytomegalovirus enhancer combined with a human β -actin promoter, a woodchuck posttranscriptional regulatory element (WPRE) and a bovine growth hormone (BGH) polyadenylation sequence. Virus production was performed by Dr. Sebastian Kügler of the Viral Vectors Lab, Department of Neurology, University Medicine Goettingen as described previously (Kügler et al., 2007).

Adenovirus serotype 5 was prepared by Samuel Young of the Department of Neuroscience of the Max Planck Florida Institute.

Virus	Titer
AAV1/2-eGFP	3.0×10^8 tu/ μ l
AAV6-eGFP	6.6×10^8 tu/ μ l
Ad-eGFP	1.1×10^7 tu/ μ l
Ad5-mOtof ^{wt} -eGFP	1.4×10^7 tu/ μ l
Ad5-mOtof ^{Pga} -eGFP	1.2×10^7 tu/ μ l
AAV1/2-Syt1-eGFP	4.0×10^8 tu/ μ l
AAV1/2-VGlut1-pHluorin	1.1×10^8 tu/ μ l

Table M1: Virus titers

All virus solutions contain $10^7 - 10^9$ transfecting units (tu)/ μ l

Immunohistochemistry

Dissection of the organ of Corti

Mice of an age from 5 to 50 days were used for immunohistochemistry. Before decapitation the mice were euthanized with CO₂, then the skull was halved along the sagittal midline and the brain was removed. The cochlea connected to the vestibule was dissected in HEPES buffered Hanks' balanced salt solution (141.7 mM NaCl, 5.36 mM KCl, 1.0 mM MgCl₂, 0.5 mM MgSO₄, 0.1 mM CaCl₂, 3.42 mM L-Glutamine, 11.1 mM Glucose, 10 mM HEPES pH 7.2). At the apex of the cochlea a small piece of bone was

removed, the stapes was detached from the oval window and the scala tympani and scala vestibuli were perfused with 0.3 ml to 0.5 ml 4% FA in PBS through the round and oval window respectively. Then the top of the cochlea was opened and the sample was fixed for one hour in 4% FA. The staining procedure for primary tissue cultures was the same as for non-cultured samples; however, non-cultured samples had to be further dissected to isolate the organ of Corti after immunohistochemistry.

Immunohistochemistry

After fixation the samples were washed three times for 10 min in phosphate buffered saline (PBS) and blocked in goat serum diluted buffer (GSDB) for one hour both at room temperature (RT). Then the samples were incubated in the antibody solution (antibodies were diluted 1:200 to 1:500 in GSDB).

In case primary and secondary antibodies were used, the samples were incubated in primary antibody solution over night at 4 °C, the next day the samples were washed 3 times for 10min in wash buffer (450 M NaCl, 20 mM phosphate buffer, 0.3% Triton X-100) at RT, then they were incubated light protected for 2-3 h at RT in secondary antibody solution. If fluorophore conjugated primary antibodies were used the samples were either only incubated light protected in the antibody solution for 2 h at RT or the conjugated antibody was added to the secondary antibody solution.

Target	Dilution	Source	Name	Provider
Otoferlin	1:500	mouse	Monoclonal Otoferlin antibody [13A9]	Abcam
Otoferlin	1:500	rabbit	Polyclonal rabbit antibody against Otoferlin	Synaptic Systems
vGlut 3	1:400	rabbit	Polyclonal rabbit antibody against vGlut 3	Synaptic Systems
Calbindin	1:1000	mouse	monoclonal anti-calbindin D-28 K	Swant
NF 200	1:400	mouse	Monoclonal Anti-Neurofilament 160/200 antibody produced in mouse	Sigma Aldrich
vGlut 1	1:400	guinea pig	Polyclonal guinea pig antibody against vGlut 1	Synaptic Systems
GFP	1:400	mouse	GFP antibody [6AT316]	Abcam
GFP	1:400	rabbit	anti-GFP, IgG, Alexa Fluor® 488 conjugate	Invitrogen

Table M3: Primary antibodies used for immunohistochemistry

- Materials and Methods -

Target	Dilution	Source	Fluoro-phore	Name	Provider
mouse	1:200	goat	Alexa 488	Alexa Fluor® 488 goat anti-mouse IgG	Invitrogen
rabbit	1:200	goat	Alexa 488	Alexa Fluor® 488 goat anti-rabbit IgG	Invitrogen
rabbit	1:200	goat	Alexa 546	Alexa Fluor® 546 goat anti-rabbit IgG	Invitrogen
guinea pig	1:200	goat	Alexa 488	Alexa Fluor® 488 goat anti-guinea pig IgG	Invitrogen
Phalloidine	1:200	-	Alexa 568	Alexa Fluor® 568 phalloidin	Invitrogen

Table M4: Secondary antibodies used for immunohistochemistry

After incubation in the antibody solutions the samples were washed for 3 times 10 min at RT in wash buffer. Finally the Organs of Corti were dissected from the cochleae in 5 mM phosphate buffer (PB) by removing the residual bony shell around the cochlea as much as possible, disattaching the stria vascularis and finally removing the organ of Corti from the modiolus. Organotypic cultures were simply incubated in 5 mM PB for 5 min. The organs of Corti were mounted on glass slides in DAKO Fluorescent Mounting Medium and imaged on a Leica SP2 confocal microscope (Leica Mikrosysteme, Wetzlar, Germany). Two lasers, a 488 nm argon laser and a 561 nm helium neon laser, were used and images were acquired with either a 10x or a 63x 1.4 N.A. objective. Image analysis was done with ImageJ and Adobe Illustrator (Adobe Systems Inc., San Jose, USA).

Real time PCR

Real time PCR was performed on cDNA from *Otof*^{Pga/Pga} and *Otof*^{+/+} organs of Corti. For each PCR 3-4 apical turns were dissected from P14 - P15 animals and the total RNA was purified using the TRIzol® Reagent (Invitrogen). Reverse transcription (10 min room temperature, 30 min 37 °C, 60 min 42 °C and 5 min 70 °C) with 9 U/μl Superscript II reverse transcriptase (Invitrogen), 1.1 pM/μl oligo dT (Invitrogen), random hexamers (Roche), 0.45 nM/μl dNTPs (Invitrogen), 9 nM/μl DTT (Invitrogen) and 1.8 U/μl RNaseOUT (Invitrogen) was used for cDNA synthesis. This cDNA was then used as template in real time PCR. Gene expression of otoferlin and the housekeeping genes TATA box binding protein (TBP) and parvalbumin was tested using TaqMan

Gene Expression Assays (Applied Biosystems, Darmstadt, Germany; for otoferlin: Mm00453306_m1; for TBP: Mm00446973_m1. For parvalbumin: assay kindly provided by P. Jonas, Freiburg).

All experiments were performed in triplicates and the average C_t value was determined by averaging and back-transforming calculated linear C_t values according to equation 3 and 4.

$$(eq. 3) \quad lin = 2^{-C_t}$$

$$(eq. 4) \quad C_{t,average} = \frac{-\ln(lin_{average})}{\ln(2)}$$

Finally the mRNA level of otoferlin in $Otof^{Pga/Pga}$ in comparison to $Otof^{+/+}$ was analyzed by the $\Delta\Delta C_t$ method, shown in equation 5, 6 and 7.

$$(eq. 5) \quad \Delta C_t = C_{t, average, otoferlin assay} - C_{t, average, TBP assay}$$

$$(eq. 6) \quad \Delta\Delta C_t = \Delta C_{t, Otof^{Pga/Pga}} - \Delta C_{t, Otof^{+/+}}$$

$$(eq. 7) \quad \frac{[mRNA \text{ of otoferlin}]_{Otof^{Pga/Pga}}}{[mRNA \text{ of otoferlin}]_{Otof^{+/+}}} = 2^{-\Delta\Delta C_t}$$

Organotypic cultures of the dissected organ of Corti

Organs of Corti of P9 mice were dissected in a sterile environment in HEPES buffered Hanks' balanced salt solution (1 mM HEPES pH 7.2, 10 U/l Penicillin G and 25 ng/l Fungizone in HBSS (Hank's balanced salt solution, Invitrogen)) and transferred onto Cell Tak (BD Biosciences) coated cover slips immersed in 300 μ l medium (DMEM + F12 1:1 (Invitrogen) + 5% FBS). The cultures were then incubated at 37 °C and 5% CO₂ over night until they were washed shortly in PBS and virus solution containing about 10⁷ infectious particles in 300 μ l medium without FBS was added. After 24 h the virus solution was exchanged by 300 μ l medium containing 5% FBS and the cultures were incubated for another 3-5 days until they were fixed in 4% FA for one hour and analyzed using immunohistochemistry.

Embryonic transuterine otocyst injections

At postcoital day 11.5 pregnant dams were anesthetized with an intraperitoneal (i.p.) injection of 125 mg/kg body weight Ketamin (Ketamin Inresa, Inresa Arzneimittel GmbH) and 2.5 mg/kg body weight Xylazin (Rompun®, Bayer), the anesthesia was maintained by applying 1 L/min oxygen enriched with 0.4 – 1.2 Vol% Isofluran via a facial mask. Additionally, 50 mg/kg body weight carprofen were injected sub cutaneously (s.c.). The anesthetized animal was shaved and the skin was sterilized at the abdomen and placed on a heated mat to prevent hypothermia. Once a stable level of anesthesia was reached, judged by the lack of paw withdrawal reflex, the laparotomy was performed. The uterus was externalized and kept moist by applying warm isotonic solution. A cold light source was used to visualize the embryos inside the uterus, each embryo was gently positioned such that the left side points up, exposing the anterior cardinal vein and fourth ventricle. These two structures were used as landmarks for the otocyst injection. The virus solution, colored with 5 mg/ml Fast Green (AppliChem), was then injected through a quartz glass injection pipette using a Pico Injector (Harvard Apparatus); The pipettes had been pulled on a P-2000 pipette puller (Sutter instruments) (settings: Heat 900, Fil 5, Vel 50, Del 126, Pul 175). The tips were snapped off at a diameter of ~20 µm with a rough angle of 45 ° to create a thin sharp tip.

After the embryos were injected the uterus was re-internalized and an abdominal suture and skin suture were performed using silk (size 06). The mice recovered and delivered 19-21 days postcoitum.

Auditory brainstem responses

Otocyst injected animals were tested for their hearing ability via auditory brainstem response (ABR) measurement using a TDT (Tucker-Davis Technologies) System III run by Matlab (MathWorks) software routines written by Gerhard Hoch and Nicola Strenzke. Some of the measurements were conducted by Nadine Herrmann and Stefan Thom with BioSig software (TDT).

The mice start hearing 12 days after birth (Sonntag et al., 2011), so measurements were performed earliest at P14. Furthermore, to avoid age-related hearing loss to alter the results measurements were always conducted before the

animals reached 40 days of age.

The animals were anesthetized with 125 mg/kg body weight Ketamine and 2.5 mg/kg body weight Xylazin i.p. (or s.c. in small animals below 10 g). For the experiments that involved destruction of the cochlea (abolition of hearing by cochlear destruction) the animals were anesthetized with 1.3 mg/kg body weight Urethane and 5.0 mg/kg body weight Xylazin. The heart rate was monitored to control for the depth of anesthesia which was maintained if necessary by s.c. injection of 0.35 – 0.75 mg Ketamine every 30 to 90 min. The animal was kept on a heated pad controlling for temperature with a rectum probe. When the animals were very small (<10 g) the probe was kept underneath the animals and was not inserted into the anal orifice).

Upon the absence of the toe reflex three needles were inserted under the skin of the anesthetized animal. One needle was positioned ventral to the outer ear (vertex), one on the midline (mastoid) of the head and a dorsal reference needle.

In order to determine the hearing threshold of AAV injected animals different noises, clicks (0.03 ms, provided as decibel (dB) sound pressure level (SPL) peak equivalent) and pure tones (4/8/12/16/24/32 kHz, 10 ms plateau, 1 ms \cos^2 rise and fall, provided as dB SPL root mean square), were played to the anesthetized animal at a 20 Hz rate at increasing SPL ranging from 20 – 80 dB in 10 dB steps. In deaf animals 100 dB were applied. The Speaker was calibrated with a 1/4 inch Brüel and Kjær microphone (model 4939).

To deal with the high number of adenovirus injected animals we developed two chirp stimuli (4 - 12 kHz and 12 - 36 kHz) for the comparison of low and high frequency hearing without the need to measure many pure tone responses in separation. In these animals the ABR threshold was determined in 5 dB steps (in case they were hearing) or a 110 dB stimulus was played to the mouse to demonstrate the absence of the ABR waves in deaf mice.

In most experiments the right cochlea was plugged with cotton tissue and electrode gel while the left ear was measured. Only in Ad5-mOtof^{MT}-eGFP injected wild type animals the right ear was destroyed as a plug only elevates the threshold coming from the right side about 20 – 30 dB.

At and above the hearing threshold of the mice the joint signal of the succeeding nuclei in the auditory pathway display characteristic electric waves which were recorded as the 50,000 times amplified difference potential between vertex and mastoid needles (filtered at 4 kHz low pass and 100 kHz high pass). The lowest SPL generating a reproducible wave, classified by visual judgement of two researchers

independently, was defined as the hearing threshold.

At suprathreshold sound pressure levels four to five peaks are recorded. They have been suggested to reflect the processing of the signal in the cochlea, cochlear nucleus complex, superior olivary complex, and probably lateral lemniscus and colliculus inferior respectively (Melcher et al., 1996).

Distortion product oto-acoustic emissions (DPOAE)

The function of OHCs was assessed by recording distortion product oto acoustic emissions on a TDT system II using a Technics SL-P320 CD player, a TDT EC1 Speaker, a Sennsheiser MKE 2 microphone with a M Audio DMP3™ dual microphone pre amplifier, a TerraTec DMX 6fire USB soundcard and BioSig (TDT) and Sony Sound Forge software. The animals were usually kept anesthetized during ABR and DPOAE measurements, however, if both tests could not be conducted after one another the animals were anesthetized again earliest on day after the first anesthesia to perform the second measurement. The animal was placed on a heated pad and a small custom made probe being connected to a microphone and two speakers was positioned directly in the external ear canal.

Oto-acoustic emissions were measured playing 5 frequency combinations (Tab. 3) always playing the lower primary frequency (f1) 10 dB lower than the higher primary frequency (f2).

f1 (kHz)	f2 (kHz)	DPOAE (kHz)
5	6	4
6.666	8	5.333
10	12	8
13.333	16	10.666
16.666	20	13.333

Table M4: Frequency combinations used for DPOAE measurements.

The ratio between both primary frequencies ($f2/f1$) was 1.2. Each frequency combination was played at f2 having a sound pressure level (SPL) of 60 dB, only f2 = 12 kHz was tested from 10 to 80 dB using 10 dB steps. Calibration used a mouse ear coupler to predict the SPL at the ear drum.

pHluorin imaging and unquenching

The pH sensitive GFP (pHluorin) was tested for functionality by neutralization of pH in acute preparations. Inside the synaptic vesicles pHluorin fluorescence is mostly quenched and upon neutralization the fluorophore can be excited. To test the maximal increase in fluorescence upon unquenching we dissected acute preparations of the organ of Corti of P5 – P8 mice and perfused in extra cellular solution (140 mM NaCl, 11.1 mM Glucose, 6 mM KCl, 2 mM sodium pyruvate, 2 mM CaCl₂, 0.5 mM MgCl₂, 10mM HEPES pH 7.2, 300 mOsm/kg). In this condition the cells were illuminated with a a Cobolt Co. Cobolt Calypso 491nm laser and the baseline fluorescence was recorded using a RedshirtImaging Neuro CCD camera on a Yokogawa CSU22 spinning disc confocal system. Then the preparation was perfused in extra cellular solution containing high ammonium chloride concentration (50 mM NH₄Cl ,90 mM NaCl, 11.1 mM Glucose, 6 mM KCl, 2 mM sodium pyruvate, 2 mM CaCl₂, 0.5 mM MgCl₂, 10 mM HEPES pH 7.2, 300 mOsm/kg). After 10 min perfusion the increased fluorescence was recorded, and perfusion was returned to normal extra cellular solution.

Results

Biochemistry and structure of otoferlin C₂F_{wt} and the *pachanga* variant

To further assess the role of otoferlin at the hair cell ribbon synapse one of the C₂ domains, C₂F, the most C-terminal of the C₂ domains, and therefore the closest to the trans-membrane domain was analyzed in detail. The wild type domain was compared to the mutant domain containing the *pachanga* mutation. Pangrsic et al. showed that *Otof*^{Pga/Pga} mice were deaf, most likely due to impaired vesicle replenishment not maintaining a standing readily releasable pool *in vivo*. In order to biochemically analyze the C₂F variants, they were expressed and purified using the pGEX expression vector and BL21-DE3 cells.

The purified protein domains were analyzed by biochemical and biophysical methods assessing secondary structure and the binding capacity to phospholipids and Ca²⁺. Moreover, the otoferlin mRNA level and protein expression in the organ of Corti of *Otof*^{+/+} mice were compared to those of *Otof*^{Pga/Pga} mice.

Ca²⁺ binding of C₂F_{wt} is unlikely

Most important for the function as Ca²⁺ sensor at the IHC ribbon synapse is the capacity to bind Ca²⁺. Therefore C₂F Ca²⁺ binding was tested with three methods. First isothermal titration calorimetry (ITC) was conducted. Ca²⁺ was titrated to the solution containing C₂F and the temperature of the sample cell containing the protein solution and a reference cell was compared. The method then determines the amount of energy consumed or released by a possible binding reaction. If no energy change is detected no binding occurred.

The ITC experiments did not provide conclusive results. One half of the experiments indicated Ca²⁺ binding, whereas the other half showed the opposite result (Figure 1A, B). Possible reasons for the diverse results include that in some experiments the protein was not pure enough, and the impurity might have bound Ca²⁺,

- Results -

thus giving a false Ca^{2+} binding, whereas in other purifications the impurities were non binding. However, on the SDS PAGE gels from the various purifications for ITC experiments no differences of contaminating proteins were evident (Figure 1C,D). On the opposite it could be that in some experiments the protein was incorrectly folded, obscuring Ca^{2+} binding.

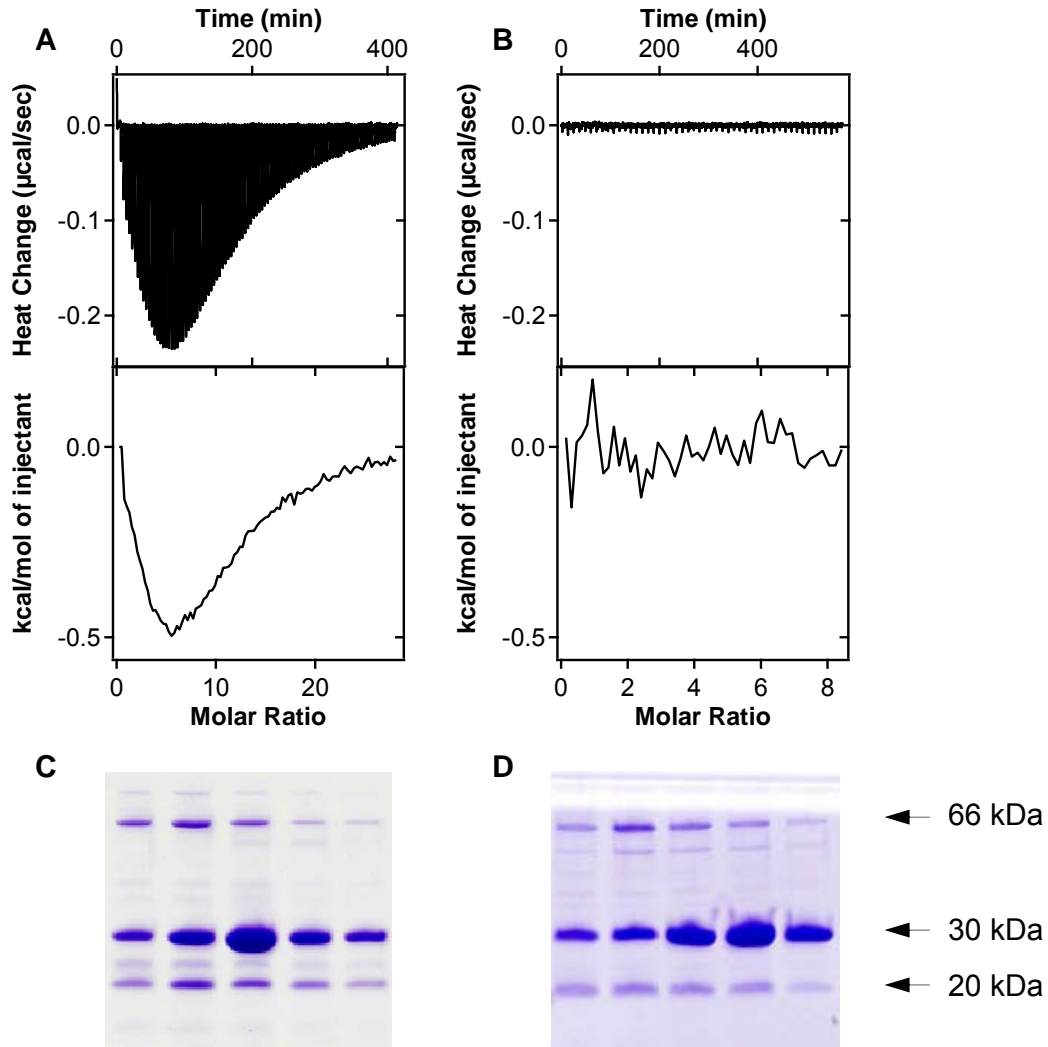


Figure 1: ITC to determine Ca^{2+} binding of $\text{C}_2\text{F}_{\text{wt}}$

Ca^{2+} binding of otoferlin $\text{C}_2\text{F}_{\text{wt}}$ was initially tested using ITC.

A-B. ITC measurements of two separately expressed and purified $\text{C}_2\text{F}_{\text{wt}}$ samples.

C-D. Corresponding SDS PAGE gels of the purified protein samples. Our $\text{C}_2\text{F}_{\text{wt}}$ construct has a size of 27.87 kDa.

To further explore the issue CD spectroscopy and fluorimetry in the presence of either Ca^{2+} or EDTA were performed. Care was taken to remove any residual Ca^{2+}

using Chelex100® pre-treatment of the buffers. In CD spectroscopy the secondary structure of proteins can be estimated, α -helices and β -sheets lead to different absorption of left and right circularly polarized light resulting in a characteristic spectrum of ellipticity specific for a particular secondary structure. A conformational change caused by Ca^{2+} binding could be detected by a change in characteristic ellipticity spectrum for Syt1 (Helfmann et al. 2011), for $\text{C}_2\text{F}_{\text{wt}}$ no such change was detected (Figure 2A).

In fluorimetry the absorption of UV light by the amino acids tryptophan, tyrosine and cysteine is dependent on protein conformation. In case of conformational changes the absorption spectrum also changes, thus putatively revealing an effect of additives or mutations on secondary structure. No changes in the fluorimetric spectrum of $\text{C}_2\text{F}_{\text{wt}}$ were detected comparing the presence of EDTA or Ca^{2+} (Figure 2B). Therefore neither CD spectroscopy nor fluorimetry indicated any effects of Ca^{2+} on secondary structure arguing against a Ca^{2+} binding ability of otoferlin C_2F domain.

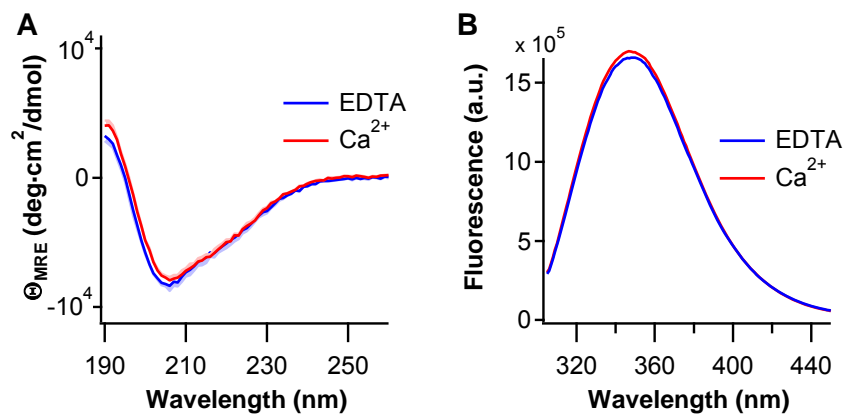


Figure 2: Ca^{2+} binding analysis of $\text{C}_2\text{F}_{\text{wt}}$

Continuative analysis of $\text{C}_2\text{F}_{\text{wt}}$ Ca^{2+} binding properties via CD spectroscopy and Fluorimetry.

A. Average CD spectroscopy traces displaying mean residual ellipticity ($n = 3$), shaded areas indicate standard error of mean (SEM) (in one direction only). Protein concentration varied from 1.5 – 2.5 μM , CaCl_2 and EDTA were used at 100 μM .

B. Fluorimetric analysis of $\text{C}_2\text{F}_{\text{wt}}$ using the same CaCl_2 and EDTA concentrations as in A. and a protein concentration of 2.36 μM . An excitation wave length of 295 nm was used and fluorescence emission was recorded from 305 – 450 nm.

Similar secondary structure of C₂F_{wt} and C₂F_{Pga}

CD spectroscopy was also used to compare the secondary structure of C₂F_{wt} and C₂F_{Pga}. The data was normalized by calculating the mean residual ellipticity and averaged (Figure 3A). Spectra, of both wild type and mutant C₂F domains, widely overlap. No major differences were detected; therefore a major change in secondary structure caused by the *pachanga* mutation is unlikely.

To support the data from CD spectroscopy, fluorimetry was conducted on the two purified domains (Figure 3B). Also using this method no major difference between the spectra of C₂F_{wt} and C₂F_{Pga} was detected, supporting the notion of only minor effects of the mutation on the secondary structure of C₂F.

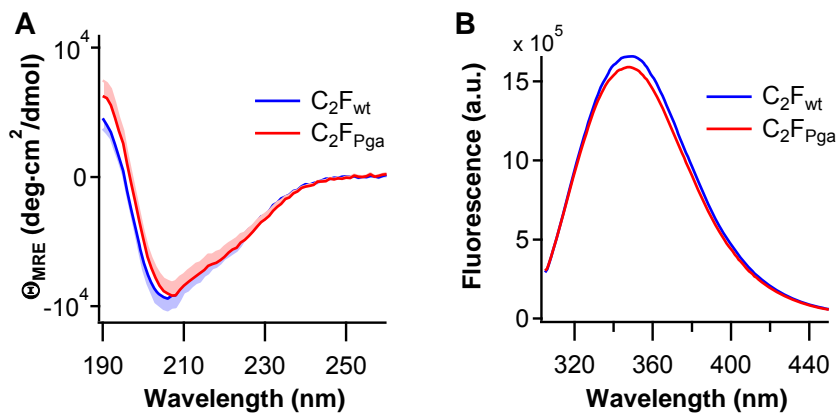


Figure 3: Secondary structure of C₂F_{wt} and C₂F_{Pga}

Biochemical structure analysis via CD spectroscopy and fluorimetry comparing C₂F_{wt} and C₂F_{Pga}.

A. Average CD spectroscopy traces of both domains displayed as mean residual ellipticity (C₂F_{wt}, C₂F_{Pga}, n = 3), shaded areas indicate SEM (displayed only in one direction for clarity). Protein concentration varied from 1.5 – 2.5 μM; EDTA was added in a concentration of 100 μM.

B. Fluorimetric analysis of C₂F_{wt} and C₂F_{Pga}. Protein concentration was adjusted to 2.36 μM. An excitation wave length of 295 nm was used and fluorescence emission was recorded from 305 – 450 nm.

Otoferlin C₂F does not seem to bind phospholipids in a Ca²⁺ dependent manner

One typical function of C₂ domains is the Ca²⁺ dependent binding to phospholipids (PL). Therefore, we tested whether otoferlin C₂F has this typical property and, if so, whether the *pachanga* mutation has an effect on it. The affinity to three phospholipid mixtures was tested in the presence of EGTA or Ca²⁺ (Figure 4). The upper phase contains liposomes and bound protein, the lower phase contains non-binding protein.

As a control synaptotagmin I C₂A (Syt1 C₂A) was used. Assays conducted in presence of EGTA or without phosphatidylserin (PS) in the liposome composition were expected not to lead to PL binding. Positive PL binding was expected in the presence of Ca²⁺ with a PL composition containing PS or PS and phosphatidylinositol-(4,5)-bisphosphate (PIP₂), which in some cases can enhance the binding affinity (Lee and Bell, 1991).

Neither C₂F_{wt} nor C₂F_{Pga} show substantial binding to any of the phospholipid mixtures tested. Only some very weak traces of the protein domains were found in some of the liposome phases which might be due to unspecific binding or denatured protein as the presence of EGTA did not abolish these protein traces.

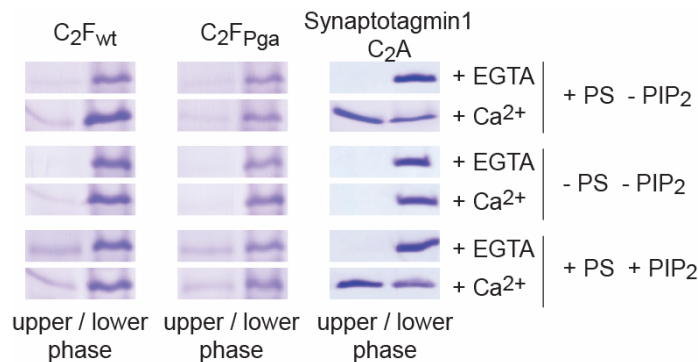


Figure 4: Floatation assay of C₂F.

Coomassie stained SDS PAGE gel of floatation assay of C₂F. The upper phase contains liposomes and bound protein, whereas the lower, aqueous phase contains the non-bound protein. 15-30 µg of protein were mixed with three types of liposomes, with and without PS and a third type containing 2% PIP₂, the mixtures were spun on a density gradient leading to the separation of two phases, liposomal and aqueous.

Otof^{Pga/Pga} mRNA level increased but protein level decreased

The minor change in secondary structure as determined via CD spectroscopy seemed unlikely to cause the phenotype of *Otof*^{Pga/Pga} mice also the otoferlin expression level was determined. The expression of mutant otoferlin was compared to wild type otoferlin by analyzing the mRNA and protein level in the organ of Corti of *Otof*^{+/+} and *Otof*^{Pga/Pga} mice. The mRNA level was assessed by real time PCR. RNA was isolated from P14 mice organs of Corti, converted to cDNA by reverse transcription and used for real time PCR. Protein levels were compared based on fluorescence intensity differences of immunohistochemically labeled organs of Corti.

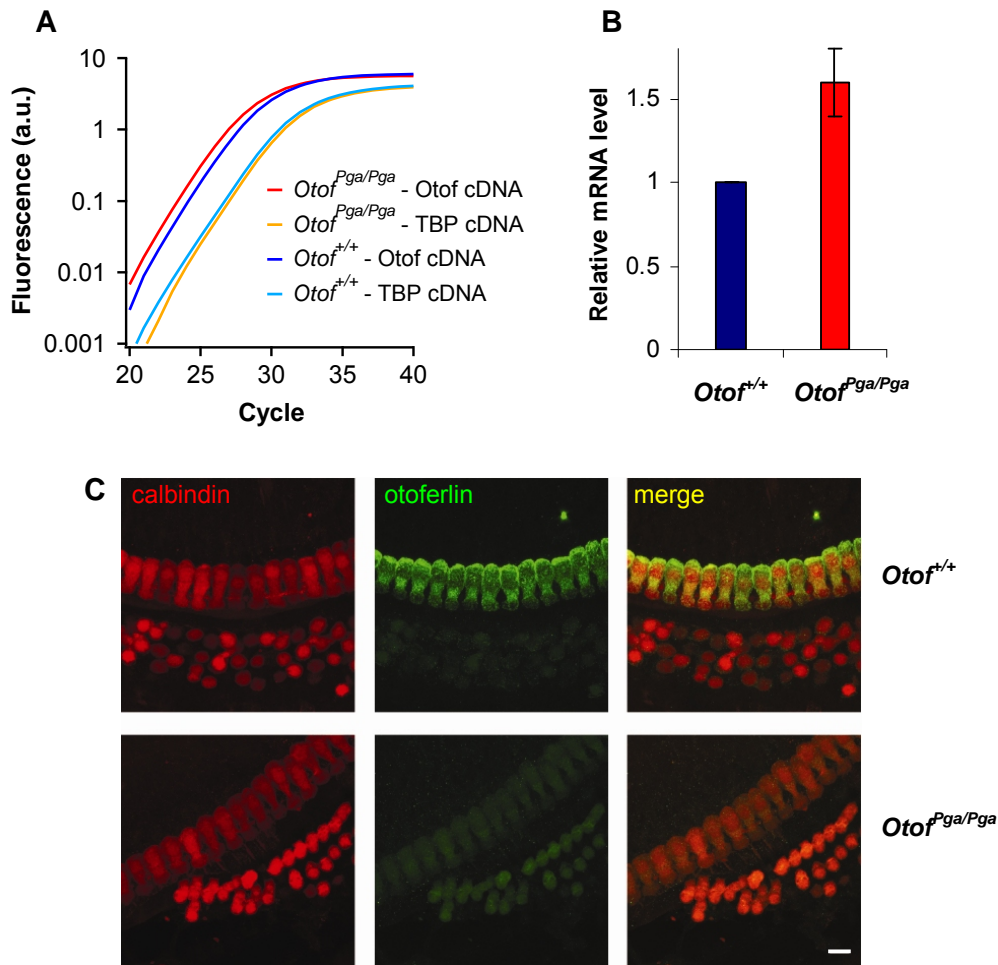


Figure 5: Expression of otoferlin_{wt} and otoferlin_{Pga}
Protein levels of otoferlin are reduced in *Otof*^{Pga/Pga} mouse IHCs whereas the mRNA levels are increased.

A. Real time PCR traces of cDNA produced from RNA of P14 wild type and *Otof*^{Pga/Pga} mouse organ of Corti. Otoferlin and TATA-box binding protein (TBP) cDNA was amplified.

B. Comparison of otoferlin wild type and mutant mRNA level determined via $\Delta\Delta C_t$ method. The mRNA level of otoferlin is not significantly increased in mutant mice. Nevertheless, a trend can be seen, it amounts to 1.56 ± 0.24 fold of wild type ($n = 4$, error bars indicate SEM).

C. Immunohistochemistry of P13 organ of Corti of wild type and mutant mice (scale bar: 10 μm). The tissue was processed in parallel using an identical protocol and the same excitation and detection conditions were used in both samples, mutant otoferlin shows lower fluorescence intensity, indicating lower protein levels.

The mRNA levels of otoferlin and the housekeeping gene TATA-box binding protein (TBP) of both mouse lines were analyzed with real time PCR (Figure 5A, B). Determination and comparison of mRNA level of wild type (wt) and mutant otoferlin via $\Delta\Delta C_t$ method revealed no significant change in mRNA level but a tendency to increased levels in the mutant mice (Figure 5A, B, $n = 4$, $P = 0.101$ in a t-test with two samples of unequal variance).

Interestingly in mutant mice the protein level appeared decreased as revealed by immunohistochemistry (Figure 5C). This was characterized by T. Pangrsic in more detail she demonstrated that *Otof*^{Pga/Pga} IHCs had clearly reduced relative otoferlin levels (otoferlin/vGlut3) with an even stronger reduction at the plasma membrane (Pangrsic et al., 2010). Interestingly also in the purifications of C₂F_{wt} and C₂F_{Pga} differences were seen in obtained protein concentrations. When the same amount of growth medium was used and the domains were purified simultaneously C₂F_{Pga} only amounted to $63.9\% \pm 8.9\%$ of C₂F_{wt}.

Towards “rescue” of otoferlin knock out mice

As a further test of the Ca^{2+} sensor of fusion hypothesis we analyzed the ability of synaptotagmin I (Syt1) to replace otoferlin in its suggested role in inner hair cells. In order to express Syt1 in the inner hair cells we used an *in vivo* transgenic approach. Furthermore, we used transgenic expression of otoferlin to test, whether this approach is capable to restore hearing in *Otof*^{-/-} mice as a first step on the way to human gene therapy.

Expression of mOtof-IRES-eGFP required the use adenovirus serotype 5, because the small genome held by adeno-associated virus (AAV) cannot accommodate otoferlin cDNA. For expression of Syt1-IRES-eGFP we chose AAV serotype 1/2 due to the low immunogenicity of AAV. Both genes were expressed using human cytomegalovirus enhancer combined with a human β -actin promoter combination, an internal ribosomal entry sites (IRES) was used for additional eGFP expression.

***In vitro* and *in vivo* transduction of IHCs**

The delivery of DNA into IHCs is more difficult than for most cell types. Semliki Forest Virus, Lentivirus and several AAV serotypes failed whereas AAV2/1 and Ad5 turned out to be able to transduce IHCs (Reisinger et al., 2011). Several methods have been tested, amongst them electro-microporation and the use of transfection media. However, with none of these methods transfection of hair cells could be achieved. We successfully used adeno-associated-virus (AAV) serotype 1/2 and 6 and adenovirus serotype 5 to deliver DNA into IHCs.

In organotypic cultures of the organ of Corti only AAV1/2 was able to reliably transduce IHCs, adenovirus serotype 5 transduced only very few hair cells and AAV6 completely failed to transduce IHCs in organotypic cultures (Figure 6A-C). All virus types were also tested *in vivo*, performing transuterine otocyst injections to deliver the virus into the developing otocyst for transduction of hair cells.

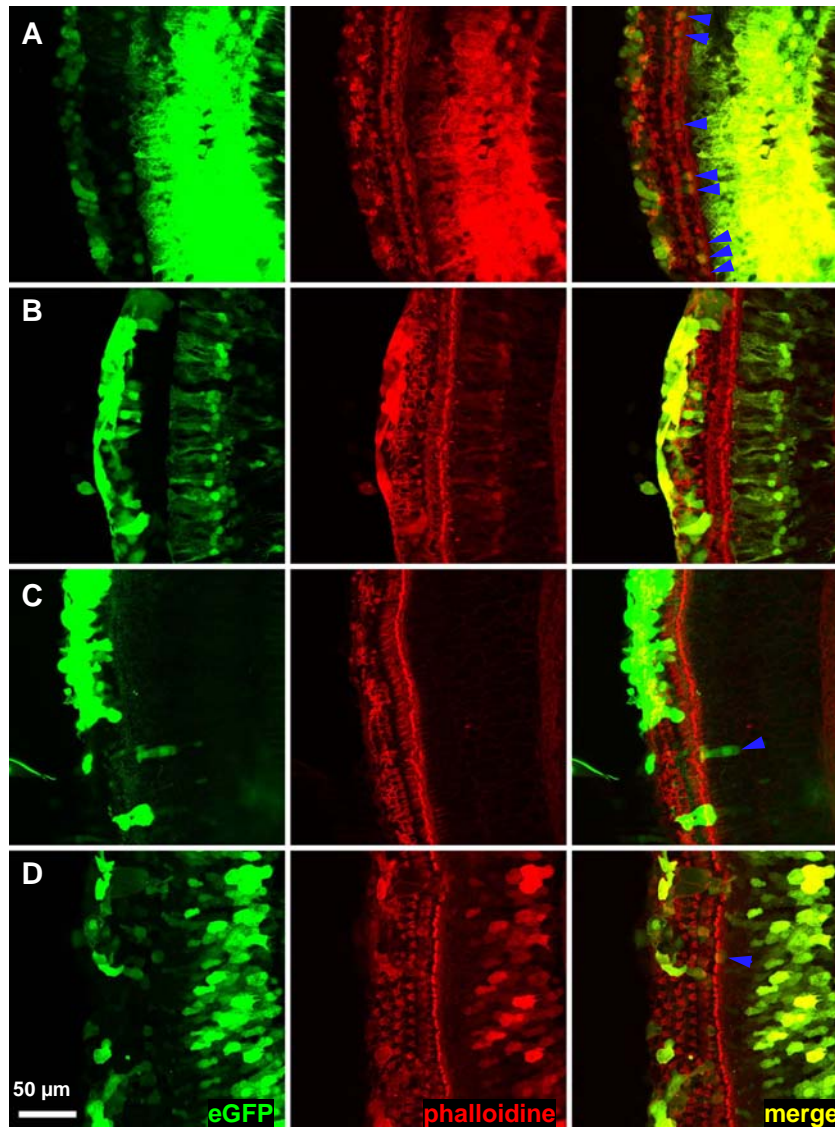


Figure 6: Viral gene expression in organotypic culture

Organotypic cultures were prepared from organs of Corti of P9 wild type mice, virus was added to the cultures and they were fixed 5 - 7 days after transduction.

A-D: eGFP expression after transduction with **A.** AAV1/2-eGFP, **B.** AAV6-eGFP, **C.** Ad-eGFP, **D.** Ad5-mOtof^{fwt}-eGFP. Blue arrowheads indicate transduced IHCs.

Embryonic transuterine otocyst injections

The method of injecting virus into the otocysts of mouse embryos was established in collaboration with Dr. John Brigande of the Oregon Hearing Research Center in Portland. In the surgeries (Figure 7) a laparotomy on pregnant dams at postcoital day 11.5 was performed, the uterus was externalized (Figure 7C) and virus was injected through uterus wall and amnion into the left otocyst of about 90% of the

embryos (Figure 8). The uterus was re-internalized and the abdominal wall and skin were sutured.

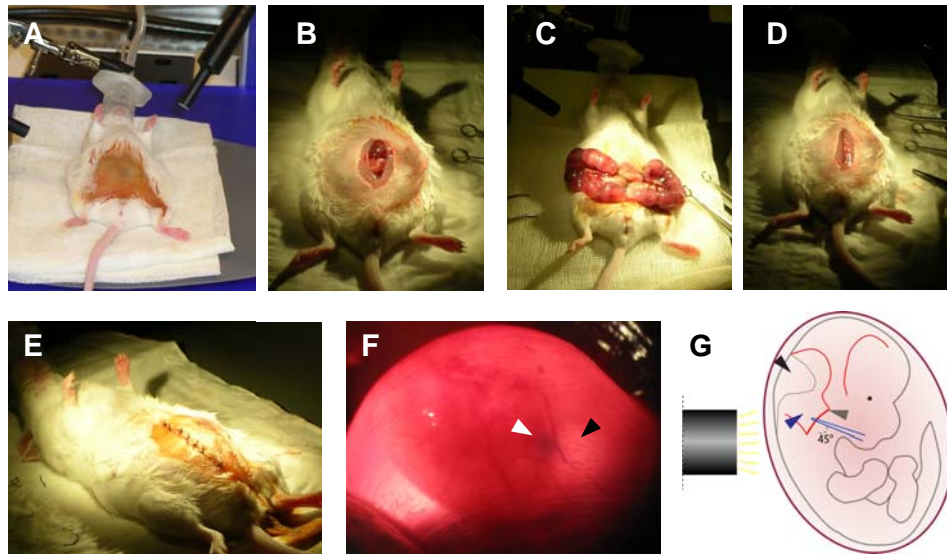


Figure 7: Embryonic trans-uterine-otocyst injections

Documentation of surgical procedure for trans-uterine-otocyst injections of various viruses for the *in vivo* transduction of IHCs.

A. Mouse before injection with breathing mask for inhalation anaesthesia with isofluran.

B-E. Surgical procedure: **B.** Mouse with laparotomy. **C.** Externalized uterus. **D.** Mouse after surgery with abdominal wall closed with continuous suture. **E.** Mouse after surgery with also the skin closed.

F. Otocyst injected embryo, white arrow: injected otocyst, black arrow: 4th ventricle.

G. Schematic of embryo with landmarks depicted grey arrow: primary head vein, blue arrow: position of otocyst, black arrow: 4th ventricle.

The mice gave birth to 70% of the embryos present at embryonic day 11.5. The offspring was analyzed for positive transduction by immunohistochemistry, labelling either the expressed gene directly or the reporter gene eGFP, and we found that 60% of the born mice expressed transgenic protein (Figure 8). Although, in principle, these viruses are able to transduce IHCs with high efficiency, the transduction rate varied following otocyst injection. This effect can only in part be explained by the possibility of non-injected embryos having higher survival rates. If all non-injected embryos were born and all injected embryos were positive for transgenic gene expression, 86% instead of 60% of all born offspring would have been expected to be positive. As this

was not the case we assume that virus transduction does not take place in all injected animals, or transduction rates are so low, that the few positive cells cannot be found in whole mount preparations.

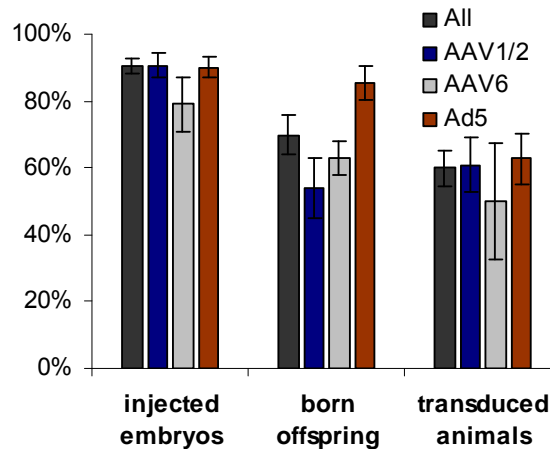


Figure 8: Statistical analysis of trans-uterine otocyst injections

The number of injected embryos and born offspring are presented as percentage of total number of embryos present at postcoital day 11.5, the number of transduced animals as percentage of born offspring. In total 19 dams gave birth to 139 mice of which 76 were expressing transgenic protein.

Immunohistochemistry was performed to assess eGFP expression and animals showing more than 20% positive IHCs in the apical, midbasal or basal region of the cochlea were counted as positive animals. Animals with some transgenic gene expression but less than 20% transduced IHCs in any cochlear region were excluded from hearing analysis to ensure that transduction rates were sufficient to unveil the effect of transgenic protein. However, we did not achieve to dissect all apical, midbasal and basal cochlear regions of all animals. In many cases the midbasal or basal region was lost, therefore some transduction rate data could not be included into the analysis.

Transgenic gene expression was superior in AAV1/2 and Ad5 injected animals compared to AAV6 (Table 1). Therefore, in further experiments those two virus types were used.

In AAV1/2-eGFP injected animals expression was predominantly found in the apical and midbasal region of the cochlea with decreasing rates from apex to base (Table 1). Of 15 AAV1/2-eGFP injected animals 7 had expression rates above 20% and in 8 animals all IHCs were negative.

In AAV6-eGFP injected animals expression was high in OHCs. Transduced IHCs were found in few samples, nevertheless, with fair rates of positive IHCs in apex and midbase. Only 4 of 18 animals showed more than 20% IHCs transfected and 9 had transduction rates below 20% and 5 were entirely negative. Therefore hearing was not

- Results -

analyzed for positive animals of expression rates below 20%.

<u>Virus</u>	<u>apical turn</u>	<u>midbasal turn</u>	<u>basal turn</u>
AAV1/2-eGFP (n = 7)	61.96% ± 5.22% (n = 7)	45.85% ± 5.52% (n = 7)	34.67% ± 3.42% (n = 2)
AAV6-eGFP (n = 4)	23.26% ± 10.18% (n = 4)	39.59% ± 8.36% (n = 3)	N.A.
Ad5-eGFP (n = 6)	33.72% ± 5.22% (n = 6)	45.77% ± 12.14% (n = 4)	38.39% ± 9.43% (n = 3)

Table 1: eGFP expression after *in vivo* viral transduction.

Average transduction rates (± SEM) of positive animals in the apical, midbasal and basal cochlear region. Animals with a transduction rate > 0 and < 20% were excluded from further data analysis. Note: some transduction rate data is missing if midbasal or basal regions were lost during preparation.

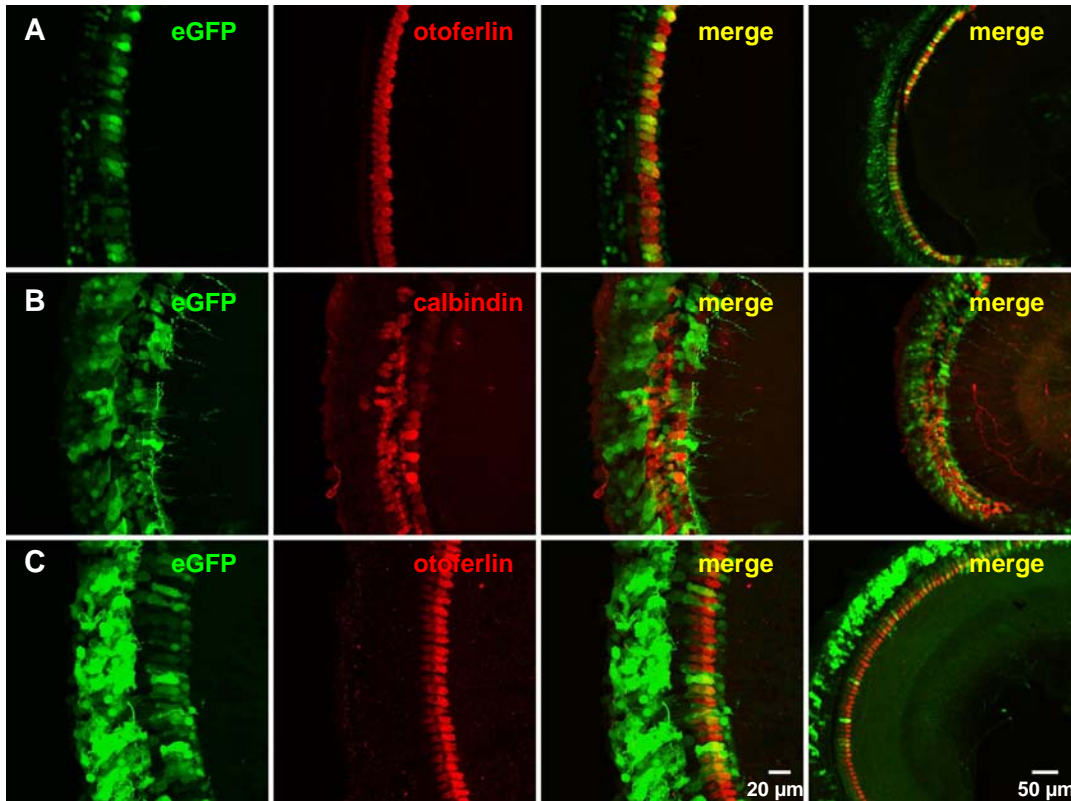


Figure 9: Transgenic eGFP expression.

Apical expression of eGFP after transuterine otocyst injection of virus. Three left images (scale bar: 20 μm), right image panel: overview of apical cochlear section (scale bar: 50 μm).

A-C. A: AAV1/2-eGFP, B: AAV6-eGFP C: Ad5-eGFP.

Finally, in Ad5-eGFP injections the IHC transduction rates were similar to those in AAV1/2-eGFP. However, transduction rates were increasing from apex to midbase and then decreasing toward the basal region, leading to similar transduction rates in apex and base. Noteworthy, in contrast to AAV1/2-eGFP injections in most Ad5-eGFP injected samples the apical-most hair cells were not transduced and transduction starts with rather high rates about ½ turn toward the base (Figure 9C). 6 of 11 animals were included in the group of positive animals and 3 were completely negative.

To test whether the hearing of the injected animals was compromised due to the surgical procedure, the penetration with the injection needle, the presence of the virus or the transgenic gene expression we performed recordings of distortion product otoacoustic emissions (DPOAE) to assess outer hair cell function and auditory brainstem responses (ABR) to study auditory signalling.

In contrast to AAVs the injection of adenovirus can harm inner ear function

Before testing the hearing of otocyst injected animals OHC function was assessed via DPOAE measurements. The DPOAE sound pressure levels (SPL) of either negative left ears or right ears of positive animals were normal in AAV injected animals at all frequencies (Figure 10A-C, F-G). Most positive ears also had normal DPOAEs except for one animal. In the group of AAV6 injections, the animal with highest midbasal expression rate had very poor DPOAE SPL in the injected ear (Figure 10C dark yellow trace extending into yellow shaded area).

In adenovirus injected animals about half the animals show impaired DPOAEs in positive ears (Figure 10D, H). This effect does not correlate with transduction rates as indicated by the colour code. The colour code shows the average transduction rates of all areas of the particular animal, apical, midbasal and basal, however, not all regions were sampled for all animals, and therefore the values may not indicate an exact representation of the entire cochlear transduction rate.

- Results -

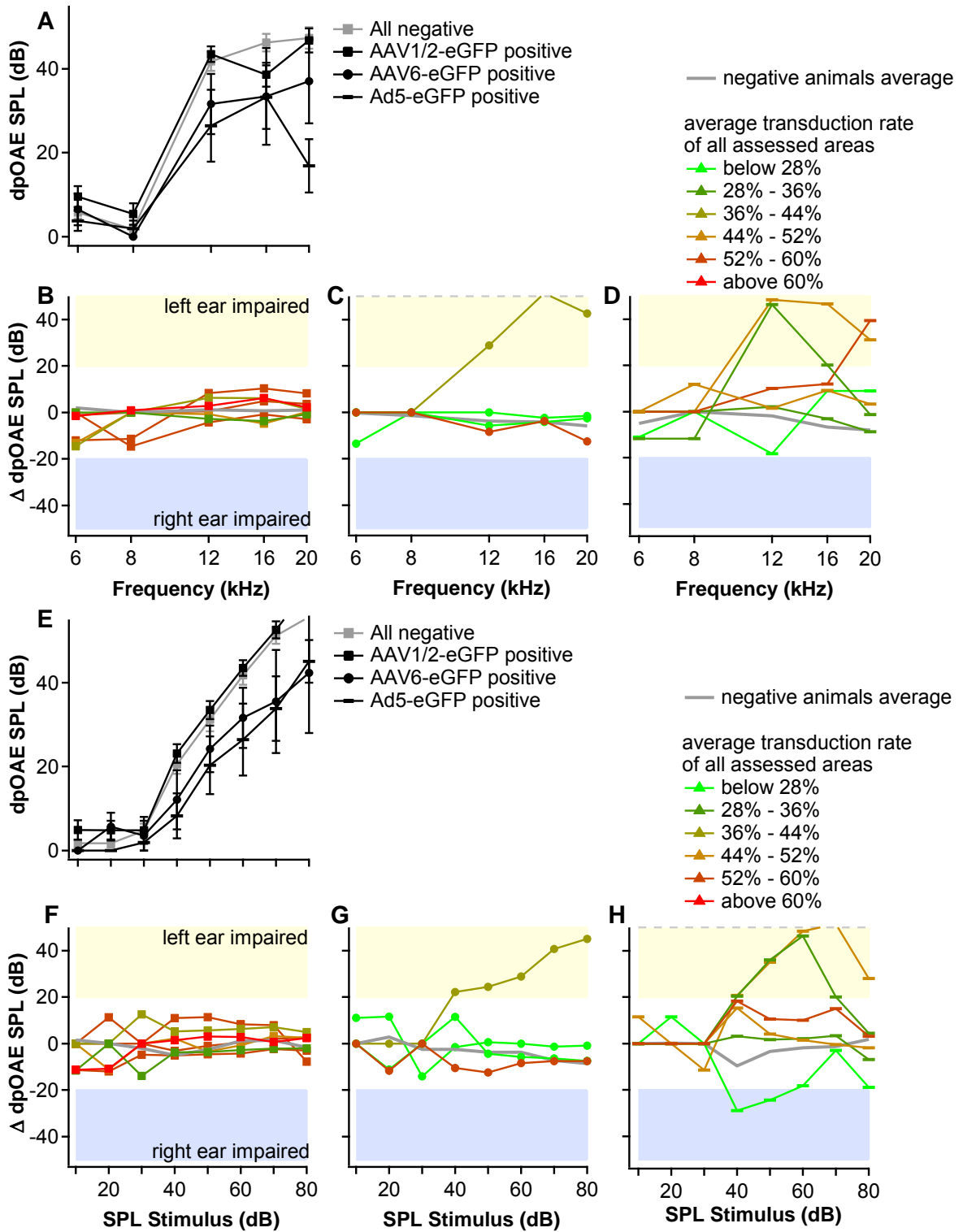


Figure 10: DPOAEs of animals expressing transgenic eGFP

Analysis of outer hair cell function of AAV1/2-eGFP, AAV6-eGFP and Ad5-eGFP injected animals via the measurement of distortion product oto-acoustic emissions.

A. DPOAEs elicited by stimulation at frequencies from 6 – 20 kHz with a SPL of 60 dB of left ears comparing negative littermates with positive animals.

B-D. Δ DPOAE: subtraction of right ear DPOAE SPL minus left ear DPOAE SPL using the same stimulus as in A. One trace represents the data of one animal; the average transduction rate is indicated with the color code. In grey the average of all negative littermates is shown. **B.** AAV1/2-eGFP, **C.** AAV6-eGFP and **D.** Ad5-eGFP injected animals.

E. Stimulation was performed at 12 kHz with SPL rising from 10 – 80 dB. DPOAEs of left ears of negative littermates and positive animals are shown.

F-H. As in B-D also for the stimulus described in E the right and left SPL of DPOAE measurements were subtracted. **F.** AAV1/2-eGFP, **G.** AAV6-eGFP and **H.** Ad5-eGFP injected animals.

Hearing of otocyst injected animals expressing eGFP in the left ear was tested by ABR recordings using click and pure tone or chirp stimuli from 20 dB (10 dB in some cases) – 80 dB sound pressure level (SPL) in 5 - 10 dB steps (Figure 11A).

One measure for auditory function is the ABR threshold; another is the amplitude of the ABR wave. For assessment of the number of functional IHCs the latter is a better measure than the ABR threshold (Khimich et al., 2005; Kujawa and Liberman, 2006). Therefore, we determined the amplitude of wave I in response to an 80 dB click stimulus from the first positive peak (p1) to first negative peak (n1) and compared negative littermates to left and right ears of injected animals (Figure 11B).

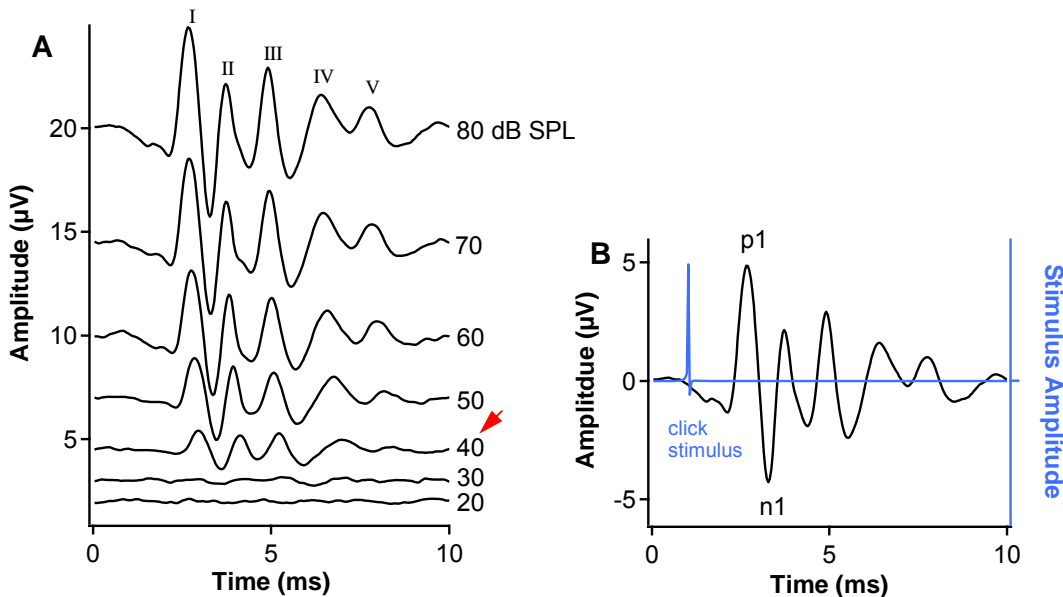


Figure 11: Threshold and wave I amplitude determination in ABR recordings

A. ABR on click stimulus at 20 – 80 dB SPL of left ear of wild type mouse, the threshold is at 40 dB indicated with the red arrow.

B. ABR after stimulation with click noise at 80 dB indicating p1 and n1 for amplitude determination.

Chirp stimulus development for mouse

Recently chirps, tones with a rising frequency, have been more frequently used for ABR measurements in several species. The time difference between the frequencies played in the chirp is adapted to the different latency of each frequency's travelling wave along the basilar membrane. Therefore, all contained frequencies generate a maximum deflection of the basilar membrane at almost the same time, leading to a well timed response. Experiential chirp stimuli elicit an ABR wave at lower SPL than the conventional click stimulus used in these measurements (Spankovich et al., 2008; Petoe et al., 2010). Therefore chirp stimuli seem superior to click stimuli for finding true hearing thresholds, and we decided to develop a chirp stimulus for the mouse (Figure 12) and to use this stimulus for the analysis of hearing in adenovirus injected animals.

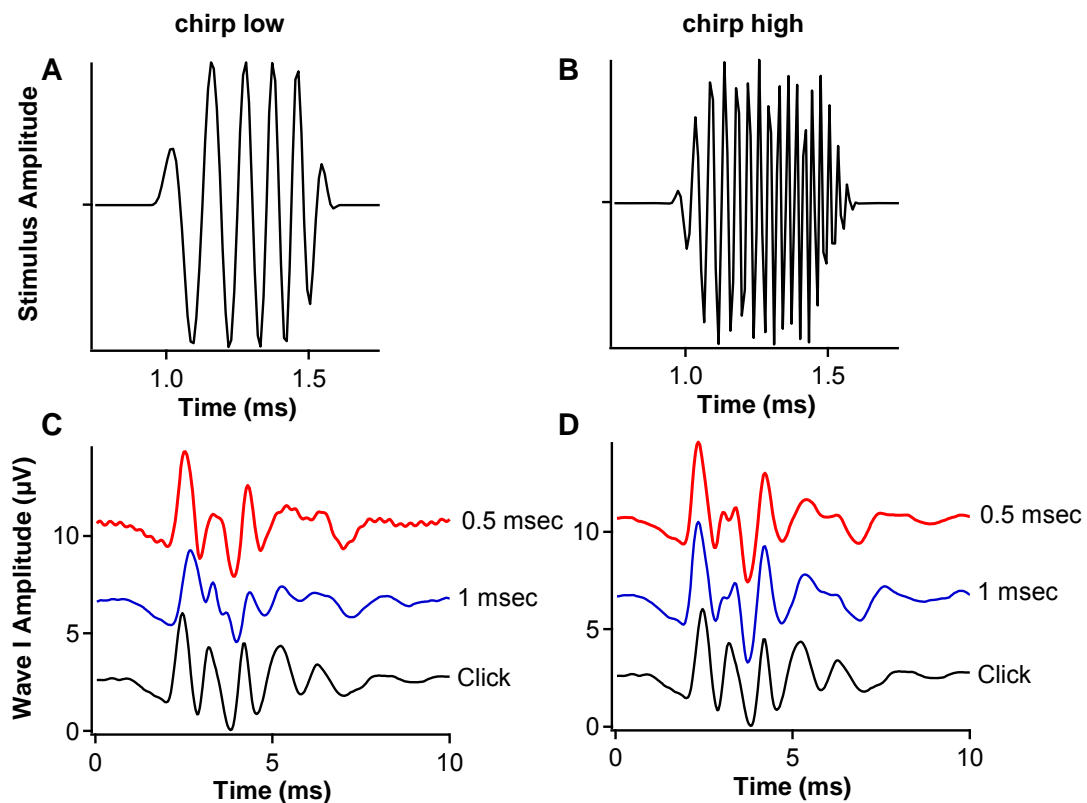


Figure 12: Chirp stimuli in mouse

A-B. Chirp stimuli for latency adapted cochlea stimulation in mouse **A.** Chirp low 4 – 12 kHz, **B.** Chirp high 12 – 36 kHz

C-D. ABR elicited by 80 dB stimulus comparing click and chirp 0.5 ms and 1 ms stimulus duration **C.** Chirp low. **D.** Chirp high.

Gerhard Hoch generated two stimuli (Figure 12A, B) similar to the linearly rising frequency chirp (L-chirp) used by C. Spankovich (2008) in rat. We use a low frequency

chirp (chirp low): 4 – 12 kHz and a high frequency chirp (chirp high): 12 – 36 kHz chirp, each stimulus spanning 1.5 octaves (Figure 12A, B). The first stimulus tested had duration of 1 msec, with a 0.1 msec rise and fall time, and then we decreased stimulus length to enhance latency adaptation. During stimulus optimization we found an optimum ABR wave shape and wave I amplitude at 0.5 msec stimulus, with 0.1 msec rise and fall time (Figure 12C, D).

Inner ear function after otocyst injections with eGFP viruses

Animals expressing eGFP after injection of AAV, showed normal ABR in response to click and pure tone stimuli. The thresholds were not increased comparing injected ears to non-injected (right) ears or to negative littermate controls (Figure 13A, B).

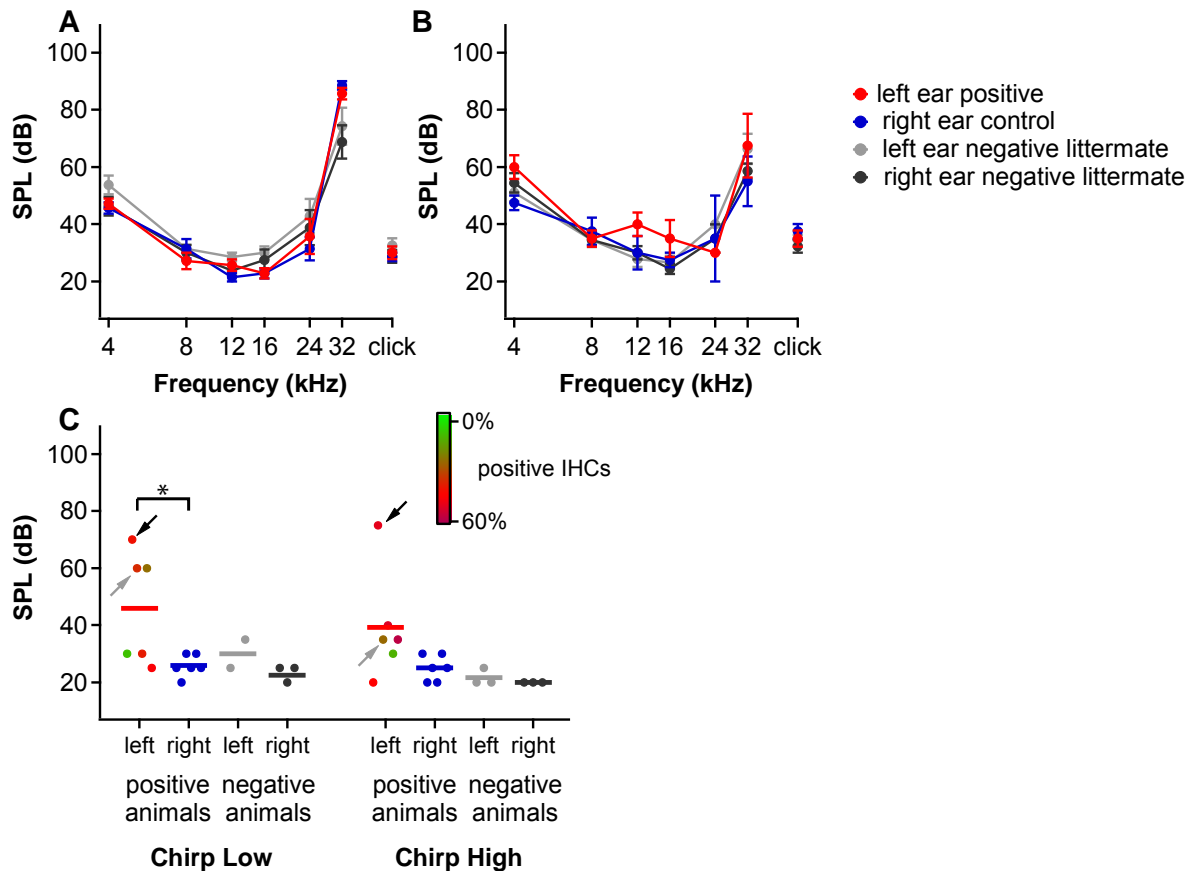


Figure 13: ABR thresholds of mouse litters injected with eGFP viruses

The offspring of dams used for trans-uterine otocyst injections with AAV1/2-eGFP, AAV6-eGFP and Ad5-eGFP was tested for their ABR thresholds. Neither the injection procedure nor the expression of eGFP in the left ear of AAV injected animals has an impact on ABR thresholds, whereas Ad5 induces a negative effect.

A-B. ABR thresholds of click noise and pure tones ranging from 20 – 80 dB SPL in 10 dB steps of wild type mice injected with **A.** AAV1/2-eGFP and **B.** AAV6-eGFP.

C. ABR thresholds using chirp stimuli from 10 – 80 dB assessing threshold values at 5 dB steps of Ad5-eGFP injected animals. Horizontal bars: average values of single animal thresholds (dots), black arrows: animal with impaired DPOAE at low and high frequencies, grey arrow: animal with decreased DPOAE SPL at 12 kHz and lower frequencies. Color scale: transduction rate at apex for chirp low and average transduction rate of midbase and base for chirp high. One star indicates $0.05 \geq P \leq 0.01$.

Ad5-eGFP injected animals showed elevated average ABR thresholds of the injected ears, similar to the decreased DPOAEs, in response to low-frequency chirps (Figure 13C red, chirp low: significantly increased, $P = 0.046$ using a Wilcoxon-Mann-Whitney Test). Most animals had almost normal thresholds using chirp high stimulus (Figure 13C), except for one animal that also had impaired DPOAEs (Figure 13C black arrow, Figure 10D bright orange trace extending into yellow shaded area). Using chirp low stimulus, however, half of the animals showed elevated ABR thresholds (Figure 11C). The black arrow indicates the same animal with elevated thresholds also for chirp high stimulus, for a second animal the DPOAE SPL was decreased at 12 kHz and lower frequencies, but not at 16 and 20 kHz (grey arrow, Figure 13C, Figure 10D dark green trace extending into shaded area) a third animal with a high ABR threshold had normal DPOAE. The loss of OHC function at 20 kHz in the dark orange trace is not detected using chirp low or chirp high stimulus for ABR threshold determination. Therefore, decreased DPOAE SPL and elevated ABR thresholds did not entirely correlate. When we found decreased DPOAE SPL we also found elevated ABR thresholds, but not all animals with elevated ABR thresholds also showed decreased DPOAE.

Another reason for decreased thresholds could be an overload of transgenic protein in IHCs, but the transduction rate does not correlate with the increased thresholds. The percentage of positive IHCs, which generally correlated well with the number of positive OHCs, is indicated by the colour scale for individual data points, low and high transduction rates are equally distributed among animals with normal and elevated ABR thresholds. The animal with normal OHC function has a fairly low transduction rate, which therefore is unlikely to account for the defect.

Apart from the ABR threshold also the ABR wave amplitudes are an interesting characteristic feature which in contrast to the threshold depends much more on the number of intact IHCs and synapses (Khimich et al., 2005; Kujawa and Liberman,

2006). Therefore, we also compared wave I amplitudes of positive and negative animals. Although ABR thresholds were normal in AAV1/2-eGFP injected animals the amplitude of the ABR recording was significantly decreased on the left, injected, side compared to the right side ($P = 0.032$ using a t-test with two samples and unequal variance) or to right ears of negative littermates ($P = 0.014$ using the same test) (Figure 14). Interestingly also the negative littermates show the same feature ($P = 0.018$ again using a t-test with two samples and unequal variance) indicating that this may be caused by the injection itself, as most negative animals were also injected. The comparison of negative and positive left ears suggests that AAV-mediated transgene expression itself does not alter auditory function.

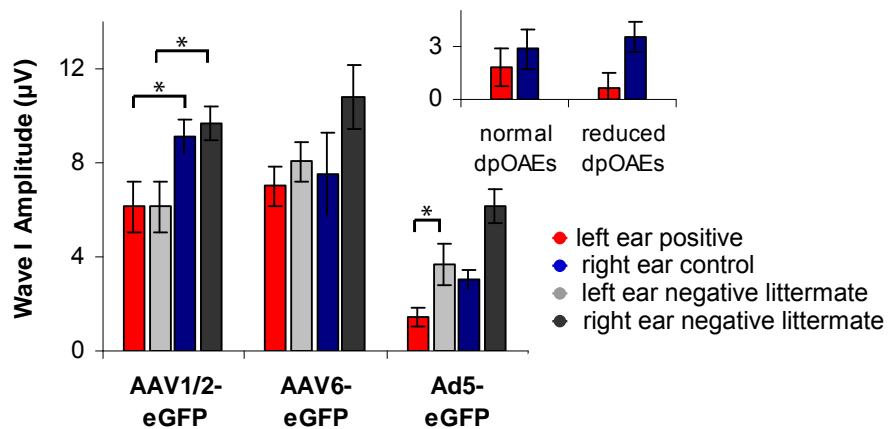


Figure 14: ABR wave I amplitudes after eGFP virus injection

Injection of AAVs does not seem to decrease the amplitude of ABR wave I. The differences seen in AAV1/2-eGFP injected animals are probably characteristic to the litter as they also occur in negative animals. However, Adenovirus clearly has a negative effect on the injected ears. The effect is more evident in animals that also showed decreased DPOAE SPL, but is also found in animals with no defect in pOAEs. Inset: left and right ears of Ad-eGFP injected positive animals separating animals with normal and reduced outer hair cell function. One star indicates $0.05 \geq P \leq 0.01$.

In AAV6-eGFP injected animals no effect on wave I amplitude could be detected (Figure 14). All animals used for Ad5-eGFP injections or for Ad5-mOtof^{wt}-eGFP injections had lower wave I amplitudes on both, injected and non-injected ears, the reasons for which are unclear. Nevertheless, Ad5-eGFP injections caused a significant decrease in wave I amplitude comparing left and right ear of positive animals ($P = 0.023$). This could be an effect of the injection as the same trend, though insignificant, is also seen in negative littermates. However, there is a trend toward smaller responses in positive than in negative ears, though insignificant. In some of these animals outer hair cell function was impaired (see Figure 10), if those animals were separated from

the group with normal outer hair cell function the effect of reduced wave I amplitude becomes non-significant due to low number of samples but the trend can still be seen (Figure 14 inset).

Syt1 does not rescue hearing ability in otoferlin knock out mice

Synaptotagmin I (Syt1) is the Ca^{2+} sensor for exocytosis in neurons and therefore might functionally replace otoferlin, the putative Ca^{2+} sensor in IHCs. It could have the potential to restore hearing in otherwise deaf *Otof*^{-/-} animals. First we tested the effects of Syt1 expression in IHCs of wild type mice. AAV1/2-Syt1-eGFP efficiently transduced the inner and outer hair cells of the injected animals (Table 2, Figure 15).

<u>Animals</u>	<u>apical turn</u>	<u>midbasal turn</u>
Wild type (n = 5)	60.00%* ± 6.00%* (n = 5)	N.A.
<i>Otof</i> ^{+/-} (n = 4)	59.27% ± 9.04% (n = 4)	2.98% ± 0.95% (n = 3)
<i>Otof</i> ^{-/-} (n = 4)	65.07% ± 7.50% (n = 4)	0.00% ± 0.00% (n = 3)

Table 2: Transgenic synaptotagmin 1 expression of positive animals.

As in other otocyst injections of AAV the highest expression rates were found in the apical region. Error indicates SEM.

* Expression rate was only estimated by eGFP fluorescence for each sample before fixation, samples were used for STED imaging by Ellen Reisinger (Reisinger et al., 2011).

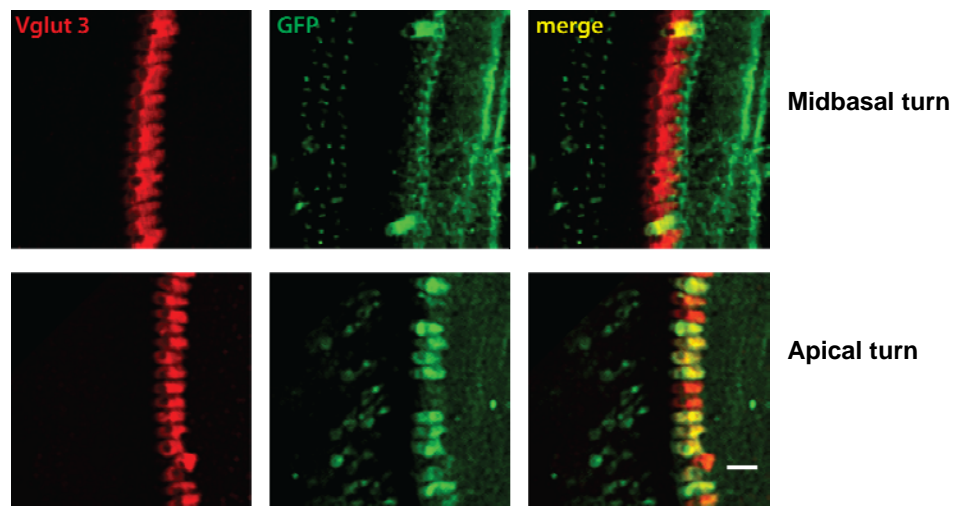


Figure 15: Transgenic Syt1 expression.

Apical and midbasal cochlear turn of AAV1/2-Syt1-eGFP injected animal (scale bar: 20 μ m).

When assessing OHC function we found that the SPL of DPOAEs were almost normal in all animals expressing Syt1 in IHCs of the left ear with only slight decreases compared to negative littermates (Figure 16A) and no effect compared to right ear controls (Figure 16B-D), indicating that the OHCs are largely unaffected by the over expression of Syt1. Two *Otof*^{±/±} mice show impaired DPOAEs, however one on the left side, the other on the right, therefore this is probably not due to the injection or Syt1 expression.

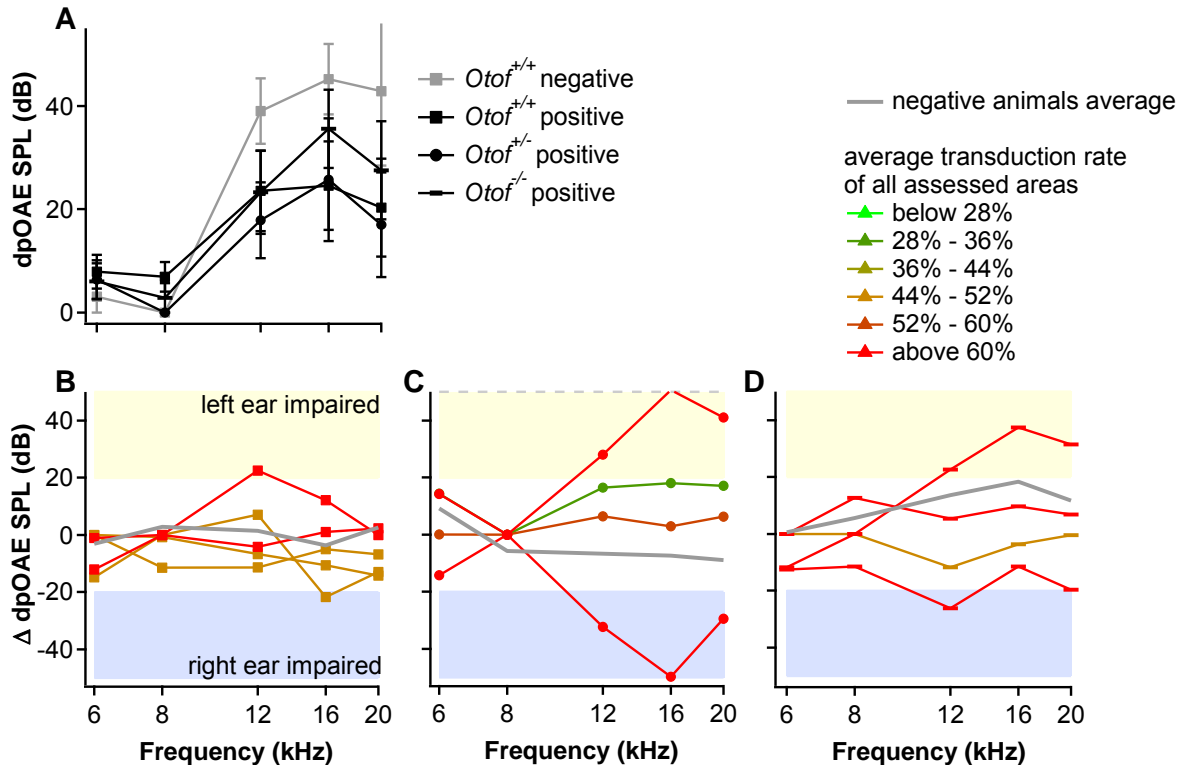


Figure 16. Effect of Syt1 expression on DPOAEs.

Mice injected with AAV1/2-Syt1-eGFP were used to find the effect of Syt1 expression on OHC function via measurement of DPOAEs elicited by stimulation at different frequencies with a SPL of 60 dB.

A. Comparison of left ears of negative wild type mice with left ears of positive animals using wild type, *Otof*^{±/±} and *Otof*^{-/-} mice.

B-D. DPOAE SPL of right ears subtracted by left ear SPLs of **B.** wild type animals, **C.** *Otof*^{±/±} and **D.** *Otof*^{-/-} mice. In grey the average of the ears of negative littermates is shown.

Furthermore we found unaffected hearing thresholds in AAV1/2-Syt1-eGFP injected left ears of wild type animals (Figure 15A) but slightly increased levels in left ears of animals heterozygous for *OTOF* (*Otof*^{±/±}) mice compared to the non-injected

- Results -

right ears (Figure 15B). Wave I amplitude was neither altered by Syt1 expression in wild type nor in *Otof^{+/−}* mice. However, we seem to observe a gene dosage effect of otoferlin in the *Otof^{+/−}* mice in which the amplitude of ABR wave I was roughly half of that of wild type mice (Figure 17C).

Regardless of finding no aversive effects of Syt1 in hearing animals it was not possible to rescue hearing of otoferlin deficient mice by transgenic expression of Syt1 in IHCs: ABR could not be detected in *Otof^{−/−}* mice expressing transgenic Syt1 (Figure 17B, bars with arrows).

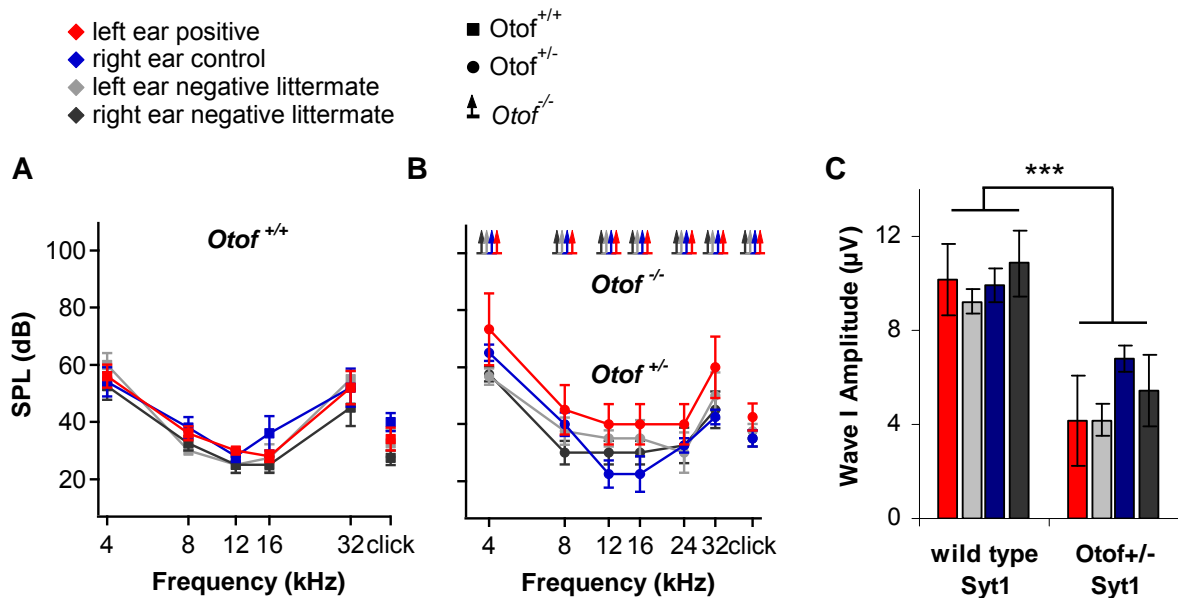


Figure 17: ABR recordings of AAV1/2-Syt1-eGFP injected animals

AAV1/2-Syt1-eGFP was injected in wild type, *Otof^{+/−}* and *Otof^{−/−}* mice and hearing ability of the mice was assessed by ABR recordings.

A-B. ABR thresholds of **A.** wild type animals and **B.** *Otof^{+/−}* (circles) and *Otof^{−/−}* (bars with arrows) mice after pure tone and click stimuli.

C. ABR wave I amplitudes. The amplitudes of positive ears are unaffected by Syt1 expression (wild type mice n = 5, *Otof^{+/−}* mice n = 4) but the heterozygote *Otof^{+/−}* mice show reduced amplitudes compared to wild type mice (P = 1.75 x 10^{−5} in a t-test using two samples with unequal variance).

It was also shown that Syt1 expression in IHCs of *Otof^{−/−}* mice did not restore Ca²⁺ dependent exocytosis (Reisinger et al., 2011). Furthermore Reisinger et al. found no regained phasic exocytosis in chromaffin cells or neurons of *Syt1^{−/−}* mice expressing otoferlin, in those neurons asynchronous release was even enhanced (Reisinger et al., 2011).

Transgenic otoferlin does not restore hearing in *Otof*^{-/-} mice

Finding that Syt1 is not capable of replacing otoferlin at the IHC synapse we intended to show that transgenic otoferlin leads to a reconstitution of hearing in *Otof*^{-/-} mice. Selectively expressing otoferlin in IHCs via a viral gene transfer also provided a test for whether otoferlin is solely required at the hair cell synapse, or is also functional in the auditory pathway beyond the IHC. Moreover, based on our findings with viral transfer of eGFP cDNA we anticipated to yield varying transduction rates. This by itself, in case of rescue would address how many functional IHCs are required for hearing. If successful in mice this experiment would also serve as a proof of principle to human gene therapy of DFNB9.

In animals injected with adenovirus for the expression of otoferlin (Ad5-mOtof^{wt}-eGFP) transduction rates were very similar to those of Ad5-eGFP (Table 3, Figure 18), and the hair bundles were intact in those preparations labelled with phalloidine (images not shown). As in Ad5-eGFP injected animals also in Ad5-mOtof^{wt}-eGFP injected animals the apical-most hair cells were often negative whereas the midbasal expression was highest, and transduction decreased slightly toward the base. Only in a few animals expression rates were high also in the very apical region. The transgenic otoferlin, expressed by viral DNA, did not localize entirely like the endogenous wild type otoferlin. Transgenic otoferlin was also found in the cuticular plate and the nucleus (Figure 18). Possible reasons include that translation stopped before the trans-membrane domain or that the trans-membrane domain was not correctly translated or inserted into the membrane. The prominent concentration at the cell membrane as found in wild type animals (Figure 18) seems reduced in injected *Otof*^{-/-} animals expressing transgenic otoferlin.

<u>Animals</u>	<u>apical turn</u>	<u>midbasal turn</u>	<u>basal turn</u>
Wild type (n = 6)	28.18% ± 9.20% (n = 6)	48.15% ± 7.79% (n = 4)	37.96% ± 3.48% (n = 2)
<i>Otof</i> ^{-/-} (n = 11)	31.40% ± 5.16% (n = 10)	55.27% ± 6.40% (n = 6)	33.12% ± 5.32% (n = 4)

Table 3: Transduction rates after injection of Ad5-mOtof^{wt}-eGFP

Otoferlin is expressed along the entire cochlea sparing only the first few apical IHCs and rising to the highest rates in the midbasal region.

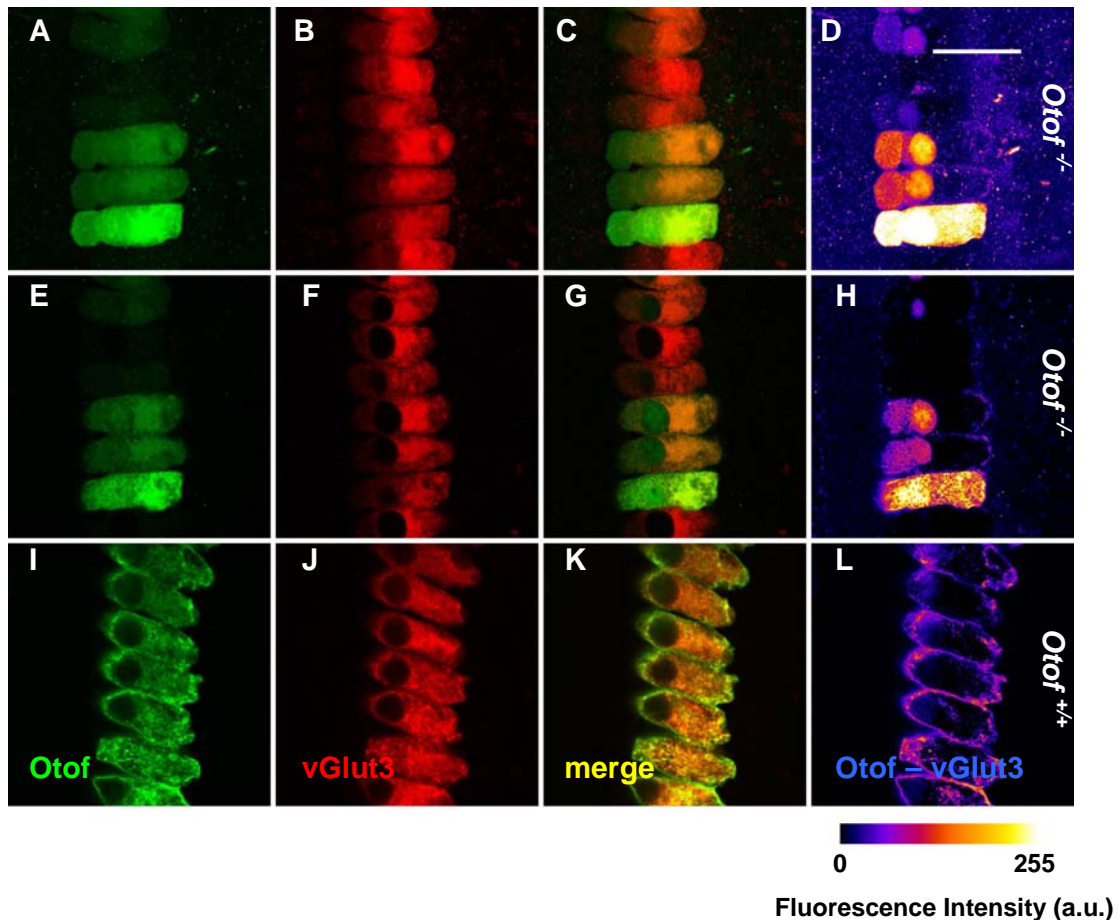


Figure 18: In vivo transduction by Ad5-mOtof^{wt}-eGFP

Immunohistochemical labeling of transgenic compared to wild type otoferlin. Expression of transgenic otoferlin is similarly distributed along the cochlea as eGFP expression after Ad5-eGFP injection (scale bar: 20 μ m).

A-D. Maximum projection of fluorescence image stack of apical cochlear section of Ad5-mOtof^{wt}-eGFP injected animal labelled in green for transgenic otoferlin and in red for vGlut3. **A.** otoferlin, **B.** vGlut3, **C.** merge, **D.** Subtraction of A and B, (only in this image the fluorescence intensity was multiplied by the factor of 2).

E-H. Single plane of fluorescence image stack shown in A-D (subtraction image was not multiplied).

I-L. Single plane of fluorescence image stack of apical cochlear coil of wild type animal labelled in green for endogenous otoferlin and in red for vGlut3. **I.** otoferlin, **J.** vGlut3, **K.** merge, **L.** Subtraction of I and J.

Hearing ability of Ad5-mOtof^{wt}-eGFP injected *Otof*^{-/-} animals

To test whether transgenic expression of otoferlin has the potential to reestablish the ability of *Otof*^{-/-} mice to hear we analyzed hearing ability of the injected mice. As control Ad5-mOtof^{wt}-eGFP was injected into wild type animals. Again only animals with > 20% of IHCs positive for transgenic gene expression were considered as positive for analysis and compared to negative littermates.

- Results -

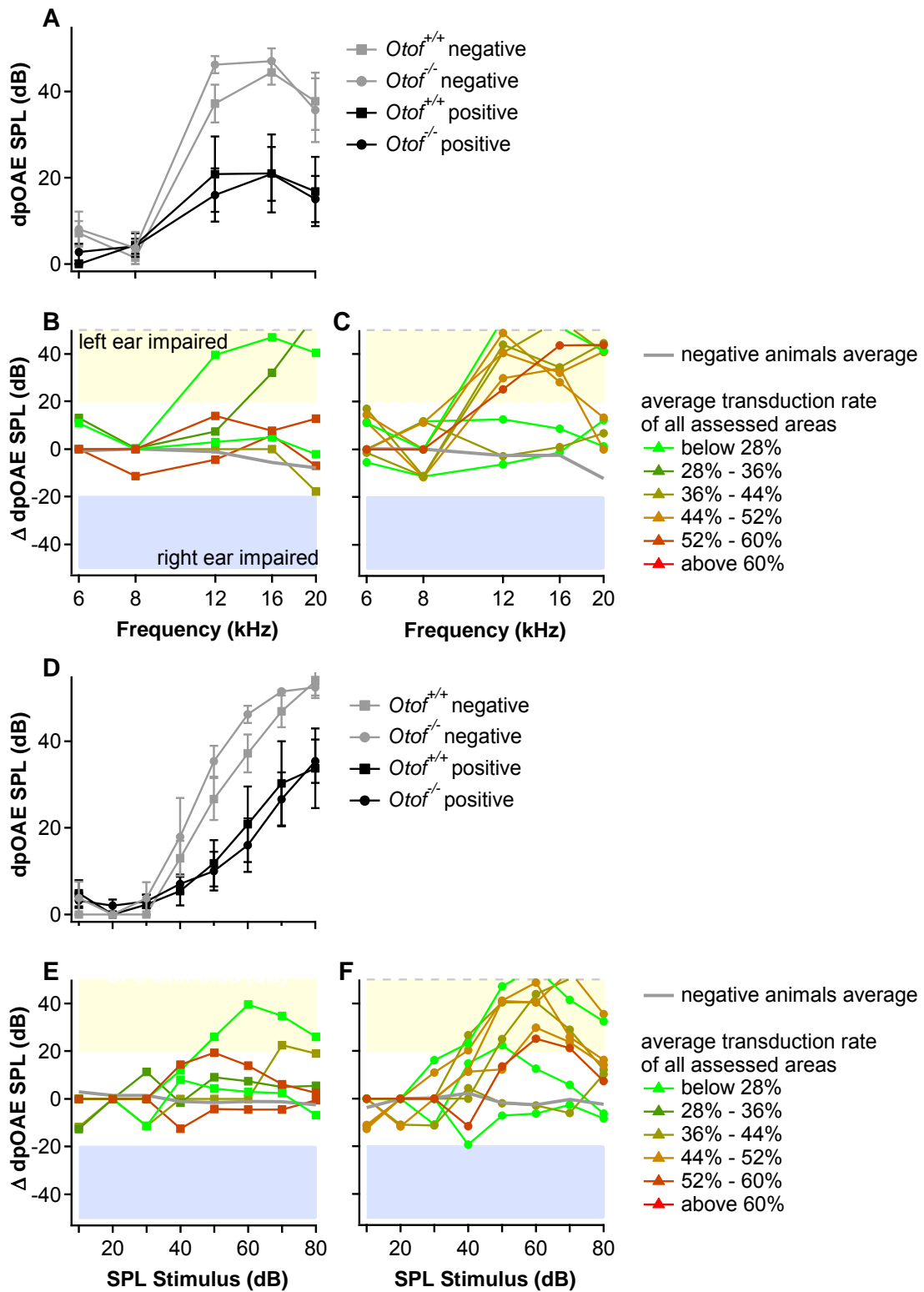


Figure 19: DPOAEs of Ad5-mOtof^{wt}-eGFP injected mice

Wild type and *Otof*^{-/-} mice were injected with Ad5-mOtof^{wt}-eGFP and their OHC function was assessed via DPOAE measurements.

A. DPOAE measurements of left ears of negative and positive wild type animals and of positive *Otof*^{-/-} mice. F1 frequencies of 6 – 20 kHz were used at 60 dB as stimulus.

B-C. Stimulus and measurements were identical as in A., right and left ear DPOAE SPL of positive animals were subtracted from each other; the average of the negative littermates is depicted in grey. **B.** wild type animals, **C.** *Otof*^{-/-} mice.

D. DPOAE were measured at f1 of 12 kHz at increasing SPL, left ears of negative animals do not show an impairment (grey trace) whereas positive ears (black traces) of wild type and *Otof*^{-/-} mice have reduced DPOAE SPL.

E-F. Stimulus and measurements as in D. As in B-C. subtraction of DPOAE of left from right ears highlights the defect of OHC function seen in positive left ears of **E.** wild type and the even bigger defect in **F.** *Otof*^{-/-} mice.

First the function of the OHCs was analyzed via detection of DPOAEs. In contrast to other used viruses DPOAEs were more strongly affected in Ad5-m*Otof*^{wt}-eGFP injected animals. At frequencies of 12 kHz and above, positive left ears were worse than negative left ears (Figure 19A). Also at increased stimulus SPL the positive left ears performed a little worse than negative left ears (Figure 19D).

The impairment found by comparing positive and negative left ears was similar for *Otof*^{+/+} and *Otof*^{-/-} animals. Only when comparing left with right ears by subtraction of the left DPOAE SPL from the right it becomes obvious that the left positive ears of *Otof*^{-/-} mice more frequently have impaired OHC function (Figure 19B, C, E, F). Negative animals did not show any impairment of DPOAE SPL. There was no correlation of transduction rate with impaired left ear DPOAEs. However, most animals with high transduction rate showed impairment, but also an animal with a fairly low transduction did so, whereas one animal with a rather high number of positive IHCs did not show any impairment (Figure 19C and F, dark yellow trace in white area).

Transgenic otoferlin does not rescue hearing

To measure the hearing ability of the injected mice we used chirps to test for ABR thresholds. The thresholds of left ears of wild type animals expressing transgenic otoferlin were significantly elevated compared to their right ears and to negative littermates (Figure 20A, chirp low: $P = 0.031$ and chirp high $P = 0.028$ in a Wilcoxon-Mann-Whitney Test). In these tests the right ear was always measured first and was then destroyed by removing the malleus and incus and making a hole into the cochlea. This was done to ensure that the ABR wave of the left side was really elicited by the cochlea of the left ear.

In contrast to Ad5-eGFP injections the effect of elevated ABR thresholds did not

correlate with decreased DPOAE SPL; animals with poor DPOAEs are marked with a black arrow in Figure 20. Again the transduction rates had no effect on the elevated thresholds. Similar as in Ad5-eGFP injected animals wave I amplitudes were significantly decreased in the positive ears (Figure 20B) compared to the corresponding right ears ($P = 0.012$ in a t-test using two samples with unequal variance). And again the same trend could be observed in negative littermates.

Taking together the ABR and DPOAE measurements performed on Ad5-eGFP and Ad5-mOtof^{wt}-eGFP injected animals, a harmful effect of the adenovirus became evident. Furthermore, we also injected Ad5-mOtof^{Pga}-eGFP (not incorporated in Figure 8) into two dams to find whether high expression rates of otoferlin_{Pga} may lead to a hearing phenotype, but only one single animal was born which was found to be negative. This strongly suggests lethality of this particular virus.

In *Otof*^{-/-} mice injected with Ad5-mOtof^{wt}-eGFP and expressing the transgenic protein in various concentrations no animal was showing ABR waves even at SPL as high as 110 dB (Figure 20A). Future Cell-physiological experiments are required to test the properties of exocytosis. However, Akil et al. (Abstract 636, Abstract book of the ARO midwinter meeting 2011) did show ABR thresholds resumed in vGlut3 knock out animals with a 40% transduction rate.

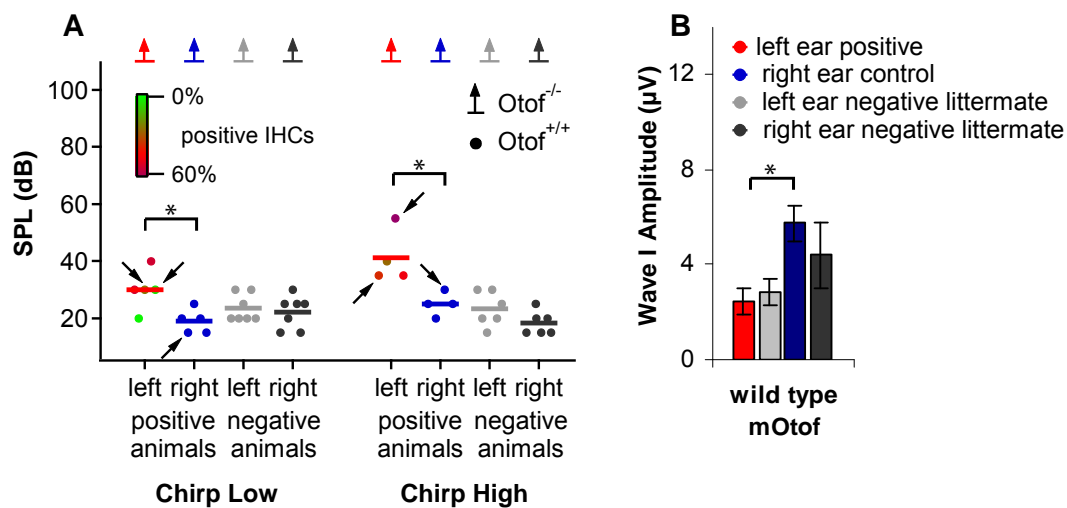


Figure 20: Effect of transgenic otoferlin on ABR thresholds of *Otof*^{-/-} mice
Ad5-mOtof^{wt}-eGFP was injected in wild type and *Otof*^{-/-} mice but had no positive effect, hearing could not be restored.

A. ABR thresholds upon chirp stimuli. In positive left ears of wild type animals thresholds are slightly increased (horizontal bars: average of single animal data: dots), in *Otof*^{-/-} mice transgenic otoferlin is not capable to restore a hearing phenotype (bars with arrows). Black arrows point toward animals with poor DPOAEs.

B. ABR wave I amplitudes of wild type animals. Amplitudes are drastically decreased in positive ears but even in negative right ears all amplitudes are lower than normal. One star indicates $0.05 \geq P \geq 0.01$.

We also analyzed the correlation of ABR wave I amplitude, as a measure of functional IHC synapses, with transduction rate, in search of a malicious effect of vast amount of transgenic protein. Plotting all animals in one graph does not demonstrate an evident negative effect of the number of transgene expressing cells (Figure 21A). However, analyzing each group (ranging from 4 – 7 animals per group) separately revealed a small negative effect of transgenic protein expression. In animals injected with one of the three eGFP viruses (AAV1/2-eGFP, AAV6-eGFP or Ad5-eGFP) only AAV6-eGFP shows an opposite trend (Figure 21B) which may be accounted to the low number of animals analyzed. The negative effect is most evident in Ad5-mOtof^{wt}-eGFP (Figure 21C) injected animals but is also present in most other groups.

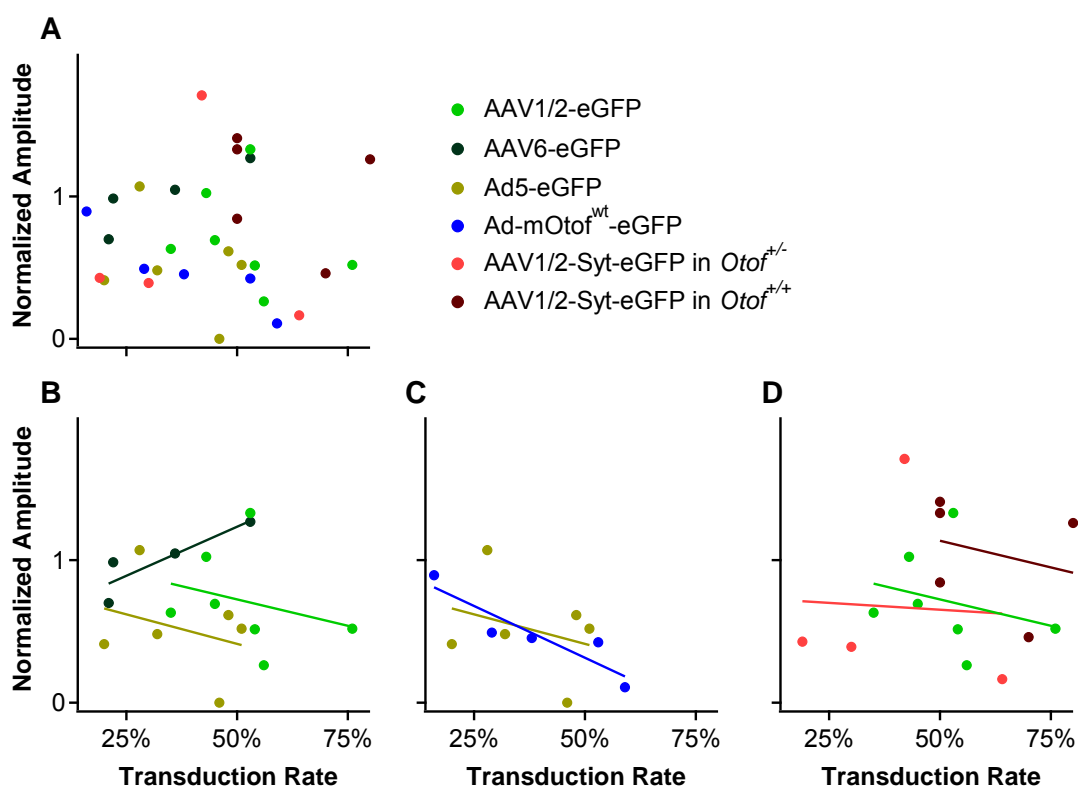


Figure 21: Correlation of transduction rate with ABR wave I amplitude

The transduction rate of IHCs was compared to relative ABR wave I amplitude of the left ears which were normalized to their corresponding right ear waves.

A. All positive animals injected with any of the 6 viruses used are shown in the graph. No correlation of the two factors, wave I amplitude and transduction rate is evident in this plot.

- Results -

B. In animals injected with the three viruses for the ectopic expression of eGFP the effects of transduction rate on wave I amplitude are minor. In AAV1/2-eGFP and Ad5-eGFP a trend to decreased amplitude with increasing transduction rate are observed. In AAV6-eGFP the trend follows the opposite direction.

C. Animals injected with Ad5-mOtof^{wt}-eGFP are compared to animals injected with Ad5-eGFP showing the most evident correlation of transduction rate and wave I amplitude for Ad5-mOtof^{wt}-eGFP injected mice.

D. In animals injected with AAV1/2-Syt1-eGFP the effect is similar as in AAV1/2-eGFP injected animals or even less strong.

Visualizing exocytosis in IHCs

Optical analysis of single synapses is of great importance for understanding sound coding. Here we attempted to utilize pH-dependent GFP (pHluorin) fused to the vesicular glutamate transporter 1 (vGlut1) for monitoring exo- and endocytosis.

Using otocyst injections of AAV1/2-vGlut1-pHluorin we were able to express vGlut1 fused to ecliptic pHluorin in IHCs of wild type mice. Most expression was found in the apical IHCs similar to eGFP expression after AAV1/2-eGFP injection (Figure 22 A).

Initial immunohistochemical analysis showed that the protein distribution of vGlut1-pHluorin was similar to that of vGlut3, the native IHC vesicular glutamate transporter (Seal et al., 2008) (Figure 22 B), in positive cells both proteins largely co-localize, however, vGlut1-pHluorin was found in slightly higher concentrations in the apex (Figure 23).

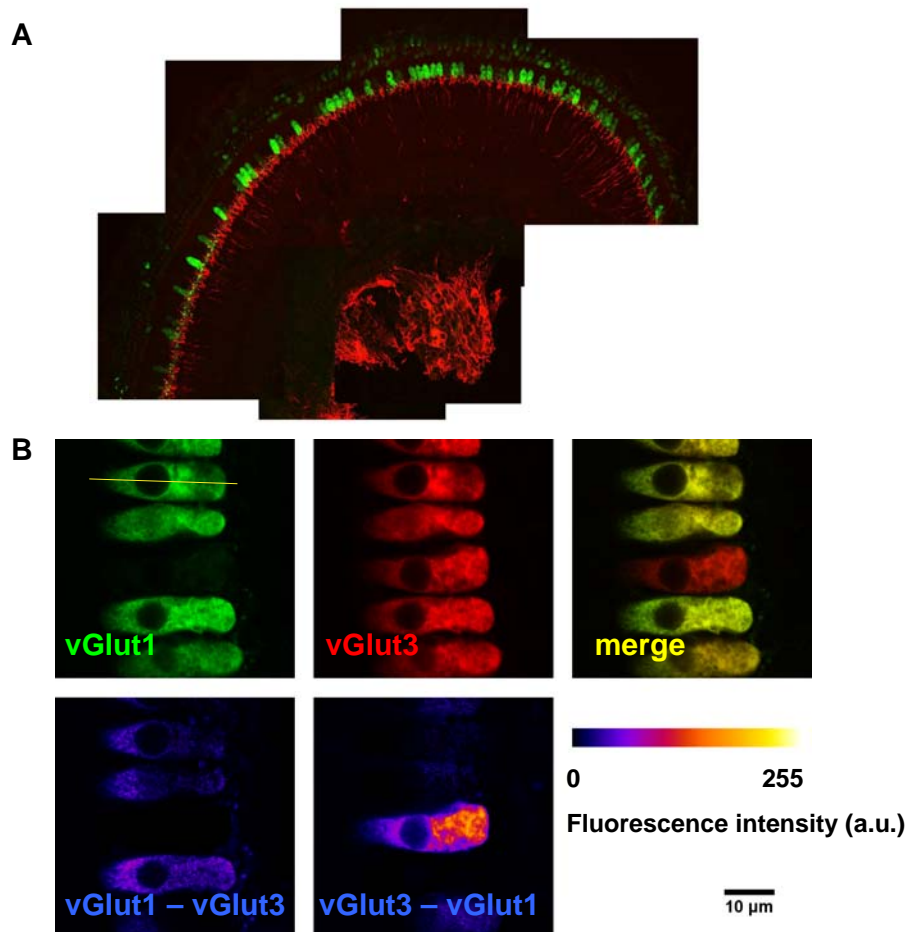


Figure 22: Expression of vGlut1-pHluorin
Transgenic vGlut1-pHluorin widely co localizes with the native vGlut3.

A. Overview of vGlut1-pHluorin expressing apical cochlear turn (green: GFP, red: Neurofilament (NF) 200).

B. Correlation of transgenic vGlut1-pHluorin and native vGlut3 expression pattern. (Green: vGlut1-pHluorin, red: vGlut3, lower left: vGlut3 stain subtracted from vGlut1-pHluorin stain, lower center: vGlut1-pHluorin stain subtracted from vGlut3 stain, lower right: color code of subtraction images, yellow line indicates position of line profile of fluorescence intensities in D.).

As the proteins were labeled with different fluorophores and as the expression level of vGlut1-pHluorin is variable no absolute comparison of protein levels can be made, thus the fluorescence in the apex was normalized to the fluorescence of the base of the cells. With this type of analysis small changes are seen in the apical expression rate; here vGlut1-pHluorin is present in higher relative concentrations, almost 20%, than the native vGlut3 (Figure 23A, C).

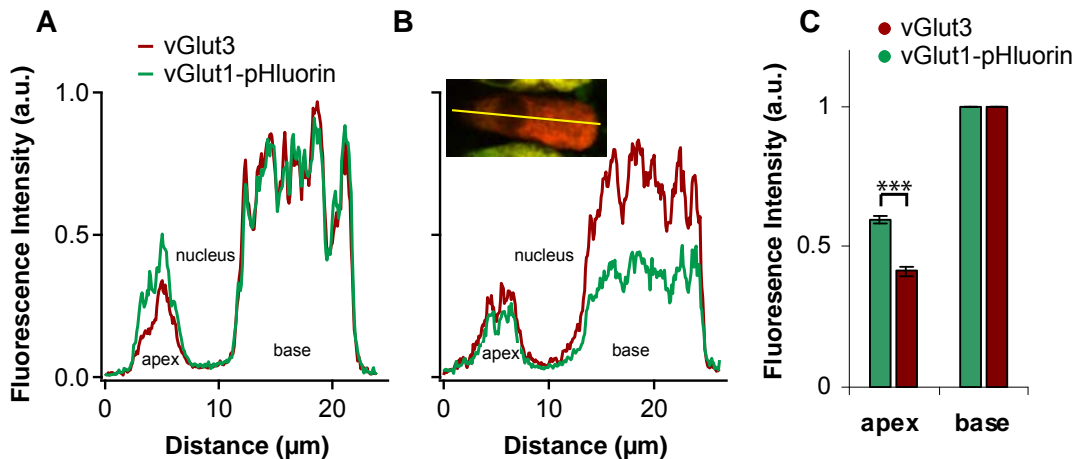


Figure 23: Apical versus basal expression of vGlut1-pHluorin in IHCs

vGlut1-pHluorin has increased levels in the apex compared to vGlut3.

A. Line profile of vGlut1-pHluorin and vGlut3 fluorescence intensity along the line of interest indicated in yellow in Figure 22B.

B. Line Profile of vGlut1-pHluorin and vGlut3 fluorescence intensity along the line of interest indicated in yellow in the inset. Inset: Fluorescence image of IHC expressing vGlut1-pHluorin in lower amounts than vGlut3 (green: vGlut1-pHluorin, red: vGlut3).

C. Fluorescence intensities of IHC labeling of the IHC apex and the IHC base, normalized to the basal fluorescence intensity, shows a relative increase in IHC apical levels of vGlut1-pHluorin compared to vGlut3. (26 cells from 3 samples have been analyzed; vGlut1-pHluorin is increased 1.442 ± 0.024 fold in the apex compared to vGlut3). Three star indicating $P \leq 0.001$.

Another important issue using non native proteins as markers in living cells is the functionality of the transduced cell and organ. Therefore we tested the function of the organ of Corti and of the IHCs. Comparison of ABR thresholds and amplitudes of injected and non-injected ears (Figure 23 A, B) showed largely unaffected hearing function in injected ears. This result is supported by preliminary data by A. Wong which indicates similar exocytosis characteristics in vGlut1-pHluorin expressing IHCs compared to negative cells and that these cells show fluorescence increase at sites of exocytosis (unpublished data, data not shown).

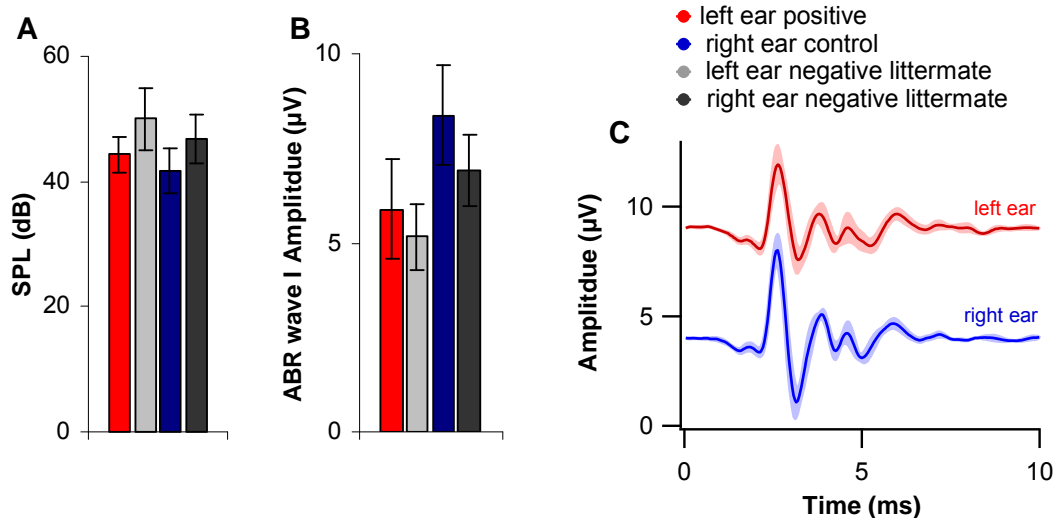


Figure 24: Phenotype of AAV1/2-VGlut1-pHluorin injected mice

ABR measurements of vGlut1-pHluorin expressing animals comparing left (injected) and right ears.

A. Thresholds of ABR recordings. No significant changes comparing the different groups were found.

B. ABR wave I amplitudes. Again no significant changes were detected analyzing positive and negative ears.

C. 80 dB ABR traces of left and right ears. (Shaded areas indicate SEM, left side: n = 7, right side: n = 6)

We then tested the ability to unquench the pHluorin inside the synaptic vesicles by perfusion of an acute preparation of the organ of Corti with NH_4Cl and found that the maximum increase in fluorescence in the entire IHC is about 2 fold higher than the background level (Figure 25). The analysis of single spots of fluorescence increase was, however, not possible due to low resolution of the used camera and needs more detailed optical analysis.

- Results -

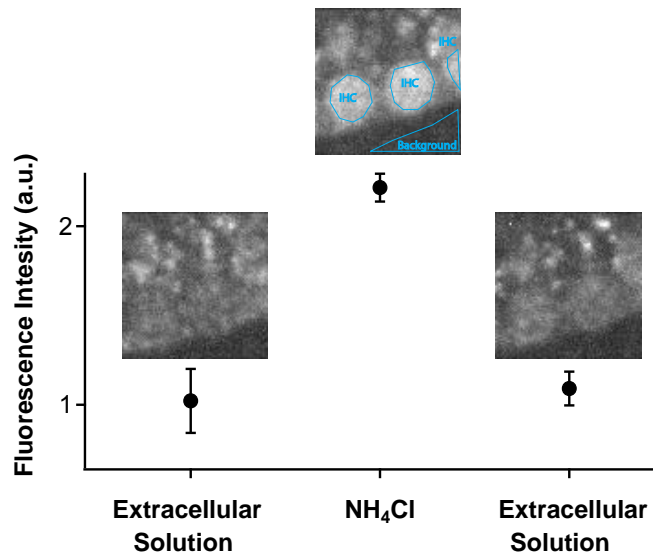


Figure 25: VGlut1-pHluorin unquenching with NH₄Cl

VGlut1-pHluorin positive organ of Corti was perfused first in extracellular solution and then for 10 min in similar solution but with 50 mM concentration of NH₄Cl in order to neutralize pH in all cellular compartments, then perfusion was set back to extracellular solution. Fluorescence was recorded before NH₄Cl perfusion, after 10 min of perfusion and after flush out. Three IHCs were analyzed for their overall fluorescence intensity.

Discussion and conclusion

The process of exocytosis in inner hair cells is not yet fully understood. The ribbon synapse of IHCs lacks several conventional components of the neurotransmitter release machinery (Mandell et al., 1990; Safieddine and Wenthold, 1997, 1999; Nouvian et al., 2011). One of the missing proteins is synaptotagmin 1 (Syt1), the putative Ca^{2+} sensor for neurotransmitter release in neurons. In IHCs, otoferlin is a major candidate for being the Ca^{2+} sensor of fusion. Here we analyzed the C-terminal C_2F domain for its Ca^{2+} and phospholipid binding characteristics and analyzed the effect of the *pachanga* mutation on this protein domain.

Furthermore we tested the rescue potential of Syt1 in *Otof*^{-/-} mice and intended to apply a gene therapeutic approach to restore hearing in *Otof*^{-/-} mice by expression of wild type otoferlin. Last, we established the expression of pHluorins in IHCs for monitoring exocytosis via fluorescence changes upon synaptic vesicle fusion.

Ca^{2+} or phospholipid binding of $\text{C}_2\text{F}_{\text{wt}}$ and $\text{C}_2\text{F}_{\text{Pga}}$ still unclear

The first question we tried to address was whether or not otoferlin C_2F binds Ca^{2+} . We performed ITC experiments which did not yield conclusive results. Therefore, we moved to measuring CD spectra and UV light absorption of purified otoferlin C_2F in the presence and absence of Ca^{2+} . We did not find changes in secondary structure induced by the presence of Ca^{2+} that could be resolved using these methods. A different conclusion was reached by Johnson and Chapman (2010), who found altered fluorescence emission spectra in the presence of 100 μM EGTA versus 1 mM Ca^{2+} . Our study used similar concentrations of additives and only slightly higher protein concentrations. Possible explanations for the contradictory results include (i) the use a different construct by Johnson et al. (2010), which may be missing one β -strand, (ii) the use of a different purification technique (iii) the use of a different device for measuring the autofluorescence of the aromatic amino acids and (iv) the different wavelengths used for excitation and emission. Johnson and Chapman (2010) used an excitation wave length of 280 nm, we used 295 nm also the emission was measured at slightly shifted wavelengths (290 – 380 nm versus 305 – 450 nm used by us).

Ca²⁺ binding of otoferlin C₂F was also reported by Ramakrishnan et al., (2009). This particular study however, was carried out using phosphate buffered saline as buffer solution for the fluorimetric analysis, which likely caused precipitation of calciumphosphate (Ca₃(PO₄)₂) at the Ca²⁺ concentrations used by the group. The same group also conducted surface plasmon resonance, a method very susceptible for aggregation, for the analysis of C₂F Ca²⁺ binding. Unfortunately, they did not show whether they controlled for protein aggregation or not.

We further analyzed the C₂F domain as wild type in comparison to the *pachanga* variant. This mutation is of high interest as in the *Otof*^{Pga/Pga} mouse vesicle replenishment was impaired (Pangrsic et al., 2010). First CD spectroscopy was performed to check for secondary structure effects caused by the mutation which may account for the loss of function. However, no such changes could be detected. Therefore, the *pachanga* mutation does not seem to disrupt the secondary structure.

We continued with the analysis of C₂F_{wt} versus C₂F_{Pga} by assessing phospholipid binding. Both, Ca²⁺ dependent as well as Ca²⁺ independent binding to phospholipids with and without phosphatidyl serine (PS) and with both PS and phosphatidylinositol-(4,5)-bis-phosphate (PIP₂) were tested. As a control, the C₂A domain of Syt1 was used. It showed clear binding to liposomes in presence of PS and Ca²⁺, but no binding in the presence of EGTA. In contrast neither otoferlin C₂F_{wt} nor C₂F_{Pga} did bind the liposomes under any condition.

Johnson and Chapman (2010) also performed a very similar analysis of otoferlin C₂F in a floatation assay. They show a dim band of C₂F on an SDS gel of the liposomal phase if the assay was conducted in the presence of Ca²⁺. They interpret this finding as phospholipid binding, however, a clear positive control like Syt1 C₂A is missing as well as the presentation of protein in the aqueous, non liposomal phase. It is well possible that both assays yielded the same result: a weak band of C₂F in the liposomal phase when Ca²⁺ was present, with deviating interpretations. Nevertheless direct comparison of the weak band of C₂F to the clear and strong band of Syt1 C₂A in the assay with liposomes containing PS and in presence of Ca²⁺ leads us to the conclusion that a moderate or strong binding to phospholipids can be excluded for otoferlin C₂F. Therefore, this protein domain might mediate other functionalities.

The *pachanga* mutation causes reduction in protein but not in mRNA levels

When starting the work with the *Otof*^{Pga/Pga} mice we found decreased protein levels of otoferlin via immunohistochemistry. T. Pangrsic performed a semi-quantitative analysis and found only ~ 30% of otoferlin as compared to wild type. Another interesting feature was that the membranous stain found in immunohistochemically labeled wild type otoferlin seemed lost in the *Otof*^{Pga/Pga} mice (Pangrsic et al., 2010). Also in biochemical purifications of C₂F_{wt} and C₂F_{Pga} less protein was produced for the mutant variant. We determined mRNA levels to test whether reduced protein levels were caused by a destabilization of otoferlin mRNA by the *pachanga* mutation. We found a tendency of the mRNA levels to be increased in organs of Corti of mutant mice. This tendency gave rise to the idea that maybe the mutation has an effect on protein synthesis or protein degradation. The reduction of protein levels might cause a compensation by increase of the mRNA level.

Embryonic transuterine otocyst injections into the inner ear

As a test of the Ca²⁺ sensor of fusion hypothesis we aimed to replace otoferlin with the neuronal Ca²⁺ sensor Syt1. Therefore we established embryonic transuterine otocyst injections in our lab. The method used to deliver the virus into the developing inner ear was derived by Dr. John Brigande, who assisted us in the effort. We performed tests to judge potential problems caused by the used viruses, by the injections or by the expression of eGFP as marker protein for positive animals.

Before performing the *in vivo* experiments, we tested adeno-associated virus serotype 1/2 (AAV1/2) and 6 (AAV6) and adenovirus serotype 5 (Ad5) for hair cell transduction using expression of eGFP in organotypic culture of mouse organ of Corti. We found that only AAV1/2-eGFP transduced cultures show eGFP expression in IHCs, whereas AAV6 and Ad5 mainly led to eGFP expression in supporting cells and OHCs. Recently Taura et al. (2010) described the use of a special reagent: trichostatin A (TSA) to enhance hair cell transduction which could be used in future experiments to test its efficiency with our used viruses. Despite this drawback all three viruses were tested *in vivo* as several studies indicate the efficiency of these virus types for *in vivo* transduction of IHCs (Lalwani et al., 1998, 2002; Holt et al., 1999; Dazert et al., 2001;

Luebke, Foster, et al., 2001; Luebke, Steiger, et al., 2001; Praetorius et al., 2002, 2007, 2009; Liu et al., 2005, 2007; Bedrosian et al., 2006; Hildebrand et al., 2008; Kesser et al., 2008).

From the three tested viruses especially AAV1/2 seems particularly efficient in transducing IHCs when used in combination with a CMV promoter and should be favored whenever the small genome of AAV suffices. Further we also showed that Ad5 leads to high transduction rates and is a good alternative to AAV1/2 if a larger genome, accepting larger constructs, is required.

We analyzed transduction rates of litters after trans-uterine otocyst injection of one of the three eGFP viruses (AAV1/2-eGFP, AAV6-eGFP or Ad5-eGFP) via immunohistochemistry, hearing ability by measurement of auditory brainstem responses (ABR) and outer hair cell (OHC) function by probing distortion product oto-acoustic emissions (DPOAE).

The number of animals expressing the transgene after transuterine injection of virus into the embryonic otocyst was lower than the number of injected embryos. Potential reasons include a preferential survival of non-injected embryos, leakage of viral particles from the otocyst after injection and a too low number of injected viral particles, which we estimated to $1 \times 10^6 - 5 \times 10^7$ particles per otocyst.

Furthermore in contrast to Bedrosian et al. (2006) we were not able to identify injected versus non-injected animals after birth. We also injected dextran bound Alexafluor 488 into the fourth ventricle in embryos that had the otocyst injected with virus. However, in contrast to Bedrosian et al. we were not able to see the fluorescence through the skull of the P0 pups upon blue light excitation. Therefore, we cannot directly compare our results to the results of Bedrosian et al. who used AAV2/1 and found 63% of injected embryos being born with much higher transduction rates than we found in our experiments. However, they did not state the number of injected and non-injected embryos or the number of injected animals that, indeed, expressed transgenic protein. As we found some animals to have very low transduction rates with less than 20% IHCs expressing transgenic protein we decided to exclude these from auditory function analysis, because functional characteristics induced by transgenic protein may not show up if it is only expressed in few cells. Transduction rates of positive animals were similar between the three viruses used, with AAV1/2 and Ad5 being slightly superior to AAV6, which were therefore used for further experiments.

Nevertheless, hearing of animals injected with any of the three viruses was tested. We found that none of the two AAV serotypes affected ABR thresholds,

amplitudes or DPOAEs. Only the amplitude of ABR wave I was slightly affected in most left ears of AAV1/2-eGFP injected animals. This effect was observed in both positive and negative ears, thus suggesting that it may be caused by the injection itself. As other studies did not report high immunogenicity of AAVs (for review see Hildebrand et al., 2008) possible reasons for the reduced wave I include: (i) there was a small bacterial contamination in the virus lot, which caused some inflammation or (ii) the injection of this litter caused more damage than usual. In contrast to AAVs Ad5-eGFP did seem to harm the inner ear of injected animals. The ABR thresholds were elevated in left, injected ears of positive animals and wave I amplitude was reduced. Similar to AAV1/2 injected animals negative animals also showed a reduction in wave I amplitude but negative left ears were still significantly better than positive left ears. These results lead us to the conclusion that in addition to a similar effect as seen in AAV1/2-eGFP injected animals the adenovirus itself has a negative effect. Possibly the virus causes an inflammatory process due to its immunogenicity, which is also supported by an impairment seen in DPOAE of left, positive ears. However, the function of OHCs may further be affected by the expression of specific virus encoded proteins.

To clarify this question further, observation of older animals is required in future experiments. If the DPOAEs degrade over time it would be likely that an inflammatory process takes place, whereas non-degrading DPOAEs would support the notion of a protein specific impairment. Further, correlation of DPOAE SPL and transduction rates in more animals could shed more light on a potential dependence of the impairment on gene dosage.

We conclude that when only few animals are needed for analysis the method of otocyst injection is very efficient, causing little harm to the injected animals. For short term applications or screens the use of virus is of great advantage as it opens the opportunity to test many constructs in a short time without the need to generate transgenic mouse lines.

Replacement of otoferlin with synaptotagmin 1 does not suffice to restore hearing ability

The neuronal calcium sensor synaptotagmin 1 (Syt1) was tested for its ability to replace otoferlin, the putative calcium sensor at the inner hair cell (IHC) ribbon synapse. Syt1 was expressed in inner hair cells lacking otoferlin via embryonic trans-

uterine otocyst injections of AAV1/2-Syt1-eGFP in *Otof*^{-/-} animals to find whether hearing can be reestablished.

First, the virus was tested in wild type animals to reveal potential, if any, negative effects of the transgenic protein, but no impairment was found. The ABR thresholds were normal as were the ABR amplitudes. The only small changes found were reduced DPOAE amplitudes in most positive animals on left and right side, indicating that the virus injection may have a minor negative effect on the OHCs with no impact on IHC function or auditory sensitivity.

Next, injections were performed on *Otof*^{+/-} mice mated with *Otof*^{-/-} mice and the offspring was separated into two groups, heterozygote *Otof*^{+/-} and homozygote *Otof*^{-/-} animals. *Otof*^{+/-} mice were expected to also show no effect of transgenic Syt1 as those mice show almost (~ 80%) normal otoferlin protein levels (Pangrsic et al., 2010). However, in the heterozygote animals the left ear ABR thresholds were slightly increased in Syt1 expressing animals compared to those of the right ear or to negative littermates. Furthermore ABR wave I amplitudes were significantly decreased in positive, but also in negative animals comparing them to the wild type animals. Possible reasons for this finding include an equal impairment of IHC function or, as wave I amplitude is a better measure for the number of functional IHCs than ABR thresholds (Khimich et al., 2005; Kujawa and Liberman, 2006), this result may also indicate that one copy of *OTOF* is not enough for normal IHC exocytosis.

Apart from the reduced wave I amplitude observed in heterozygote animals no effect on the amplitude was seen in the comparison of left and right ear of positive *Otof*^{+/-} mice. This strongly suggests that the seen effect is only due to the heterozygote genotype and not due to Syt1 expression or injection of AAV itself. Again minimally reduced DPOAE levels were detected having probably no consequence for ABR.

Finally we analyzed *Otof*^{-/-} mice expressing Syt1 and found reasonably high transduction rates in 4 animals. Despite normal DPOAE levels none of these animals showed any ABR wave at 100 dB SPL. Additionally, Reisinger et al. (2011) found a lack of exocytosis in Syt1 positive IHCs of *Otof*^{-/-} animals.

Therefore, it seems that the expression of Syt1 does not cause any negative effect in HCs, but also it is also not able to restore IHC function by replacing otoferlin in *Otof*^{-/-} animals. The much larger protein otoferlin may have more or even different functions at the ribbon synapse than Syt1 has in the neuronal synapse. However, also the lack of native interaction partners of Syt1 like SNAP25 or Syntaxin 1 (Nouvian et al., 2011) or the lack of complexins, facilitating exocytosis in neuronal synapses

(Strenzke et al., 2009), could prevent exocytosis in the Syt1 positive IHCs of *Otof*^{-/-} animals.

To confirm these results Reisinger et al. (2011) also performed the opposite experiment. Otoferlin was expressed in neuronal cultures lacking Syt1, but again no synchronous exocytosis was found. Therefore, we conclude that there is no simple functional equivalence of the two proteins. This suggests that otoferlin functions in a different manner than Syt1. A study by Johnson et al. (2010) also indicates that the two proteins fulfill deviating Ca²⁺ sensing function. They found high order Ca²⁺ dependence in immature IHCs which they account to Syt1 and 2 opposing the linear Ca²⁺ dependence found in mature IHCs (Johnson et al., 2010). In mature IHCs which do not express Syt1 and 2 anymore they conclude that synaptotagmin 4 makes the relationship of Ca²⁺ entry and vesicle fusion linear. In a study by Beurg et al. (2010) the role of synaptotagmins and otoferlin at the IHC ribbon synapse is further discussed. They show otoferlin independent exocytosis in immature IHCs which switches to an otoferlin dependent mode at P4 when synaptic reorganization and maturation occurs. Synaptotagmin 1, 2 and 7 are shown to be dispensable for exocytosis in immature IHCs and it is indicated that Syt1 - dependent recovery of the readily releasable pool of synaptic vesicles (Beurg et al., 2010). They assume the involvement of a still unknown Ca²⁺ sensor at immature IHC synapses that are still lacking otoferlin.

One way to further the knowledge of otoferlin function could be the generation of mutants lacking single or multiple C₂ domains, and expressing those proteins in the *Otof*^{-/-} animals analyzing the overall hearing ability as well as cellular morphology and exocytosis. For this purpose initially wild type otoferlin needs to be expressed via viral transduction in those animals to characterize the difference of wild type and mutant otoferlin. Another interesting experiment would be to replace one or two otoferlin C₂ domains with Syt1 C₂A or C₂B to see whether exocytosis can be reestablished in *Otof*^{-/-} mice and to conclude on the ability of single protein domains to replace each other.

Expression of transgenic otoferlin in IHCs does not restore hearing in *Otof*^{-/-} mice

Wild type otoferlin was expressed *in vivo* in *Otof*^{-/-} mouse inner ears for several reasons. We intended to characterize transgenic otoferlin in comparison to native protein at various transduction rates in order to find whether the deafness of *Otof*^{Pga/Pga}

mice might be caused by reduced protein levels. A successful recovery of hearing in the injected *Otof*^{-/-} mice could be taken as starting point for the injection and expression of otoferlin mutants to analyze their effects in future experiments. Furthermore we attempted to evaluate viral gene transfer for future gene therapy in case of otoferlin dependent deafness.

Initially the virus (Ad5-mOtof^{wt}-eGFP) was tested on wild type animals and as already seen with Ad5-eGFP a slight increase in ABR thresholds, a decrease in wave I amplitude and decreased DPOAE SPL were found. The harmful effect of Ad5-mOtof^{wt}-eGFP on OHC function was stronger than that in Ad5-eGFP injected animals. A third virus, Ad5-mOtof^{f^{ga}}-eGFP, which was originally meant to be used for analyzing whether increasing the concentration of otoferlin_{Pga} may suffice to restore hearing, appears to be even lethal to the injected embryos. This is likely caused by a contamination of this particular lot of virus. The generally more harmful effects of adenovirus compared to AAV are probably caused by its high immunogenicity and the ensuing inflammatory response in the inner ear after injection.

As the hearing impairment caused by Ad5-mOtof^{wt}-eGFP did not entirely abolish ABR waves or DPOAEs the virus was also injected into otoferlin knock out mice (*Otof*^{-/-}). In these animals we were able to show successful expression of transgenic otoferlin in IHCs via embryonic transuterine otocyst injection of adenovirus. Similar as done for the supplementation experiment with Syt1 the animals were tested for their hearing ability, analyzing whether it was possible to replace native protein with transgenically expressed otoferlin. As in *Otof*^{-/-} animals expressing Syt1 no ABR waves could be detected at even higher sound pressure levels (110 dB) and using an even more efficient stimulus (chirp low and high).

There are several potential causes for the missing ABR waves. First, if OHCs are not fully functional (as suggested by affected DPOAEs) and the number of successfully transduced IHCs is low, the neurotransmitter release might not be strong or synchronous enough for the generation of a detectable ABR wave. There is evidence that a lack of synchronous release leads to the absence of proper ABR waves (Starr et al., 1996). Secondly, it is possible that other neurons in the auditory pathway also require otoferlin; however, it is unlikely that these neurons are SGN as cochlea implants work well in DFNB9 patients (Rouillon et al., 2006) and in many experiments SGN were also found to express transgenic otoferlin. Further, a potential inflammatory process due to viral immunogenicity or injection itself might damage the cochlea to a degree that does not support hearing despite successful and sufficient transfection.

Currently, there is some evidence for malformations of semicircular canals, reduced size of cochlea, lag in maturation of hair cells and possible disorganization of stereocilia in some injected inner ears. Finally, it is possible that otoferlin expressed after otocyst injection of Ad5-mOtofwt-eGFP can not rescue exocytosis in IHCs. Currently, the last option seems most likely as preliminary data by T. Pangrsic and E. Reisinger (data not shown) demonstrated the absence of exocytosis in IHCs of *Otof*^{-/-} mice positive for Ad5-mOtofwt-eGFP transduction.

It is unclear what causes the failure to re-establish exocytosis in IHCs using the transuterine otocyst injections. The embryonic expression of otoferlin, long before endogenous otoferlin expression starts (at postnatal day 4; Beurg et al., 2010), may have a negative effect or damage by an inflammatory response might be too strong. Another reason could be the mislocalization of the transgenic protein; the amount of properly localized and functional protein could be too low or possibly the protein is not expressed correctly.

To test whether transgenic otoferlin is expressed correctly and to analyze its localization in more detail we will perform more immunohistochemical labeling of both the C- and the N-terminus of the protein and also ultra thin section analysis comparing wild type and transgenic otoferlin localization. To overcome possible negative effects of premature otoferlin expression the injection of virus could be shifted from E11.5 to prenatal P3 – P14 mice. Alternatively, different virus type or a different promoter could be used to start the expression later in development. A different virus type might also be less harmful to the cells, therefore reducing the possible inflammation.

pH sensitive GFP variants for monitoring exocytosis in IHCs

To establish a tool for optical monitoring of exocytosis in IHCs we expressed a pH sensitive GFP variant, ecliptic pHluorin (Sankaranarayanan et al., 2000), fused to the vesicular glutamate transporter 1 (vGlut1) in inner hair cells (IHC). The native vesicular glutamate transporter in IHCs is vGlut3 (Seal et al., 2008), therefore we analyzed localization of the fusion protein and co localization with the native vGlut3. VGlut1-pHluorin localizes throughout the cell with exception of the nucleus, the concentration is slightly increased in the base of the cell, similar to the localization of vGlut3. However, in a more detailed analysis of co localization we compared the fluorescence intensities of immunolabeled vGlut3 and the fusion protein along a line of

interest through the IHC from apex to base. With this method we found that vGlut1-pHluorin concentration is higher in the apex relative to the base compared to vGlut3.

Although we cannot compare absolute protein levels with this method we can show that this change in localization is not an effect of higher protein levels and therefore of a potential saturation of synaptic vesicles with vGlut1-pHluorin as we also analyzed cells with a rather low vGlut1-pHluorin expression level and found the same relative effect. Therefore we conclude that this effect results from a slightly less efficient targeting of the transgene compared to native vGlut3.

Nevertheless vGlut1-pHluorin does not seem to intervene with any inner ear function as hearing thresholds as well as DPOAEs (data not shown) are normal. The overall fluorescence increase in IHCs expressing vGlut1-pHluorin after pH neutralization was 2 fold to background fluorescence. Further a detailed analysis of hot spots of fluorescence increase, the readout of pHluorin fluorescence of silent and stimulated cells and also the exocytosis characteristics of wild type animals expressing vGlut1-pHluorin in IHCs need to be further studied in detail.

Despite the promising results however, for a tool like this, which will probably be applied also for other studies a transgenic mouse line expressing the protein in IHCs would serve better than needing to inject a virus for every experiment. Another possibility would be the generation of virus for simultaneous expression of the protein of interest; in this case otoferlin and the pHluorin construct, then exocytosis characteristics of the altered protein can be easily assessed.

Summary

In humans deafness is caused by environmental but also by genetic factors. Mutations in the gene encoding otoferlin are one genetic cause of deafness, leading to DFNB9 an autosomal recessive nonsyndromic hearing loss. The function of otoferlin is still not fully understood. It is suspected to act as the Ca^{2+} sensor for synaptic vesicle fusion at the inner hair cell ribbon synapse, and as a regulator of vesicle replenishment. We analyzed the most C-terminal C_2 domain C_2F in detail via CD-spectroscopy, fluorimetry and using a floatation assay. We did not find convincing evidence for Ca^{2+} and phospholipid binding.

We also tested the effect of the *pachanga* mutation, a mutation that causes reduced speed of vesicle replenishment. $\text{C}_2\text{F}_{\text{Pga}}$ did not show any differences to $\text{C}_2\text{F}_{\text{wt}}$ in the biochemical assays, however analyzing protein and mRNA level we found that $\text{Otof}^{\text{Pga/Pga}}$ animals have reduced otoferlin protein levels compared to wild type animals but increased mRNA levels. This may suggest that the cells try to compensate the lack of protein.

To test the hypothesis that otoferlin is a synaptotagmin 1 (Syt1) - like Ca^{2+} sensor we tried to replace otoferlin with Syt1, the major Ca^{2+} sensor at conventional synapses. We established viral gene transfer into IHCs using transuterine injection of the embryonic otocyst and expressed Syt1 in IHCs of deaf $\text{Otof}^{-/-}$ mice. However, we did not find a rescue of the deafness phenotype. As a control experiment but also as a potential gene therapy approach we expressed otoferlin in the $\text{Otof}^{-/-}$ mice via the same technique and again we were not able to restore hearing. Nevertheless this may open up a strategy to test mutated otoferlin in vitro.

Last. we adapted the pHluorin optical assay of exocytosis to inner hair cells. We expressed pHluorin coupled to the vesicular glutamate transporter 1 (vGlut1). PHluorin is a pH dependent GFP variant already used in neurons, its fluorescence unquenches upon vesicles fusion with the plasma membrane and requenches upon acidification of vesicular lumen after endocytosis, thus enabling visualization of exocytosis and endocytosis. We found that the construct is expressed at high rates but does not entirely co localize with endogenous vGlut3. Preliminary data by A. Wong shows that fluorescence increases at spots of exocytosis, promising that the method can indeed be used as optical assay for exo- and endocytosis in IHCs.

References

- Adato, A., Raskin, L., Petit, C., Bonne-Tamir, B., 2000. Deafness heterogeneity in a Druze isolate from the Middle East: novel OTOF and PDS mutations, low prevalence of GJB2 35delG mutation and indication for a new DFNB locus. *Eur. J. Hum. Genet* 8, 437-442.
- Bartlett, J.S., Samulski, R.J., McCown, T.J., 1998. Selective and rapid uptake of adeno-associated virus type 2 in brain. *Hum. Gene Ther* 9, 1181-1186.
- Bedrosian, J.C., Gratton, M.A., Brigande, J.V., Tang, W., Landau, J., Bennett, J., 2006. In vivo delivery of recombinant viruses to the fetal murine cochlea: transduction characteristics and long-term effects on auditory function. *Mol. Ther* 14, 328-335.
- Beurg, M., Fettiplace, R., Nam, J.-H., Ricci, A.J., 2009. Localization of inner hair cell mechanotransducer channels using high-speed calcium imaging. *Nat Neurosci* 12, 553-558.
- Beurg, M., Michalski, N., Safieddine, S., Bouleau, Y., Schneggenburger, R., Chapman, E.R., Petit, C., Dulon, D., 2010. Control of Exocytosis by Synaptotagmins and Otoferlin in Auditory Hair Cells. *J. Neurosci.* 30, 13281-13290.
- Bonifacino, J.S., Glick, B.S., 2004. The Mechanisms of Vesicle Budding and Fusion. *Cell* 116, 153-166.
- Brownell, W., Bader, C., Bertrand, D., de Ribaupierre, Y., 1985. Evoked mechanical responses of isolated cochlear outer hair cells. *Science* 227, 194 -196.
- Chapman, E.R., 2002. Synaptotagmin: A Ca²⁺ sensor that triggers exocytosis? *Nat Rev Mol Cell Biol* 3, 498-508.
- Choi, B.Y., Ahmed, Z.M., Riazuddin, S., Bhinder, M.A., Shahzad, M., Husnain, T., Riazuddin, S., Griffith, A.J., Friedman, T.B., 2009. Identities and frequencies of mutations of the otoferlin gene (OTOF) causing DFNB9 deafness in Pakistan. *Clinical Genetics* 75, 237-243.
- Coura, R. dos S., Nardi, N.B., 2008. A role for adeno-associated viral vectors in gene therapy. *Genet. Mol. Biol.* 31.
- Dallos, P., Harris, D., 1978. Properties of auditory nerve responses in absence of outer hair cells. *J. Neurophysiol* 41, 365-383.
- Dallos, P., 1992. The Active Cochlea. *J. Neurosci* 12, 4575 - 4585.

- References -

- Dallos, P., Fakler, B., 2002. Prestin, a new type of motor protein. *Nat. Rev. Mol. Cell Biol* 3, 104-111.
- Davletov, B.A., Südhof, T.C., 1993. A single C2 domain from synaptotagmin I is sufficient for high affinity Ca²⁺/phospholipid binding. *J. Biol. Chem* 268, 26386-26390.
- Dazert, S., Aletsee, C., Brors, D., Gravel, C., Sendtner, M., Ryan, A., 2001. In vivo adenoviral transduction of the neonatal rat cochlea and middle ear. *Hear. Res* 151, 30-40.
- Fernandez-Chacon, R., Königstorfer, A., Gerber, S.H., Garcia, J., Matos, M.F., Stevens, C.F., Brose, N., Rizo, J., Rosenmund, C., Südhof, T.C., 2001. Synaptotagmin I functions as a calcium regulator of release probability. *Nature* 410, 41-49.
- Fettiplace, R., Fuchs, P.A., 1999. Mechanisms of hair cell tuning. *Annu. Rev. Physiol.* 61, 809-834.
- Fettiplace, R., Hackney, C.M., 2006. The sensory and motor roles of auditory hair cells. *Nat. Rev. Neurosci* 7, 19-29.
- Frank, T., Rutherford, M.A., Strenzke, N., Neef, A., Pangrsic, T., Khimich, D., Fejtova, A., Gundelfinger, E.D., Liberman, M.C., Harke, B., Bryan, K.E., Lee, A., Egner, A., Riedel, D., Moser, T., 2010. Bassoon and the Synaptic Ribbon Organize Ca²⁺ Channels and Vesicles to Add Release Sites and Promote Refilling. *Neuron* 68, 724-738.
- Geppert, M., Goda, Y., Hammer, R.E., Li, C., Rosahl, T.W., Stevens, C.F., Südhof, T.C., 1994. Synaptotagmin I: A major Ca²⁺ sensor for transmitter release at a central synapse. *Cell* 79, 717-727.
- Gillespie, P.G., Walker, R.G., 2001. Molecular basis of mechanosensory transduction. *Nature* 413, 194-202.
- Han, R., Campbell, K.P., 2007. Dysferlin and Muscle Membrane Repair. *Curr Opin Cell Biol* 19, 409-416.
- Heidrych, P., Zimmermann, U., Breß, A., Pusch, C.M., Ruth, P., Pfister, M., Knipper, M., Blin, N., 2008. Rab8b GTPase, a protein transport regulator, is an interacting partner of otoferlin, defective in a human autosomal recessive deafness form. *Hum. Mol. Genet* 17, 3814 -3821.
- Heidrych, P., Zimmermann, U., Kuhn, S., Franz, C., Engel, J., Duncker, S.V., Hirt, B., Pusch, C.M., Ruth, P., Pfister, M., Marcotti, W., Blin, N., Knipper, M., 2009. Otoferlin interacts with myosin VI: implications for maintenance of the

- References -

- basolateral synaptic structure of the inner hair cell. *Hum. Mol. Genet* 18, 2779-2790.
- Helfmann, S., Neumann, P., Tittmann, K., Moser, T., Ficner, R., Reisinger, E., 2011. The Crystal Structure of the C(2)A Domain of Otoferlin Reveals an Unconventional Top Loop Region. *J Mol Biol.*
- Hildebrand, M.S., Newton, S.S., Gubbels, S.P., Sheffield, A.M., Kochhar, A., de Silva, M.G., Dahl, H.-H.M., Rose, S.D., Behlke, M.A., Smith, R.J.H., 2008. Advances in molecular and cellular therapies for hearing loss. *Mol. Ther* 16, 224-236.
- Hildinger, M., Auricchio, A., Gao, G., Wang, L., Chirmule, N., Wilson, J.M., 2001. Hybrid Vectors Based on Adeno-Associated Virus Serotypes 2 and 5 for Muscle-Directed Gene Transfer. *J. Virol.* 75, 6199-6203.
- Holt, J.R., Johns, D.C., Wang, S., Chen, Z.Y., Dunn, R.J., Marban, E., Corey, D.P., 1999. Functional expression of exogenous proteins in mammalian sensory hair cells infected with adenoviral vectors. *J. Neurophysiol* 81, 1881-1888.
- Houseman, M., Jackson, A., Al-Gazali, L., Badin, R., Roberts, E., Mueller, R., 2001. A novel mutation in a family with non-syndromic sensorineural hearing loss that disrupts the newly characterised OTOF long isoforms. *J Med Genet* 38, e25-e25.
- Hui, E., Johnson, C.P., Yao, J., Dunning, F.M., Chapman, E.R., 2009. Synaptotagmin-Mediated Bending of the Target Membrane Is a Critical Step in Ca²⁺-Regulated Fusion. *Cell* 138, 709-721.
- Hutchin, T., Coy, N.N., Conlon, H., Telford, E., Bromelow, K., Blaydon, D., Taylor, G., Coghill, E., Brown, S., Trembath, R., Liu, X.Z., Bitner-Glindzicz, M., Mueller, R., 2005. Assessment of the genetic causes of recessive childhood non-syndromic deafness in the UK - implications for genetic testing. *Clin. Genet* 68, 506-512.
- Jahn, R., Scheller, R.H., 2006. SNAREs - engines for membrane fusion. *Nat Rev Mol Cell Biol* 7, 631-643.
- Jeffreys, A.J., Wilson, V., Neumann, R., Keyte, J., 1988. Amplification of human minisatellites by the polymerase chain reaction: towards DNA fingerprinting of single cells. *Nucleic Acids Res* 16, 10953-10971.
- Johnson, C.P., Chapman, E.R., 2010. Otoferlin is a calcium sensor that directly regulates SNARE-mediated membrane fusion. *J Cell Biol* 191, 187 -197.
- Johnson, S.L., Franz, C., Kuhn, S., Furness, D.N., Ruttiger, L., Munkner, S., Rivolta, M.N., Seward, E.P., Herschman, H.R., Engel, J., Knipper, M., Marcotti, W.,

- References -

2010. Synaptotagmin IV determines the linear Ca²⁺ dependence of vesicle fusion at auditory ribbon synapses. *Nat Neurosci* 13, 45-52.
- Johnson, S.L., Beurg, M., Marcotti, W., Fettiplace, R., 2011. Prestin-Driven Cochlear Amplification Is Not Limited by the Outer Hair Cell Membrane Time Constant. *Neuron* 70, 1143-1154.
- Kachar, B., Brownell, W.E., Altschuler, R., Fex, J., 1986. Electrokinetic shape changes of cochlear outer hair cells. *Nature* 322, 365-368.
- Kelley, M.W., 2006. Regulation of cell fate in the sensory epithelia of the inner ear. *Nat. Rev. Neurosci* 7, 837-849.
- Kesser, B.W., Hashisaki, G.T., Holt, J.R., 2008. Gene Transfer in Human Vestibular Epithelia and the Prospects for Inner Ear Gene Therapy. *Laryngoscope* 118, 821-831.
- Khimich, D., Nouvian, R., Pujol, R., tom Dieck, S., Egnér, A., Gundelfinger, E.D., Moser, T., 2005. Hair cell synaptic ribbons are essential for synchronous auditory signalling. *Nature* 434, 889-894.
- Kneen, M., Farinas, J., Li, Y., Verkman, A.S., 1998. Green fluorescent protein as a noninvasive intracellular pH indicator. *Biophys. J* 74, 1591-1599.
- Kügler, S., Hahnewald, R., Garrido, M., Reiss, J., 2007. Long-Term Rescue of a Lethal Inherited Disease by Adeno-Associated Virus-Mediated Gene Transfer in a Mouse Model of Molybdenum-Cofactor Deficiency. *Am J Hum Genet* 80, 291-297.
- Kujawa, S.G., Liberman, M.C., 2006. Acceleration of Age-Related Hearing Loss by Early Noise Exposure: Evidence of a Misspent Youth. *J Neurosci* 26, 2115-2123.
- Lalwani, A., Walsh, B., Reilly, P., Carvalho, G., Zolotukhin, S., Muzyczka, N., Mhatre, A., 1998. Long-term in vivo cochlear transgene expression mediated by recombinant adeno-associated virus. *Gene Ther* 5, 277-281.
- Lalwani, A.K., Jero, J., Mhatre, A.N., 2002. Current issues in cochlear gene transfer. *Audiol. Neurootol* 7, 146-151.
- Lee, M.H., Bell, R.M., 1991. Mechanism of protein kinase C activation by phosphatidylinositol 4,5-bisphosphate. *Biochemistry* 30, 1041-1049.
- LeMasurier, M., Gillespie, P.G., 2007. Hair bundles: keeping it together. *Nat Neurosci* 10, 11-12.
- Liberman, M.C., Gao, J., He, D.Z.Z., Wu, X., Jia, S., Zuo, J., 2002. Prestin is required for electromotility of the outer hair cell and for the cochlear amplifier. *Nature* 419, 300-304.

- References -

- Liu, Y., Okada, T., Nomoto, T., Ke, X., Kume, A., Ozawa, K., Xiao, S., 2007. Promoter effects of adeno-associated viral vector for transgene expression in the cochlea in vivo. *Exp. Mol. Med* 39, 170-175.
- Liu, Y., Okada, T., Sheykholslami, K., Shimazaki, K., Nomoto, T., Muramatsu, S.-I., Kanazawa, T., Takeuchi, K., Ajalli, R., Mizukami, H., Kume, A., Ichimura, K., Ozawa, K., 2005. Specific and efficient transduction of Cochlear inner hair cells with recombinant adeno-associated virus type 3 vector. *Mol. Ther* 12, 725-733.
- Luebke, A.E., Foster, P.K., Muller, C.D., Peel, A.L., 2001. Cochlear function and transgene expression in the guinea pig cochlea, using adenovirus- and adeno-associated virus-directed gene transfer. *Hum. Gene Ther* 12, 773-781.
- Luebke, A.E., Steiger, J.D., Hodges, B.L., Amalfitano, A., 2001. A modified adenovirus can transfect cochlear hair cells in vivo without compromising cochlear function. *Gene Ther* 8, 789-794.
- Mandell, J.W., Townes-Anderson, E., Czernik, A.J., Cameron, R., Greengard, P., De Camilli, P., 1990. Synapsins in the vertebrate retina: Absence from ribbon synapses and heterogeneous distribution among conventional synapses. *Neuron* 5, 19-33.
- Martens, S., Kozlov, M.M., McMahon, H.T., 2007. How Synaptotagmin Promotes Membrane Fusion. *Science* 316, 1205 -1208.
- McNeil, P.L., Kirchhausen, T., 2005. An emergency response team for membrane repair. *Nat Rev Mol Cell Biol* 6, 499-505.
- Melcher, J.R., Knudson, I.M., Fullerton, B.C., Guinan, J.J., Jr, Norris, B.E., Kiang, N.Y., 1996. Generators of the brainstem auditory evoked potential in cat. I. An experimental approach to their identification. *Hear. Res* 93, 1-27.
- Meyer, A.C., Frank, T., Khimich, D., Hoch, G., Riedel, D., Chapochnikov, N.M., Yarin, Y.M., Harke, B., Hell, S.W., Egner, A., Moser, T., 2009. Tuning of synapse number, structure and function in the cochlea. *Nat Neurosci* 12, 444-453.
- Miesenbock, G., De Angelis, D.A., Rothman, J.E., 1998. Visualizing secretion and synaptic transmission with pH-sensitive green fluorescent proteins. *Nature* 394, 192-195.
- Migliosi, V., Modamio-Hoybjor, S., Moreno-Pelayo, M., Rodriguez-Ballest..., M., Villamar, M., Telleria, D., Menendez, I., Moreno, F., del Castillo, I., 2002. Q829X, a novel mutation in the gene encoding otoferlin (OTOF), is frequently found in Spanish patients with prelingual non-syndromic hearing loss. *J Med Genet* 39, 502-506.

- References -

- Mirghomizadeh, F., Pfister, M., Apaydin, F., Petit, C., Kupka, S., Pusch, C.M., Zenner, H.P., Blin, N., 2002. Substitutions in the Conserved C2C Domain of Otoferlin Cause DFNB9, a Form of Nonsyndromic Autosomal Recessive Deafness. *Neurobiol Dis* 10, 157-164.
- Nouvian, R., Beutner, D., Parsons, T.D., Moser, T., 2006. Structure and function of the hair cell ribbon synapse. *J. Membr. Biol* 209, 153-165.
- Nouvian, R., Neef, J., Bulankina, A.V., Reisinger, E., Pangrsic, T., Frank, T., Sikorra, S., Brose, N., Binz, T., Moser, T., 2011. Exocytosis at the hair cell ribbon synapse apparently operates without neuronal SNARE proteins. *Nat Neurosci* advance online publication.
- Oliver, D., He, D.Z.Z., Klöcker, N., Ludwig, J., Schulte, U., Waldegger, S., Ruppertsberg, J.P., Dallos, P., Fakler, B., 2001. Intracellular Anions as the Voltage Sensor of Prestin, the Outer Hair Cell Motor Protein. *Science* 292, 2340-2343.
- Pangrsic, T., Lasarow, L., Reuter, K., Takago, H., Schwander, M., Riedel, D., Frank, T., Tarantino, L.M., Bailey, J.S., Strenzke, N., Brose, N., Muller, U., Reisinger, E., Moser, T., 2010. Hearing requires otoferlin-dependent efficient replenishment of synaptic vesicles in hair cells. *Nat Neurosci* 13, 869-876.
- Petoe, M.A., Bradley, A.P., Wilson, W.J., 2010. On chirp stimuli and neural synchrony in the suprathreshold auditory brainstem response. *J. Acoust. Soc. Am.* 128, 235-246.
- Poirier, M.A., Xiao, W., Macosko, J.C., Chan, C., Shin, Y.-K., Bennett, M.K., 1998. The synaptic SNARE complex is a parallel four-stranded helical bundle. *Nat Struct Mol Biol* 5, 765-769.
- Praetorius, M., Baker, K., Brough, D.E., Plinkert, P., Staecker, H., 2007. Pharmacodynamics of adenovector distribution within the inner ear tissues of the mouse. *Hear. Res* 227, 53-58.
- Praetorius, M., Brough, D.E., Hsu, C., Plinkert, P.K., Pfannenstiel, S.C., Staecker, H., 2009. Adenoviral vectors for improved gene delivery to the inner ear. *Hear. Res* 248, 31-38.
- Praetorius, M., Knipper, M., Schick, B., Tan, J., Limberger, A., Carnicero, E., Alonso, M.T., Schimmang, T., 2002. A novel vestibular approach for gene transfer into the inner ear. *Audiol. Neurootol* 7, 324-334.

- References -

- Qing, K., Mah, C., Hansen, J., Zhou, S., Dwarki, V., Srivastava, A., 1999. Human fibroblast growth factor receptor 1 is a co-receptor for infection by adeno-associated virus 2. *Nat Med* 5, 71-77.
- Ramakrishnan, N.A., Drescher, M.J., Drescher, D.G., 2009. Direct Interaction of Otoferlin with Syntaxin 1A, SNAP-25, and the L-type Voltage-gated Calcium Channel CaV1.3. *J Biol Chem* 284, 1364-1372.
- Reisinger, E., Bresee, C., Neef, J., Nair, R., Reuter, K., Bulankina, A., Nouvian, R., Koch, M., Bückers, J., Kastrup, L., Roux, I., Petit, C., Hell, S.W., Brose, N., Rhee, J.-S., Kügler, S., Brigande, J.V., Moser, T., 2011. Probing the Functional Equivalence of Otoferlin and Synaptotagmin 1 in Exocytosis. *The Journal of Neuroscience* 31, 4886 -4895.
- Rickman, C., Archer, D.A., Meunier, F.A., Craxton, M., Fukuda, M., Burgoyne, R.D., Davletov, B., 2004. Synaptotagmin Interaction with the Syntaxin/SNAP-25 Dimer Is Mediated by an Evolutionarily Conserved Motif and Is Sensitive to Inositol Hexakisphosphate. *J Biol Chem* 279, 12574 -12579.
- Rizo, J., Südhof, T.C., 1998. C2-domains, structure and function of a universal Ca²⁺-binding domain. *J. Biol. Chem* 273, 15879-15882.
- Rizo, J., Rosenmund, C., 2008. Synaptic vesicle fusion. *Nat Struct Mol Biol* 15, 665-674.
- Rodríguez-Ballesteros, M., del Castillo, F.J., Martín, Y., Moreno-Pelayo, M.A., Morera, C., Prieto, F., Marco, J., Morant, A., Gallo-Terán, J., Morales-Angulo, C., Navas, C., Trinidad, G., Tapia, M.C., Moreno, F., del Castillo, I., 2003. Auditory neuropathy in patients carrying mutations in the otoferlin gene (OTOF). *Hum. Mutat* 22, 451-456.
- Rodríguez-Ballesteros, M., Reynoso, R., Olarte, M., Villamar, M., Morera, C., Santarelli, R., Arslan, E., Medá, C., Curet, C., Völter, C., Sainz-Quevedo, M., Castorina, P., Ambrosetti, U., Berrettini, S., Frei, K., Tedín, S., Smith, J., Cruz Tapia, M., Cavallé, L., Gelvez, N., Primignani, P., Gómez-Rosas, E., Martín, M., Moreno-Pelayo, M.A., Tamayo, M., Moreno-Barral, J., Moreno, F., del Castillo, I., 2008. A multicenter study on the prevalence and spectrum of mutations in the otoferlin gene (OTOF) in subjects with nonsyndromic hearing impairment and auditory neuropathy. *Hum. Mutat* 29, 823-831.
- Rosenmund, C., Rettig, J., Brose, N., 2003. Molecular mechanisms of active zone function. *Current Opinion in Neurobiology* 13, 509-519.

- References -

- Rouillon, I., Marcolla, A., Roux, I., Marlin, S., Feldmann, D., Couderc, R., Jonard, L., Petit, C., Denoyelle, F., Garabédian, E.N., Loundon, N., 2006. Results of cochlear implantation in two children with mutations in the OTOF gene. *Int J Pediatr Otorhinolaryngol* 70, 689-696.
- Roux, I., Safieddine, S., Nouvian, R., Grati, M., Simmler, M.-C., Bahloul, A., Perfettini, I., Le Gall, M., Rostaing, P., Hamard, G., Triller, A., Avan, P., Moser, T., Petit, C., 2006. Otoferlin, Defective in a Human Deafness Form, Is Essential for Exocytosis at the Auditory Ribbon Synapse. *Cell* 127, 277-289.
- Safieddine, S., Wenthold, R.J., 1999. SNARE complex at the ribbon synapses of cochlear hair cells: analysis of synaptic vesicle- and synaptic membrane-associated proteins. *Eur. J. Neurosci* 11, 803-812.
- Safieddine, S., Wenthold, R.J., 1997. The Glutamate Receptor Subunit delta 1 Is Highly Expressed in Hair Cells of the Auditory and Vestibular Systems. *J. Neurosci.* 17, 7523-7531.
- Sakaguchi, H., Tokita, J., Müller, U., Kachar, B., 2009. Tip links in hair cells: molecular composition and role in hearing loss. *Curr Opin Otolaryngol Head Neck Surg* 17, 388-393.
- Sankaranarayanan, S., De Angelis, D., Rothman, J.E., Ryan, T.A., 2000. The use of pHluorins for optical measurements of presynaptic activity. *Biophys. J* 79, 2199-2208.
- Schwander, M., Sczaniecka, A., Grillet, N., Bailey, J.S., Avenarius, M., Najmabadi, H., Steffy, B.M., Federe, G.C., Lagler, E.A., Banan, R., Hice, R., Grabowski-Boase, L., Keithley, E.M., Ryan, A.F., Housley, G.D., Wiltshire, T., Smith, R.J.H., Tarantino, L.M., Muller, U., 2007. A Forward Genetics Screen in Mice Identifies Recessive Deafness Traits and Reveals That Pejvakin Is Essential for Outer Hair Cell Function. *J. Neurosci.* 27, 2163-2175.
- Seal, R.P., Akil, O., Yi, E., Weber, C.M., Grant, L., Yoo, J., Clause, A., Kandler, K., Noebels, J.L., Glowatzki, E., Lustig, L.R., Edwards, R.H., 2008. Sensorineural deafness and seizures in mice lacking vesicular glutamate transporter 3. *Neuron* 57, 263-275.
- Söllner, T., Whiteheart, S.W., Brunner, M., Erdjument-Bromage, H., Geromanos, S., Tempst, P., Rothman, J.E., 1993. SNAP receptors implicated in vesicle targeting and fusion. *Nature* 362, 318-324.

- References -

- Sonntag, M., Englitz, B., Typlt, M., Rübtsamen, R., 2011. The Calyx of Held Develops Adult-Like Dynamics and Reliability by Hearing Onset in the Mouse In Vivo. *The Journal of Neuroscience* 31, 6699-6709.
- Spankovich, C., Hood, L.J., Wesley Grantham, D., Polley, D.B., 2008. Application of frequency modulated chirp stimuli for rapid and sensitive ABR measurements in the rat. *Hearing Research* 245, 92-97.
- Starr, A., Picton, T.W., Sininger, Y., Hood, L.J., Berlin, C.I., 1996. Auditory neuropathy. *Brain* 119, 741-753.
- Strenzke, N., Chanda, S., Kopp-Scheinpflug, C., Khimich, D., Reim, K., Bulankina, A.V., Neef, A., Wolf, F., Brose, N., Xu-Friedman, M.A., Moser, T., 2009. Complexin-I is required for high-fidelity transmission at the endbulb of Held auditory synapse. *J. Neurosci* 29, 7991-8004.
- Südhof, T.C., Scheller, R.H., 2003. Mechanism and regulation of neurotransmitter release, in: *Synapses* ed. W. M. Cowan, T. C. Südhof, and C. F. Stevens. JHU Press.
- Summerford, C., Bartlett, J.S., Samulski, R.J., 1999. α V β 5 integrin: a co-receptor for adeno-associated virus type 2 infection. *Nat Med* 5, 78-82.
- Summerford, C., Samulski, R.J., 1998. Membrane-Associated Heparan Sulfate Proteoglycan Is a Receptor for Adeno-Associated Virus Type 2 Virions. *J. Virol.* 72, 1438-1445.
- Sutton, R.B., Fasshauer, D., Jahn, R., Brunger, A.T., 1998. Crystal structure of a SNARE complex involved in synaptic exocytosis at 2.4 Å resolution. *Nature* 395, 347-353.
- Taura, A., Taura, K., Choung, Y.H., Masuda, M., Pak, K., Chavez, E., Ryan, A.F., 2010. Histone deacetylase inhibition enhances adenoviral vector transduction in inner ear tissue. *Neuroscience* 166, 1185-1193.
- Tekin, M., Akcayoz, D., Incesulu, A., 2005. A novel missense mutation in a C2 domain of OTOF results in autosomal recessive auditory neuropathy. *Am. J. Med. Genet. A* 138, 6-10.
- Varga, R., Avenarius, M.R., Kelley, P.M., Keats, B.J., Berlin, C.I., Hood, L.J., Morlet, T.G., Brashears, S.M., Starr, A., Cohn, E.S., Smith, R.J.H., Kimberling, W.J., 2006. OTOF mutations revealed by genetic analysis of hearing loss families including a potential temperature sensitive auditory neuropathy allele. *J Med Genet* 43, 576-581.

- References -

- Varga, R., Kelley, P., Keats, B., Starr, A., Leal, S., Cohn, E., Kimberling, W., 2003. Non-syndromic recessive auditory neuropathy is the result of mutations in the otoferlin (OTOF) gene. *J Med Genet* 40, 45-50.
- Wang, D.-Y., Wang, Y.-C., Weil, D., Zhao, Y.-L., Rao, S.-Q., Zong, L., Ji, Y.-B., Liu, Q., Li, J.-Q., Yang, H.-M., Shen, Y., Benedict-Alderfer, C., Zheng, Q.-Y., Petit, C., Wang, Q.-J., 2010. Screening mutations of OTOF gene in Chinese patients with auditory neuropathy, including a familial case of temperature-sensitive auditory neuropathy. *BMC Medical Genetics* 11, 79.
- Washington, N.L., Ward, S., 2006. FER-1 regulates Ca²⁺-mediated membrane fusion during *C. elegans* spermatogenesis. *J. Cell. Sci* 119, 2552-2562.
- Waters, M.G., Hughson, F.M., 2000. Membrane tethering and fusion in the secretory and endocytic pathways. *Traffic* 1, 588-597.
- Whyte, J.R.C., Munro, S., 2002. Vesicle tethering complexes in membrane traffic. *J Cell Sci* 115, 2627-2637.
- Wu, E., Nemerow, G.R., 2004. Virus yoga: the role of flexibility in virus host cell recognition. *Trends in Microbiology* 12, 162-169.
- Wu, Z., Asokan, A., Samulski, R.J., 2006. Adeno-associated Virus Serotypes: Vector Toolkit for Human Gene Therapy. *Mol Ther* 14, 316-327.
- Xie, Q., Bu, W., Bhatia, S., Hare, J., Somasundaram, T., Azzi, A., Chapman, M.S., 2002. The atomic structure of adeno-associated virus (AAV-2), a vector for human gene therapy. *Proc Natl Acad Sci U S A* 99, 10405-10410.
- Yasunaga, S., Grati, M., Chardenoux, S., Smith, T.N., Friedman, T.B., Lalwani, A.K., Wilcox, E.R., Petit, C., 2000. OTOF encodes multiple long and short isoforms: genetic evidence that the long ones underlie recessive deafness DFNB9. *Am. J. Hum. Genet* 67, 591-600.
- Yasunaga, S., Grati, M., Cohen-Salmon, M., El-Amraoui, A., Mustapha, M., Salem, N., El-Zir, E., Loiselet, J., Petit, C., 1999. A mutation in OTOF, encoding otoferlin, a FER-1-like protein, causes DFNB9, a nonsyndromic form of deafness. *Nat. Genet* 21, 363-369.
- Yoshihara, M., Littleton, J.T., 2002. Synaptotagmin I Functions as a Calcium Sensor to Synchronize Neurotransmitter Release. *Neuron* 36, 897-908.

Acknowledgements

I would like to thank Tobias Moser for the opportunity to work on this interesting and challenging project in his laboratory, which provides an excellent working environment. I very much appreciate my PhD committee Nils Brose and Reinhard Jahn for the efforts they took to support me and for their helpful advice during my PhD thesis.

I thank the Boehringer Ingelheim Fonds for providing me with a PhD Fellowship, the federal state of Lower Saxony for granting me with a Georg-Christoph-Lichtenberg Stipend, and the SFB 889 TPA4 for funding my work.

Further I would like to thank Tobias Moser, Ellen Reisinger and Victor Hernandez for repeated help, new ideas and constant support during my PhD thesis. Many thanks also to Gerhard Hoch and Nicola Strenzke for guidance and help in systems physiology and thanks to the other members of the InnerEarLab, for having a pleasant working atmosphere and for patience with the numerous questions I had, special thanks go to Sarah Helfmann for her friendship and company.

In addition, I want to express special thankfulness to Reinhard Jahn and Nils Brose giving me access to fully equipped workspace while the facilities of the InnerEarLab were not yet provided with molecular biology and biochemistry equipment. Furthermore I would like to thank Kai Tittmann for the opportunity to work in his laboratory.

Another big 'thank you' deserve Dirk Jessen and Sarah Helfmann for enlightening debates. I also want to express my appreciation towards the coordination office of the neuroscience program for all the organizational help.

Finally I would like to deeply thank my friends, my parents Ingolf and Renate Reuter and my sister Janina Reuter for the constant support I enjoyed throughout all these years: I am very grateful about that.

Appendix 1

Abbreviations

Aa – Amino Acid

ABR – Auditory Brainstem Response

APS – Ammonium Persulfate

ATP – Adenosine 5'-triphosphate

BGH – bovine growth hormone polyadenylation sequence

CCD – Charge Coupled Device

CD – Circular Dichroism

ΔF – change in Fluorescence

dNTP – Deoxyribonucleotide triphosphate

Da – Daltons

DPOAE – Distortion Product Oto-Acoustic Emissions

DTT – Dithiothreitol

EDTA – Ethylenediaminetetraacetic acid

EGTA – Ethylene glycol tetraacetic acid

GST – Glutathione-S-transferase

HBA – human CMV enhancer – human β -Actin promoter combination

IHC – Inner Hair Cell

IRES – Internal Ribosomal Entry Site

ITR – Inverted Terminal Repeat

kDa – kilo Dalton

LB – Lysogeny Broth

LSO – Lateral Superior Olive

MCS – Multiple Cloning Site

mOtof – murine Otoferlin

MSO – Medial Superior Olive

MWCO – Molecular Weight Cut Off

OD – Optical Density

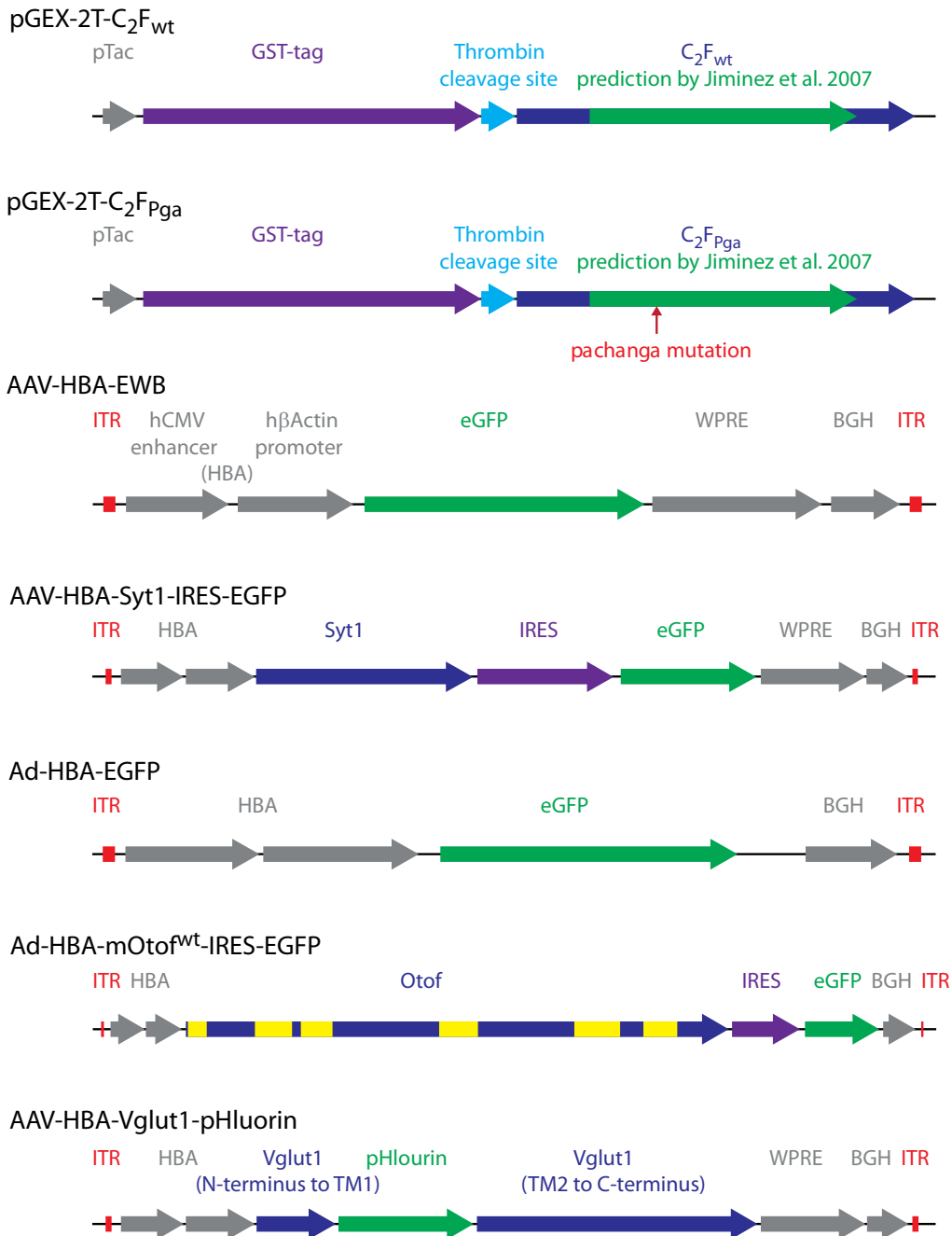
Otof – Otoferlin

OHC – Outer Hair Cell

PAGE – Polyacrylamide Gel Electrophoresis
PC – Phosphatidylcholine
PCR – Polymerase Chain Reaction
PE – Phosphatidylethanolamine
Pga – Pachanga mutation
PI – Phosphatidylinositol
PIP₂ – Phosphatidylinositol-(4,5)bis-phosphate
PMSF – Phenylmethanesulfonyl Fluoride
PMT – Photomultiplier tube
PS – Phosphatidylserine
RT – Room Temperature
SGN – Spiral Ganglion Neurons
SDS – Sodium Dodecylsulphate
SEM – Standard Error of Mean
TAE – Tris-acetate-EDTA
TB – Terrific Broth
TBP – TATA-box Binding Protein
TEMED – N,N,N',N'-Tetramethylethylenediamine
TM – Trans-Membrane Domain
TSA - trichostatin A
tu – transfecting units
WPRE – Woodchuck Posttranscriptional Regulatory Element

Appendix 2

Vector Maps



Curriculum Vitae

Kirsten Reuter

InnerEarLab

Department of Otolaryngology
University Medical Center Goettingen
Robert-Koch-Str. 40
37075 Goettingen

MSc/PhD program Neurosciences
International Max Planck Research School
Georg August University Goettingen

Scientific Activities

Dissertation

Title: Biochemistry and physiological role of otoferlin
Thesis committee: Prof. Tobias Moser (Georg August University Goettingen),
Prof. Reinhard Jahn (Max Planck Institute for Biophysical Chemistry), Prof. Nils
Brose (Max Planck Institute for Experimental Medicine Goettingen)
Supervisor: Prof. Tobias Moser

Oct 2007 – Sep 2011

Research assistant

continuation of BSc thesis project

Mar 2006 – Aug 2006

BSc thesis

Title: Selective Labeling of Presynaptic Protein in the Calyx of
Held Mediated by the Genetically Encoded AGT-tag

Sep 2005 – Feb 2006

Internship

Title: Fine mapping of large deletions in *MECP2*

Aug 2004 – Jan 2005

Scholarships

Boehringer Ingelheim Fonds PhD Fellowship

Jan 2009 – Dec 2010

Georg-Christoph-Lichtenberg Stipend

by the federal state of Lower Saxony

Oct 2007 – Dec 2008

Education

MSc/PhD program Neurosciences

International Max Planck Research School
Georg August University Goettingen

Oct 2007 – Sep 2011

BSc program Biotechnology

University of Applied Sciences Mannheim

Oct 2002 – Feb 2006

Secondary School

Luise-Büchner-Schule, Freudenstadt

Aug 1998 – Jun 2002

Publications

Probing the Functional Equivalence of Otoferlin and Synaptotagmin 1 in Exocytosis.

Reisinger E, Bresee C, Neef J, Nair R, Reuter K, Bulankina A, Nouvian R, Koch M, Bückers J, Kastrup L, Roux I, Petit C, Hell SW, Brose N, Rhee JS, Kügler S, Brigande JV, Moser T.
J Neurosci. 2011 Mar 30;31(13):4886-4895.

Hearing requires otoferlin-dependent efficient replenishment of synaptic vesicles in hair cells.

Pangrsic T, Lasarow L, Reuter K, Takago H, Schwander M, Riedel D, Frank T, Tarantino LM, Bailey JS, Strenzke N, Brose N, Müller U, Reisinger E, Moser T.
Nat Neurosci. 2010 Jul;13(7):869-76. Epub 2010 Jun 20.

Delineation of large deletions of the MECP2 gene in Rett syndrome patients, including a familial case with a male proband.

Hardwick SA, Reuter K, Williamson SL, Vasudevan V, Donald J, Slater K, Bennetts B, Bebbington A, Leonard H, Williams SR, Smith RL, Cloosterman D, Christodoulou J.
Eur J Hum Genet. 2007 Dec;15(12):1218-29. Epub 2007 Aug 22.